Wearable biosensors enabled by cell-free synthetic biology

Wearable Biosensors Enabled by Cell-Free Synthetic Biology

Peter Q. Nguyen[1,2‡], Luis R. Soenksen[1,3,5‡], Nina M. Donghia[1], Nicolaas M. Angenent-Mari[1,4,5], Helena de Puig[1,5], Ally Huang[1,4,5], Rose Lee[1], Shimyn Slomovic[1], Tommaso Galbersanini[6], Geoffrey Lansberry[1], Hani M. Sallum[1], Evan M. Zhao[1], James B. Niemi[1], and James J. Collins[1,4,5,7,8,9*]

[‡] Co-first authors.
[1] Wyss Institute for Biologically Inspired Engineering, Harvard University, Boston, MA 02115.
[2] School of Engineering and Applied Sciences, Harvard University, Cambridge, MA 02138.
[3] Department of Mechanical Engineering, Massachusetts Institute of Technology (MIT), Cambridge, MA 02139.
[4] Department of Biological Engineering, MIT, Cambridge, MA 02139.
[5] Institute for Medical Engineering and Science, MIT, Cambridge, MA 02139.
[6] DREAMLUX, Samsara S.r.l, Milan, MI 20123, Italy.
[7] Synthetic Biology Center, MIT, Cambridge, MA 02139, USA.
[8] Harvard-MIT Program in Health Sciences and Technology, Cambridge, MA 02139, USA.
[9] Broad Institute of MIT and Harvard, Cambridge, MA 02142, USA.

*Corresponding author: James J. Collins
email: jimjc@mit.edu

Abstract

Wearable biosensors have become increasingly relevant as promising solutions for monitoring of physiological status, disease states, and pathogen/toxin exposure. The integration of synthetic biology tools into such formats could improve and expand on this potential. However, the use of synthetic gene circuits in wearables has been limited by the challenges of sustaining engineered organisms for operation. Here, we report on the development of a wearable sensing platform based on cell-free synthetic biology reactions freeze-dried into flexible substrates and textiles. We present a colorimetric wearable device capable of reacting to specific target exposures, as well as a highly sensitive textile-based wearable system containing inter-weaved optical fibers for the detection of fluorescent and luminescent outputs. These wearable systems are functionally validated using a variety of relevant engineered biological circuits and regulatory components for detecting metabolites, chemicals, and pathogen nucleic acids. We also show that lyophilized programmable CRISPR-based detection systems can be incorporated into the wearable devices, enabling detection limits that rival current laboratory-based methods such as qPCR. These sensors are integrated into garments with sensing electronics and wireless networking capabilities for real-time dynamic monitoring of target exposure. Finally, we present a face mask-integrated lyophilized cell-free synthetic biology sensor system allowing for on-patient diagnosis of SAR-CoV-2 at room temperature within 90 min, requiring no user intervention other than the press of a button.

Main text

Synthetic biology has enabled unprecedented control of biological systems and has led to transformational developments in biotechnology and medicine[1]. A rich palette of modular biosensors, genetic logic gates, and output effectors already populate the design toolkit of custom biological circuits[2]. In parallel, recent developments in wireless technology, wearable electronics, smart materials, and functional fibers with novel mechanical, electrical and optical properties have marked the dawn of next-generation biosensing systems[3]. Even though genetically encoded sensors have been readily incorporated into bench-top diagnostics, examples of wearable devices using these tools are limited. Only a few demonstrations of hygroscopically actuated vents and response to induction molecules have been achieved using living engineered bacteria encapsulated in flexible substrates and hydrogels in a wearable format[4-7]. While seminal, such examples encounter several limitations, particularly that of sustaining living organisms within these devices for extended periods. In practice, retaining viability and function of wearable sensing systems based on living cells requires nutrient delivery, waste extraction, as well as temperature and gas regulation, all of which involve numerous technological hurdles. Genetically engineered cells can also pose biocontainment or biohazard concerns, particularly if integrated into consumer-level garments, leading to stringent regulatory pathways in many critical applications. Moreover, continually evolving cell populations suffer mutational pressures over time, resulting in potential loss of the genetic phenotype and function. Thus, a new approach in synthetic biology is needed to resolve the mismatch between practical requirements of wearable use and operational limitations of available biomolecular circuits for sensing and response. Achieving this goal could enable many applications for synthetic biology, allowing utilization in a wide range of wearable substrates (e.g., functional fibers or fabrics) to assess molecular targets difficult to detect through other technologies[8].

Cell-free synthetic biology reactions are self-contained abiotic chemical systems with all the biomolecular components required for efficient transcription and translation. Such systems can be freeze-dried into shelf-stable formats utilizing porous substrates, which allow for robust distribution, storage and use without specialized environmental or biocontainment requirements[9]. Genetically engineered circuits, encoded in DNA or RNA, can be added to freeze-dried, cell-free (FDCF) reactions for activation by simple rehydration. Robust FDCF systems have already been developed for inexpensive paper-based nucleic acid diagnostics[9], highly sensitive programmable CRISPR-based nucleic acid sensors[10-12], on-demand production of antimicrobials, antibodies, and enzymes[13], and low-cost educational kits for teaching[14-16]. Here, we propose the use of freeze-dried, cell-free genetic circuits in combination with specifically designed flexible and textile substrates as a new direction towards practical wearable biosensors. In this study, we report on the design and validation of various wearable freeze-dried, cell-free synthetic biology (wFDCF) sensors for small molecule, nucleic acid, and toxin detection. These sensors are integrated into flexible multi-material substrates (e.g., silicone elastomers and textiles) using genetically engineered components, including toehold switches, transcriptional factors, riboswitches, fluorescent aptamers, and CRISPR-Cas12a complexes.

For our first wFDCF demonstration, we embedded colorimetric genetic circuits into cellulose substrates surrounded by a fluid wicking and containment assembly made of flexible elastomers (Fig. 1a). These prototypes were assembled layer-by-layer to form reaction chambers fluidically connected to top sample portals (Fig. 1b and Supplementary Fig. S1a). The devices

are flexible, elastic, and can rapidly wick in splashed fluids through capillary action (Fig. 1c, d). Pinning geometries throughout the device direct sample fluids towards enclosed hydrophilic paper networks allowing for reaction rehydration (Fig. 1b and Supplementary Fig. S3b). Using a *lacZ* β-galactosidase operon as the circuit output to hydrolyze chlorophenol red-β-D-galactopyranoside (CPRG), a yellow to purple color change develops upon exposure to a target (Supplementary Fig. S1b, S3a).

Key environmental factors were considered for the design of these prototypes. For instance, sample exposure in the field likely occurs with variable splash volumes (as little as 50-100 μL), relative humidity (RH, 20-40%), and temperature (20-37ºC). Thus, we optimized our design to reduce inhibition of genetic circuit operation due to evaporation or excessive dilution of components. In particular, our devices use impermeable chambers exhibiting low evaporation rates (<20% volume/hour), which also constrain the rehydration volume to ~50 μL per sensor. In addition, the wFDCF reactions were optimized to generate a higher concentrated reaction upon rehydration. We found that a 1.5x-concentrated cell-free reaction increased the reaction kinetics to enable signal output at least 10 min faster, ensuring that the desired circuit is completed before eventual evaporation in the device terminates the reaction (Supplementary Fig. S2). The resulting stand-alone colorimetric system is modular and can be used in garments such as bracelets (Supplementary Fig. S3c).

Functional testing of this colorimetric wearable platform was performed utilizing four different synthetic biology biosensors with *lacZ* as the output (Fig. 1e-h). These various demonstrations include a constitutive *lacZ* expression reaction (Fig. 1e), a transcription factor-regulated circuit using the tetracycline repressor (TetR) (Fig. 1f), a toehold switch for Ebola virus RNA detection (Fig. 1g), and a theophylline riboswitch for small-molecule sensing (Fig. 1h). Genetic circuits using transcriptional regulators are among some of the most common elements used in synthetic biology. Our wFDCF TetR sensor demonstrates the capacity of our colorimetric platform for facile integration of well-established genetic modules into a wearable format (Fig. 1f). Similarly, toehold switches have been developed as highly programmable nucleic acid sensors capable of detecting any target RNA[17]. We show that a wFDCF Ebola virus RNA toehold sensor in our wearable device is capable of rapid and sensitive detection of biothreats (Fig. 1g). This paves the way for the development of similar viral or bacterial wearable nucleic acid sensors. Furthermore, a functional theophylline riboswitch wFDCF circuit is functionally validated in our platform for the environmental detection of small molecules via engineered cis-regulated RNA circuits (Fig. 1h). This specific riboswitch was selected as a model test case, although a plethora of similar riboswitches for various targets have been reported and could be used in a modular fashion. All of the colorimetric wFDCF sensors reported here exhibited visible changes within ~40-60 min after exposure to the respective trigger molecules or inducer, and were performed at ambient conditions of 30-40% RH and 30ºC to simulate the average skin surface temperature[18].

Expanding on the attractiveness and versatility of textiles as ubiquitous wearable substrates, we immobilized and activated FDCF synthetic biology systems within wearable woven fabrics and individual threads. Figure 2 presents various demonstrations of a highly sensitive, textile-based system (Fig. 2a, b) capable of containing and monitoring the activation of wFDCF reactions with fluorescent (Fig. 2c-e and Supplementary Fig. S7, S13-S15) or luminescent (Fig.

2f and Supplementary Fig. S10) outputs. To achieve this, we fabricated a second wearable platform that integrates: (a) hydrophilic threads (85% polyester / 15% polyamide) for cell-free reagent immobilization, (b) patterns of skin-safe hydrophobic silicone elastomers for reaction containment, and (c) inter-weaved polymeric optic fibers (POFs) for signal interrogation (Fig. 2a-b and Supplementary Fig.S8-S9). This fabric was chosen as our main immobilization substrate after conducting a compatibility screening of over 100 textiles (e.g., silks, cotton, rayon, linen, hemp bamboo, wool, polyester, polyamide, nylon, and combination materials) using a lyophilized constitutive *lacZ* cell-free reaction (Supplementary Fig. S4-S6). The analysis of sensor outputs was done using a custom-built wearable POF spectrometer (Fig. 2b and Supplementary Fig S17) that could be monitored with a mobile phone application (Supplementary Fig. S18). Using this integrated platform, we performed distributed on-body sensing of various target exposures as shown in Fig. 2c-f. A sample activation through fluid splashing can be seen in Fig. 2a, where the sample wicks through the entry ports with blackout fabrics to rehydrate the freeze-dried, cell-free synthetic biology reactions immobilized within the hydrophilic textile fibers. These fibers are located within the excitation and emission layers of the device as shown in Fig. 2a,b. Trigger presence in the splash fluid leads to activation of the sensor circuits, which produce fluorescent or luminescent reporters.

The versatility of this textile platform in fluorescence mode was first verified using two independent synthetic biology modules upstream of a superfolder green fluorescent protein (sfGFP) operon. These demonstrations included the activation of constitutive sfGFP expression (Fig. 2c) and sensing of theophylline using an inducible riboswitch (Fig. 2d). A third fluorescence demonstration was done via activation of a 49-nucleotide Broccoli aptamer (Fig. 2e) with substrate-specificity to *(Z)-4-(3,5-difluoro-4-hydroxybenzylidene)-1,2-dimethyl-1H-imidazol-5(4H)-one* (DFHBI-1T), evincing functionality of this emerging class of fluorescent sensors in synthetic biology[19]. Furthermore, demonstrations utilizing luminescence outputs were conducted using a nanoLuciferase[20] operon downstream of an HIV RNA toehold switch (Fig. 2f and Supplementary S10a), as well as a *B. burgdorferi* RNA toehold switch for the wearable detection of Lyme disease (Supplementary Fig. S10b).

Additionally, we tested the operation of our platform for the detection of chemical threats such as organophosphate nerve agents used in chemical warfare and the pesticide industry, both of which constitute prime targets for wearable detection. To achieve this, we modified our POF platform optics for excitation and detection at near-infrared (NIR) fluorescence, generated from a lyophilized acetylcholinesterase (AChE)-choline oxidase (ChOx)-HRP coupled enzyme reaction (Figure 2g). In the presence of acetylcholine, this reaction can produce NIR fluorescence that is readily detectable with our wearable prototype (see Supplementary Methods). When exposed to an organophosphate AChE inhibitor, the sensor fluorescence is ameliorated as compared to unexposed controls. Our wearable nerve agent sensor was validated using paraoxon-ethyl as a nerve agent simulant at levels that are four orders of magnitude lower than the reported lethal dose (LD_{50}) by dermal absorption in mammals[21] (Fig. 2g).

Despite the single-activation nature of our wFDCF synthetic biology sensors, the presence of fluorescence outputs is continuously monitored to allow for automatic detection of rehydration events containing the desired target. This is achieved by illuminating the wFDCF textile reaction with blue light (447 nm) via etched excitation POFs (Fig. 2b and Supplementary Fig.S9a). The

light emitted from the activated system is then collected by the second set of emission POFs (Fig. S17), which exit the fabric weave and bundle into a connection to the optical sensor (Fig. 2b) of our wearable spectrometer (Supplementary Fig.S9 and Fig.S17). Signals coming from each of the devices are filtered (Supplementary Fig.S17d) and processed to generate temporally and spatially resolved fluorescence images of the POF bundle-ends (510 nm) and averaged pixel intensity traces per channel for quantitative analysis (Fig. 2b). In the case of luminescence demonstrations, all POFs bundles are treated as signal inputs, without the need for sample illumination. All reported wFDCF fluorescence and luminescence sensor replicates ($n \geq 3$) exhibited visible fluorescence or luminescence within 5-20 min after exposure to relevant trigger conditions, at 30-40% RH and 30ºC.

Recent advances in programmable clustered regularly interspaced short palindromic repeat (CRISPR) and CRISPR-associated (Cas) enzymes have enabled the development of new classes of rapid and reliable sensing platforms[10, 11, 22, 23]. The advantages of CRISPR-based systems over existing biosensors include high sensitivity, rapid output, single base-pair resolution, freeze-drying compatibility, and the notable programmability to target any DNA or RNA sequence through interchangeable guide RNAs (gRNAs). Thus, we integrated CRISPR-based Specific High Sensitivity Enzymatic Reporter UnLOCKing (SHERLOCK) sensors into our fluorescence wFDCD platform to demonstrate this detection technique in wearable applications (Fig. 3a). We used Cas13a and Cas12a for the detection of RNA and DNA, respectively. For DNA detection, we used a Cas12a ortholog from *Lachnospiraceae* bacterium (LbaCas12a)[22, 24] that displays a non-specific collateral cleavage activity towards single-stranded DNA (ssDNA) after detection of a gRNA-defined double-stranded DNA (dsDNA) target. This Cas12a-based sensor was paired with recombinase polymerase amplification (RPA)[25] and freeze-dried into a one-pot reaction to demonstrate state-of-the-art detection limits for wearable clinical applications. In the presence of a target dsDNA sequence, isothermally generated RPA amplicons activate Cas12a-gRNA complexes. Then, active Cas12a engages in trans-ssDNase activity and cleaves quenched ssDNA fluorophore probes, resulting in a fluorescence output (Fig. 3a). For our wearable CRISPR-based demonstrations, we designed gRNAs against three common resistance markers in *Staphylococcus aureus*: specifically, the *mecA* gene common in methicillin-resistant *S. aureus* (MRSA)[26], the *spa* gene which encodes the protein A virulence factor[27], and the *ermA* gene conferring macrolide resistance[28]. When tested in wFDCF format, our RPA-Cas12a sensors displayed detectable signals within 56-78 min ($P<0.05$) with femtomolar limits of detection (Fig. 3b-d). Moreover, using our *mecA* wFDCF sensor (Fig. 3e, Supplementary Fig. S11), we were able to confirm single-digit femtomolar sensitivity (2.7 fM). Compatibility with RNA inputs and other CRISPR enzymes such as Cas13a, an ortholog from *Leptotrichia wadei* bacterium (LwaCas13a)[10] was also confirmed (Supplementary Fig. S12), exhibiting similar in-device activation dynamics as that of cell-free reactions conducted in a plate reader. These results suggest that our wearable textile platform could be adapted to achieve sensitivities rivaling that of current laboratory diagnostic tests such as qPCR for monitoring contamination or spread of bacteria and viruses.

To further demonstrate the modularity of our CRISPR-Cas12a wearable sensors, we tested wFDCF devices containing three orthogonal Cas12a-gRNA complexes in isolated reaction wells (Fig. 3f). In this experiment, each device was splashed with dd-H_2O containing different targets, each specific to only one Cas12a-gRNA complex. The orthogonal behavior of our CRISPR-

based wearable sensors is shown in Fig. 3g-h, where higher fluorescence was observed for the cases in which the dsDNA trigger matched the pre-defined Cas12a-gRNA complex at each sensor location. These results suggest the broad applicability of CRISPR-based synthetic biology sensors for multiplexing or logic-gating in wearable synthetic biology applications.

Our wFDCF reactions and networked optical fiber detection system can be integrated into flexible textiles to create an autonomous wearable platform enabling real-time monitoring of environmental exposure and biohazard detection. We designed a jacket that contained a distributed arrangement of wFDCF multi-sensor arrays (Fig. 3i). The various optical fibers carrying the output emission signals can be routed into a single bundle for centralized imaging analysis or interrogated as separate modules, which we demonstrate using a wFDCF CRISPR-Cas12a based MRSA-sensing array containing spa, ermA and mecA sensors, that was activated in the wearable prototype with a fluid splash containing 100 fM of spa DNA trigger (Supplementary Fig. S13). Only the well containing the spa sensor generated a fluorescent signal upon activation. The platform is also compatible with transcription-only outputs, such as rehydrated fluorescent aptamer reactions (Supplementary Fig. S14), where the fluorescence signal is monitored by microscopy over time.

In addition, the optical sensor allows for facile fluorescent output multiplexing simply by using fluorescent proteins with orthogonal emission profiles (Supplementary Fig. S15). In this example, wFDCF reactions for three constitutively expressed fluorescent output proteins (eforRed[29], dTomato[30], and sfGFP[31]) were used to demonstrate detection of distinguishable output signals in a single bundle. It is possible that additional fluorescent outputs, including orthogonal quenched fluorophore probes for SHERLOCK-based sensors, can be employed to increase the signal multiplexing of our wearable platform. We also show that the wFDCF POF system is fully compatible with integrated lyophilized lysis components, allowing for the release and detection of a plasmid-borne *mecA* gene when challenged with intact bacterial cells (Supplementary Fig. S16). Finally, to develop a complete data feedback cycle between the platform and the user, we integrated the detector system with a custom wireless mobile application that enables continuous cloud-based data logging, signal processing, geolocation tracking, and on-the-fly control of various detector components through a smart phone or other networked digital device (Fig. 3j). All images and spectral data presented in Figs 2 and 3 were collected and processed using wFDCF devices fully integrated with our wearable spectrometer and mobile phone application. Further details on the hardware (Supplementary Fig. S17) and software design (Supplementary Fig. S18), as well an implementation of a novel *Opuntia microdasys* bioinspired fluid collection[32] add-on for improved sample harvesting and routing splashes outside of the sensor zones into the wFDCF modules (Supplementary Fig. S19), can be found in the Supplemental Information.

The wearable synthetic biology sensors demonstrated here thus imbue programmable and highly sensitive diagnostic sensing to protective apparel. With the current SARS-CoV-2 pandemic that has led to significant strain on the medical system of all impacted countries and considerable delays in diagnostic testing, we explored whether our wFDCF system could be adapted to key wearable gear, face masks, that have been shown to be critical in reducing the transmission of this highly infectious virus[33, 34]. Although face masks are placed on all incoming patients that are presumptive SARS-CoV-2 carriers, confirmation through burdened laboratory diagnostics may result in delays that could negatively impact rapid triaging or effective contact

tracing of patients[35-37]. Patients suspected of an infectious respiratory disease are fitted with a face mask upon clinical admission as a preventative measure to reduce transmission. Diagnosis is commonly undertaken by nasopharyngeal sampling, which may cause reflexive sneezing and increase exposure risk to clinical workers[38]. Respiratory droplets and aerosols are the transmission routes for respiratory infectious diseases, but their use as a non-invasive diagnostic sample has been underutilized historically. Work on breath-based sensing has focused on the detection of volatile organic compound biomarkers in infected patients using electrochemical sensors[39, 40] or downstream mass spectrometry analysis[41, 42], which may be challenging to implement on a wide scale. The NIH Rapid Acceleration of Diagnostics (RADx) Initiative has identified SARS-CoV-2 detection from breath sampling technologies as an active area of interest for alleviating testing bottlenecks[43]. Here, we demonstrate that our freeze-dried synthetic biology sensors can be adapted for a rapid point-of-care SARS-CoV-2 sensor fully integrated into any standard face mask, which takes advantage of the accumulation of virus on the inside of the mask as a result of coughing, talking or normal respiration, as demonstrated in numerous studies[34, 44-49]. Unlike other current nucleic acid tests (NATs) that require laboratory equipment and trained technicians[50-54], the SARS-CoV-2 face-mask NAT sensor we describe here requires no power source, operates autonomously without liquid handling, is shelf-stable, functions at near-ambient temperatures, provides a visual output in under 2 hours, and is only ~3 g in weight. All the user has to do is press a button to activate a reservoir containing nuclease-free water.

Our SARS-CoV-2 sensor contains four modular components: a reservoir for hydration, a large surface area collection sample pad, a wax-patterned μPAD (microfluidic paper-based analytical device), and a lateral flow assay (LFA) strip (Figure 4a-b). Each module can be oriented on the outside or inside of the face mask, with the exception of the collection pad, which must be positioned on the mask interior facing the mouth and nose of the patient. Capillary action wicks any collected fluid and viral particles from the sample collection pad to the μPAD, which contains an arrangement of freeze-dried lysis and detection components (Figure 4c). The use of the μPAD format allowed us to rapidly prototype and optimize a passively regulated multi-step reaction process. Each reaction zone is separated by polyvinyl alcohol (PVA) time delays that enable tunable incubation times between each reaction, greatly improving the efficiency of the sensor compared to that of a one-pot lyophilized reaction (Supplementary Fig. S20). The first μPAD reaction zone contains lyophilized lysis reagents including components known to lyse viral membranes[55-58]. The second μPAD reaction zone is an RT-RPA reaction zone containing a customized isothermal amplification reaction developed to target a non-overlapping region of the SARS-CoV-2 S gene. The final μPAD reaction zone contains a Cas12a SHERLOCK sensor with an optimized gRNA for detection of the amplified dsDNA amplicon. In the presence of SARS-CoV-2 derived amplicons, the activated Cas12a enables trans-cleavage of a co-lyophilized 6-FAM-(TTATTATT)-Biotin ssDNA probe. To enable a simple colorimetric visual readout, an integrated LFA strip is used to detect probe cleavage. The output strip orientation is adjustable to preserve patient confidentiality. Details on the design, performance, and relevant molecular sensor sequences are presented in Supplementary Fig. S21-S22.

From activation of the face-mask sensor to a final readout only takes ~1.5 hours. The limit of detection observed for our sensors is 500 copies (17 aM) of SARS-CoV-2 in vitro transcribed (IVT) RNA, which matches that of WHO-endorsed standard laboratory-based RT-PCR assays[59] (Fig. 4d-e). The sensors also do not cross react to RNA from other commonly circulating human

coronavirus strains (HCoVs) (Fig. 4f-e). Most critically, our hands-off diagnostic reaction proceeds to full completion even at room temperature, which is considered sub-optimal for RT, RPA, and Cas12a activities. We also validated the SARS-CoV-2 face-mask sensor using a precision lung simulator attached to a high-fidelity human airway model (Fig. 4h, Supplementary Fig. 23). The target RNA was nebulized to replicate lung emissions with aerosol diameters matching those naturally occurring in breath exhalation plumes. The breath temperature was regulated to 35°C and the relative humidity in the mask microclimate was measured to be 100% RH. Under these realistic simulation conditions, the face-mask sensor was able to detect SARS-CoV-2 vRNA after a breath sample collection period of 30 minutes, with a calculated accumulation of 10^6-10^7 vRNA copies on the sample pad, as determined by RT-qPCR (Fig. 4i-j). Clinical measurements have previously shown that the SARS-CoV-2 breath emission rate of infected patients could reach an output 10^3-10^5 copies/min.[49] To our knowledge, this is the first SARS-CoV-2 NAT that is able to achieve high sensitivity and specificity while operating fully at ambient temperature ranges, thus obviating the need for any heating instruments and allowing for integration into a wearable format. We believe our rapid face-mask-integrated SARS-CoV-2 diagnostic presented here could relieve strained medical systems by combining protection and sensing into a simple and easy-to-deploy wearable system, greatly improving patient outcomes. Our face-mask system could be adapted to discriminate between SARS-CoV-2 and other respiratory viruses, as well as different emerging SARS-CoV-2 variants[60-62], allowing rapid triaging of patient populations and isolation of specific positive cases to minimize the spread of infection.

We view the wFDCF platform as being complementary to cell-based synthetic biology sensors. Such living sensors are capable of self-replication, can operate continuously to provide dynamic sensing, and can actively draw upon environmental resources for energy. However, storage and biocontainment concerns limit their use for wearable technologies. We have shown that cell-free synthetic biology systems can be used to build practical wearable biosensors that are shelf-stable, genetically programmable, and highly sensitive. However, the current wFDCF technology does have a number of limitations, including the single-use nature of the sensors and inability to operate in particular environmental conditions (such as high humidity or underwater). These challenges are also shared by other sensors in which operation requires open access to the environment and will require further engineering to surmount.

Our wFDCF sensors are responsive to external rehydration events, such as splashes with contaminated fluids, and withstand inhibitory evaporative and dilutive effects in open-environment conditions (30-40% RH and ~25-30ºC). Alternatively, user-generated samples such as breath emissions can be used if an on-demand hydration system is employed, as we demonstrate for the SARS-CoV-2 sensing face mask. We showed that these freeze-dried systems generate measurable colorimetric, fluorescence, or luminescence outputs upon exposure to relevant real-world targets such as MRSA, Ebola virus, or SARS-CoV-2 virus. In the wFDCF POF sensors, continuous monitoring enables rapid alert to an exposure event. We also demonstrated the integration of our device designs into garments that are compatible with wireless sensor networks to provide real-time dynamic monitoring of exposure using custom smartphone applications. Although laboratory testing may be more sensitive, our wFDCF sensors have the distinct advantages of a wearable format, autonomous functioning, and rapid results.

To our knowledge, the platform presented here is the first wearable technology demonstrated to detect viral or bacterial nucleic acid signatures in fluid samples with sensitivities rivaling those of traditional laboratory tests at ambient temperatures. Our wFDCF platform evinces a number of distinct advantages over existing POC diagnostics, which similarly attempt to eliminate the need for time-consuming and resource-intensive laboratory tests. Current field-portable POC systems typically use a swabbed or directly applied sample to provide a readout. Our wearable platform accomplishes field sensing in one of the most critical environmental spaces for testing – that is, the surface of the user or wearable areas that are exposed to patient samples, such as the inside of a face mask. Moreover, in contrast to batch-mode POC sensors, our wFDCF synthetic biology sensors can be networked to provide spatial sensing arrays of lyophilized reactions and lightweight polymer fabrics, thus cloaking the user and continuously generating high-density, real-time outputs without sacrificing comfort or agility in the field. Our platform is also designed to operate autonomously, unlike most current POC instruments that require training for use and multiple operations by the user to acquire the final results. This feature removes the need to perform regular exposure checks, freeing those in the field to focus on their core tasks. In comparison to current wearable sensors that primarily employ electronic devices to monitor physiological signals such as heart rate or blood oxygen levels, our modular wearable sensors can detect environmental threats or patient samples through nucleic acid, protein, or small molecule detection. Although recently electrochemical sensors have been integrated into a wearable format[40, 63], they only detect chemicals and an easily programmable wearable form for sensitive nucleic acid detection does not currently exist. Integration of our wearable synthetic biology reactions with these advances in electrochemical devices[64-66] could be a fertile area for expanding the functionality of wearable sensors. The key functional differences of our platform over current related technologies, including traditional bench-top assays, are summarized in Supplementary Table 4. Finally, the wFDCF components are inexpensive, with cell-free reactions costing only \$0.01 – 0.03 per μL[15, 67]. Thus, a single 10 mm-diameter sensor would currently only cost ~\$1 in reagents. The optical fiber textiles are woven from common polymer fibers and are also inexpensive. At these price points, our wearables could be utilized as disposable protective garments with advanced sensing technology. We have also shown that the sensors can be highly modular and adapted to various form factors, such as clothing or face masks.

Field applications that would greatly benefit from our wFDCF synthetic biology platform include warfighters and first responders operating in environments where a specific chemical or biological threat is suspected. In this situation, our apparel of disposable wFDCF sensors could be used to maintain situational awareness, with continuous spatio-temporal monitoring of exposure and bodily resolution down to centimeters. Another set of potential uses for our platform involves the environmental awareness of clinicians, health workers, and researchers working in high-risk areas. In contrast to laboratory-based exposure testing, our wearable platform enables swift responses to contagion exposure so that users could begin decontamination and neutralization procedures in a timely manner. Similarly, wFDCF-enabled coats and gowns in hospitals could provide alerts to prevent the spread of nosocomial infections to vulnerable populations, such as immune-compromised patients or newborns. An additional promising application is patient-worn sensor-enabled PPE wearables such as the face mask presented here that can provide inexpensive, shelf-stable, and labor-saving POC diagnostics to

rapidly inform clinicians in outbreak events, such as the current COVID-19 pandemic that has overwhelmed the resources of our medical infrastructure.

References

1. Kim, J., Campbell, A.S., de Avila, B.E. & Wang, J. Wearable biosensors for healthcare monitoring. *Nat Biotechnol* **37**, 389-406 (2019).
2. Khalil, A.S. & Collins, J.J. Synthetic biology: applications come of age. *Nat Rev Genet* **11**, 367-379 (2010).
3. Tao, X. Smart fibres, fabrics and clothing: fundamentals and applications. (Elsevier, 2001).
4. Liu, X. et al. Stretchable living materials and devices with hydrogel-elastomer hybrids hosting programmed cells. *Proc Natl Acad Sci U S A* **114**, 2200-2205 (2017).
5. Liu, X. et al. 3D printing of living responsive materials and devices. *Adv Mater* **30** (2018).
6. Moser, F., Tham, E., González, L.M., Lu, T.K. & Voigt, C.A. Light-controlled, high-resolution patterning of living engineered bacteria onto textiles, ceramics, and plastic. *Adv Func Mater* **29**, 1901788 (2019).
7. Wang, W. et al. Harnessing the hygroscopic and biofluorescent behaviors of genetically tractable microbial cells to design biohybrid wearables. *Sci Adv* **3**, e1601984 (2017).
8. Slomovic, S., Pardee, K. & Collins, J.J. Synthetic biology devices for in vitro and in vivo diagnostics. *Proc Natl Acad Sci U S A* **112**, 14429-14435 (2015).
9. Kumar, R.M. et al. Deconstructing transcriptional heterogeneity in pluripotent stem cells. *Nature* **516**, 56-61 (2014).
10. Gootenberg, J.S. et al. Nucleic acid detection with CRISPR-Cas13a/C2c2. *Science* **356**, 438-442 (2017).
11. Gootenberg, J.S. et al. Multiplexed and portable nucleic acid detection platform with Cas13, Cas12a, and Csm6. *Science* **360**, 439-444 (2018).
12. English, M.A. et al. Programmable CRISPR-responsive smart materials. *Science* **365**, 780-785 (2019).
13. Pardee, K. et al. Portable, on-demand biomolecular manufacturing. *Cell* **167**, 248-259 e212 (2016).
14. Huang, A. et al. BioBits Explorer: A modular synthetic biology education kit. *Sci Adv* **4**, eaat5105 (2018).
15. Stark, J.C. et al. BioBits Bright: A fluorescent synthetic biology education kit. *Sci Adv* **4**, eaat5107 (2018).
16. Stark, J.C. et al. BioBits Health: Classroom activities exploring engineering, biology, and human health with fluorescent readouts. *ACS Synth Biol* **8**, 1001-1009 (2019).
17. Green, A.A., Silver, P.A., Collins, J.J. & Yin, P. Toehold switches: de-novo-designed regulators of gene expression. *Cell* **159**, 925-939 (2014).
18. Choi, J.K., Miki, K., Sagawa, S. & Shiraki, K. Evaluation of mean skin temperature formulas by infrared thermography. *Int J Biometeorol* **41**, 68-75 (1997).
19. Filonov, G.S., Kam, C.W., Song, W. & Jaffrey, S.R. In-gel imaging of RNA processing using broccoli reveals optimal aptamer expression strategies. *Chem Biol* **22**, 649-660 (2015).
20. Hall, M.P. et al. Engineered luciferase reporter from a deep sea shrimp utilizing a novel imidazopyrazinone substrate. *ACS Chem Biol* **7**, 1848-1857 (2012).
21. Handbook of Pesticide Toxicology. (Academic Press, London, UK; 2010).
22. Chen, J.S. et al. CRISPR-Cas12a target binding unleashes indiscriminate single-stranded DNase activity. *Science* **360**, 436-439 (2018).

23. Harrington, L.B. et al. Programmed DNA destruction by miniature CRISPR-Cas14 enzymes. *Science* **362**, 839-842 (2018).
24. Li, S.-Y. et al. CRISPR-Cas12a has both cis-and trans-cleavage activities on single-stranded DNA. *Cell Res* **28**, 491 (2018).
25. Piepenburg, O., Williams, C.H., Stemple, D.L. & Armes, N.A. DNA detection using recombination proteins. *PLoS Biol* **4**, e204 (2006).
26. Lee, A.S. et al. Methicillin-resistant Staphylococcus aureus. *Nat Rev Dis Primers* **4**, 18033 (2018).
27. Falugi, F., Kim, H.K., Missiakas, D.M. & Schneewind, O. Role of protein A in the evasion of host adaptive immune responses by Staphylococcus aureus. *MBio* **4**, e00575-00513 (2013).
28. Westh, H., Hougaard, D.M., Vuust, J. & Rosdahl, V.T. Prevalence of erm gene classes in erythromycin-resistant Staphylococcus aureus strains isolated between 1959 and 1988. *Antimicrob Agents Chemother* **39**, 369-373 (1995).
29. Alieva, N.O. et al. Diversity and evolution of coral fluorescent proteins. *PLoS One* **3**, e2680 (2008).
30. Shaner, N.C. et al. Improved monomeric red, orange and yellow fluorescent proteins derived from Discosoma sp. red fluorescent protein. *Nat Biotechnol* **22**, 1567-1572 (2004).
31. Pedelacq, J.D., Cabantous, S., Tran, T., Terwilliger, T.C. & Waldo, G.S. Engineering and characterization of a superfolder green fluorescent protein. *Nat Biotechnol* **24**, 79-88 (2006).
32. Ju, J. et al. A multi-structural and multi-functional integrated fog collection system in cactus. *Nat Commun* **3**, 1247 (2012).
33. Wang, X., Ferro, E.G., Zhou, G., Hashimoto, D. & Bhatt, D.L. Association Between Universal Masking in a Health Care System and SARS-CoV-2 Positivity Among Health Care Workers. *JAMA* (2020).
34. Leung, N.H.L. et al. Respiratory virus shedding in exhaled breath and efficacy of face masks. *Nat Med* **26**, 676-680 (2020).
35. Tang, Y.W., Schmitz, J.E., Persing, D.H. & Stratton, C.W. Laboratory Diagnosis of COVID-19: Current Issues and Challenges. *J Clin Microbiol* **58** (2020).
36. Rong, X.M., Yang, L., Chu, H.D. & Fan, M. Effect of delay in diagnosis on transmission of COVID-19. *Math Biosci Eng* **17**, 2725-2740 (2020).
37. Kretzschmar, M.E. et al. Impact of delays on effectiveness of contact tracing strategies for COVID-19: a modelling study. *Lancet Public Health* **5**, e452-e459 (2020).
38. Mohammadi, A., Esmaeilzadeh, E., Li, Y., Bosch, R.J. & Li, J.Z. SARS-CoV-2 detection in different respiratory sites: A systematic review and meta-analysis. *EBioMedicine* **59**, 102903 (2020).
39. Gouma, P.I., Wang, L., Simon, S.R. & Stanacevic, M. Novel Isoprene Sensor for a Flu Virus Breath Monitor. *Sensors (Basel)* **17** (2017).
40. Maier, D. et al. Toward Continuous Monitoring of Breath Biochemistry: A Paper-Based Wearable Sensor for Real-Time Hydrogen Peroxide Measurement in Simulated Breath. *ACS Sens* **4**, 2945-2951 (2019).
41. Gould, O., Ratcliffe, N., Krol, E. & de Lacy Costello, B. Breath analysis for detection of viral infection, the current position of the field. *J Breath Res* **14**, 041001 (2020).
42. Ruszkiewicz, D.M. et al. Diagnosis of COVID-19 by analysis of breath with gas chromatography-ion mobility spectrometry - a feasibility study. *EClinicalMedicine* **29**, 100609 (2020).

43. Tromberg, B.J. et al. Rapid Scaling Up of Covid-19 Diagnostic Testing in the United States - The NIH RADx Initiative. *N Engl J Med* **383**, 1071-1077 (2020).
44. Liu, Y. et al. Aerodynamic analysis of SARS-CoV-2 in two Wuhan hospitals. *Nature* **582**, 557-560 (2020).
45. Fennelly, K.P. Particle sizes of infectious aerosols: implications for infection control. *Lancet Respir Med* (2020).
46. van Doremalen, N. et al. Aerosol and Surface Stability of SARS-CoV-2 as Compared with SARS-CoV-1. *N Engl J Med* **382**, 1564-1567 (2020).
47. Santarpia, J.L. et al. Aerosol and surface contamination of SARS-CoV-2 observed in quarantine and isolation care. *Sci Rep* **10**, 12732 (2020).
48. Liu, L., Li, Y., Nielsen, P.V., Wei, J. & Jensen, R.L. Short-range airborne transmission of expiratory droplets between two people. *Indoor Air* **27**, 452-462 (2017).
49. Ma, J. et al. Exhaled breath is a significant source of SARS-CoV-2 emission. *medRxiv*, 2020.2005.2031.20115154 (2020).
50. Baek, Y.H. et al. Development of a reverse transcription-loop-mediated isothermal amplification as a rapid early-detection method for novel SARS-CoV-2. *Emerg Microbes Infect* **9**, 998-1007 (2020).
51. Joung, J. et al. Point-of-care testing for COVID-19 using SHERLOCK diagnostics. *medRxiv* (2020).
52. Arizti-Sanz, J. et al. Integrated sample inactivation, amplification, and Cas13-based detection of SARS-CoV-2. *bioRxiv* (2020).
53. Yan, C. et al. Rapid and visual detection of 2019 novel coronavirus (SARS-CoV-2) by a reverse transcription loop-mediated isothermal amplification assay. *Clin Microbiol Infect* **26**, 773-779 (2020).
54. Broughton, J.P. et al. CRISPR-Cas12-based detection of SARS-CoV-2. *Nat Biotechnol* **38**, 870-874 (2020).
55. Lezin, G., Kosaka, Y., Yost, H.J., Kuehn, M.R. & Brunelli, L. A one-step miniprep for the isolation of plasmid DNA and lambda phage particles. *PLoS One* **6**, e23457 (2011).
56. Darnell, M.E., Subbarao, K., Feinstone, S.M. & Taylor, D.R. Inactivation of the coronavirus that induces severe acute respiratory syndrome, SARS-CoV. *J Virol Methods* **121**, 85-91 (2004).
57. Shen, S. et al. The severe acute respiratory syndrome coronavirus 3a is a novel structural protein. *Biochem Biophys Res Commun* **330**, 286-292 (2005).
58. Gui, M. et al. Electron microscopy studies of the coronavirus ribonucleoprotein complex. *Protein Cell* **8**, 219-224 (2017).
59. Vogels, C.B.F. et al. Analytical sensitivity and efficiency comparisons of SARS-COV-2 qRT-PCR primer-probe sets. *medRxiv* (2020).
60. Koyama, T., Weeraratne, D., Snowdon, J.L. & Parida, L. Emergence of Drift Variants That May Affect COVID-19 Vaccine Development and Antibody Treatment. *Pathogens* **9** (2020).
61. Wang, Z. et al. mRNA vaccine-elicited antibodies to SARS-CoV-2 and circulating variants. *bioRxiv* (2021).
62. Li, Q. et al. The Impact of Mutations in SARS-CoV-2 Spike on Viral Infectivity and Antigenicity. *Cell* **182**, 1284-1294 e1289 (2020).
63. Barfidokht, A. et al. Wearable electrochemical glove-based sensor for rapid and on-site detection of fentanyl. *Sens Actuators B Chem* **296** (2019).

64. Bruch, R., Urban, G.A. & Dincer, C. Unamplified gene sensing via Cas9 on graphene. *Nat Biomed Eng* **3**, 419-420 (2019).
65. Dincer, C. et al. Disposable Sensors in Diagnostics, Food, and Environmental Monitoring. *Adv Mater* **31**, e1806739 (2019).
66. Dai, Y. et al. Exploring the Trans-Cleavage Activity of CRISPR-Cas12a (cpf1) for the Development of a Universal Electrochemical Biosensor. *Angew Chem Int Ed Engl* **58**, 17399-17405 (2019).
67. Shepherd, T.R. et al. De novo design and synthesis of a 30-cistron translation-factor module. *Nucleic Acids Res* **45**, 10895-10905 (2017).

Figures and Figure Legends:

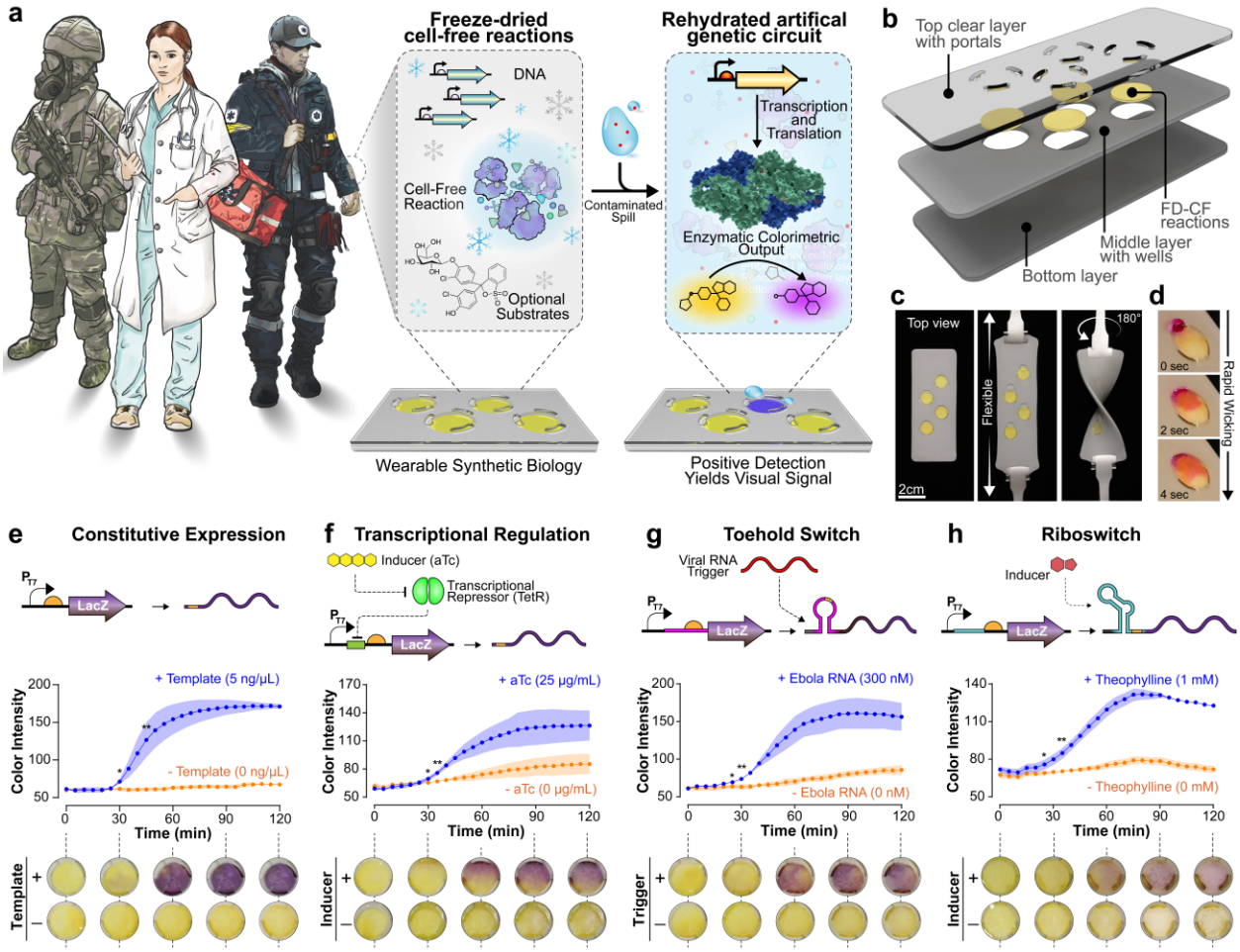

Fig. 1. Wearable cell-free synthetic biology. a, Freeze-dried cell-free reactions can be embedded in reaction sachets that are distributed throughout garments for use by warfighters, clinicians, and first responders. Upon exposure to an external splash, the reactions are rehydrated, activating dormant synthetic gene circuits that detect pathogens, metabolites, and toxins. **b**, Schematic of the layer-by-layer assembly of the wearable devices. Each layer is fabricated from skin-safe silicone elastomer. The FDCF reactions are embedded in a cellulose matrix placed within each chamber. **c**, An array of assembled reaction chambers showing the elasticity (center) and flexibility (right) of the devices. **d**, Portals cut into the outermost layer allow sample access, which is rapidly drawn into the reaction chambers through capillary action. The hydrophobic chamber walls prevent inhibitory dilution through lateral diffusion. **e**-**f**, Various types of synthetic biology circuits can be freeze-dried in these wearable devices, including constitutively expressed outputs (e), transcription factor-regulated circuits for small molecule detection (f), toehold switches for nucleic acid-sensing (g), and riboswitches to detect various small molecules (h). Each graph shows color deconvoluted values, n=3. Statistical significance is indicated for specific time points (*$P \leq 0.05$ and **$P \leq 0.01$). Bottom images are representative color images of the wearable device.

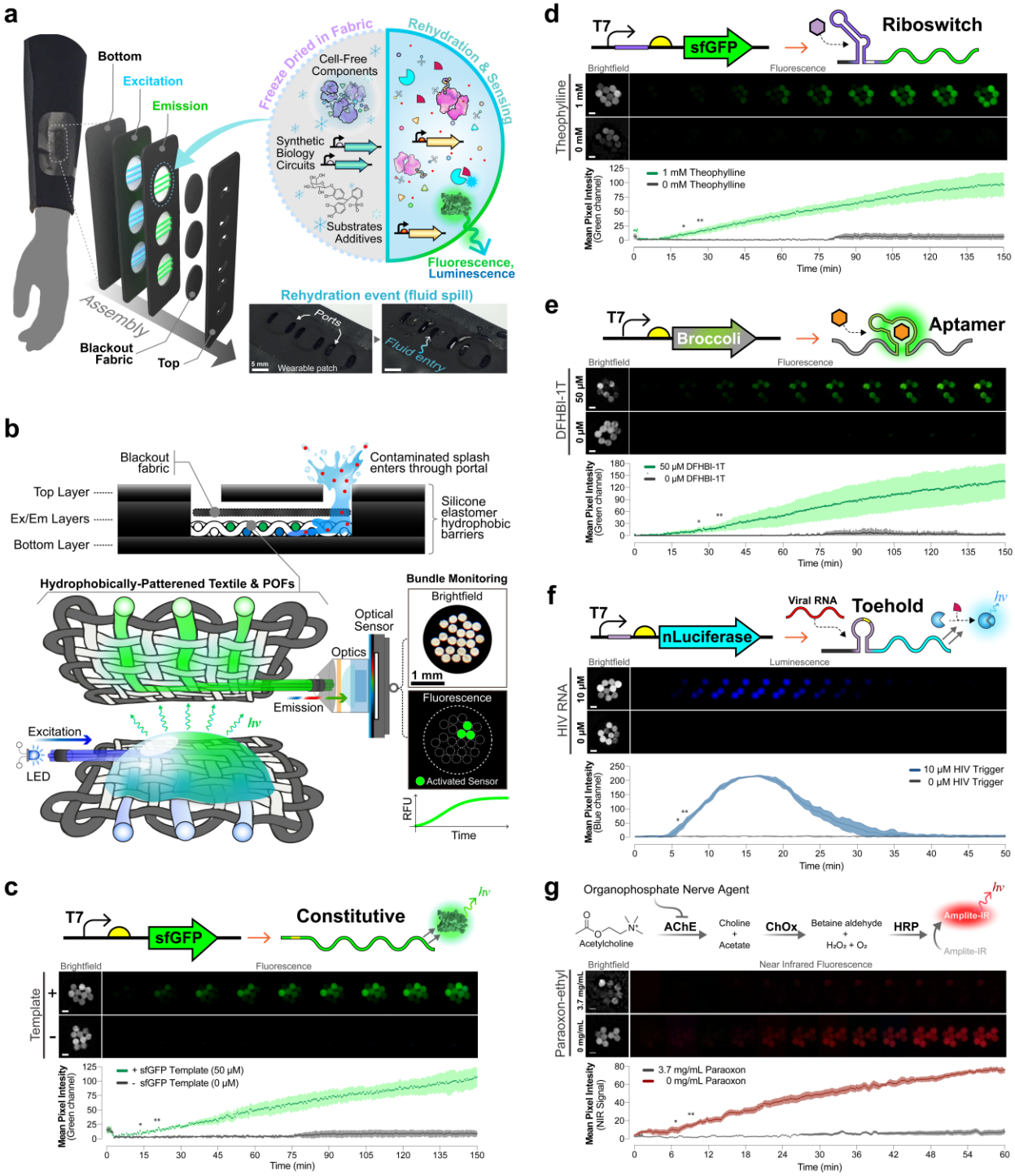

Fig. 2. Design and validation of fluorescent and luminescent freeze-dried cell-free synthetic biology wearables. a, Details of assembly and activation of fiber-optic based wFDCF module for fluorescence/luminescence output, with a schematic of module layers and components of embedded cell-free reactions. Fiber-optic embedded textiles allow excitation of the samples and detection by sensing emission light. A single layer of blackout cover made of polyester fabric is used to prevent the entry of environmental light into the reaction well. Bottom: An example rehydration event over the device shows the aqueous sample being wicked through the portals and blackout fabric and into internal reaction wells. **b**, Top: Diagram showing the layers of the assembled device. Contaminated splashes access the interior of the device through portals in the top layer. Bottom: A cross-sectional view of the interior of the device, where two layers of hydrophobically patterned fabric inter-woven with polymeric optic fibers are placed in a coplanar arrangement to allow for rehydration of freeze-dried cell-free reaction components as well as to provide light input/output for excitation and emission signals. Excitation POFs are illuminated with a 447-470 nm LED arrangement, and emission fibers are bundled and aligned with an optical sensor containing an amber filter (for fluorescence readings only) and a collimating lens

for magnification. The amber filter can be removed from the device in luminescence mode. **c**, Rapid fluorescent signal after rehydration of wFDCF constitutive sfGFP template as compared to control. Fluorescent signal in-device is statistically distinguishable from the control after 11 min (P<0.05). **d**, Activation of FDCF riboswitch with 1 mM theophylline in a wearable device as compared to 0 mM theophylline control. Fluorescent signal in-device is statistically distinguishable from the control after 19.5 min (P<0.05). **e**, Wearable demonstration of fluorescent aptamer being activated by the presence of 50 µM DFHBI-1T substrate as compared to 0 µM DFHBI-1T control. Fluorescent signal in-device is statistically distinguishable from the control after 24.5 min (P<0.05). **f**, Luminescence output detected from an HIV toehold sensor with nanoLuciferase operon. HIV RNA trigger was added at 10 µM and was statistically distinguishable from the control after 6 min (P<0.05) post-rehydration. **g**, Wearable detection of organophosphate nerve agents using a lyophilized HRP-coupled enzyme sensor rehydrated with 50 mM acetylcholine with and without 3.7 mg/mL paraoxon-ethyl (acetylcholinesterase inhibitor). When the acetylcholinesterase is active, the Amplite-IR substrate is oxidized to generate near-IR fluorescence emission. All images above graphs correspond to time sequences of the recorded POF images in each sensor demonstration with bundle pictures synchronized with reaction profiles. Each experiment is from three independent wells each having three fiber optic sensors, for a total of 9 fiber optic outputs. Any fibers that were 1 S.D. below the mean of all nine fiber outputs were excluded from analysis. Statistical significance is indicated for specific time points (*$P \leq 0.05$ and **$P \leq 0.01$). Scale bars in brightfield images are 250 µm. LED = light-emitting diode, POFs = Polymer Optic Fibers, sfGFP =S uperfolder Green Fluorescent Protein, DFHBI-1T = *difluoro-4-hydroxybenzylidene-1,2-dimethyl-1H-imidazol-5(4H)-one,* HIV = Human Immunodeficiency Virus, AChE = Acetylcholinesterase, ChOx = Choline oxidase, HRP = Horseradish peroxidase, NIR = Near Infrared.

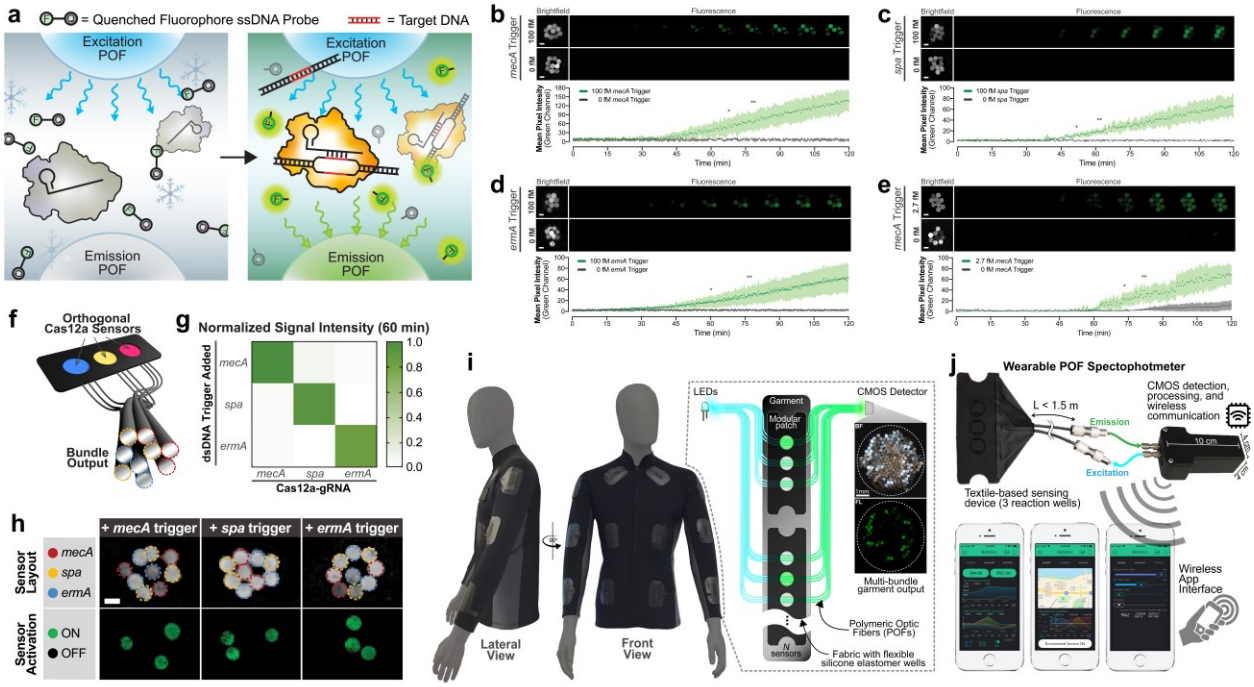

Fig. 3. Validation of CRISPR-based FDCF wearable sensors. a, The sensing mechanism of CRISPR-Cas12a system is based on catalytic trans-cleavage of fluorophore-quencher ssDNA probes after activation by an RPA-amplified dsDNA trigger. **b**, wFDCF mecA CRISPR-based sensor exposed to sample containing 100 fM mecA trigger. **c**, wFDCF spa CRISPR-based sensor exposed to 100 fM spa trigger. **d**, wFDCF ermA CRISPR-based sensor exposed to 100 fM ermA trigger. Statistically distinguishable signals ($P<0.05$) were observed after 72, 56 and 78 min for mecA, spa and ermA sensors respectively. **e**, Experimental detection of mecA CRISPR-based sensor at 2.7 fM trigger was statistically distinguishable after 75 min ($P<0.05$), corresponding to 10,000 dsDNA-copies per µL. Each experiment is from three independent wells, each having three fiber optic sensors, for a total of 9 fiber optic outputs. Any fibers that were 1 S.D. below the mean of all nine fiber outputs were excluded from analysis. Statistical significance is indicated for specific time points ($*P \leq 0.05$ and $**P \leq 0.01$). **f**, Orthogonality demonstration of mecA / spa / ermA CRISPR-based multi-sensor wearable. **g-h**, Rehydration only yielded activation of sensors when the Cas12a-gRNA sensor was in the presence of its programmed trigger dsDNA. Scale bars are 250 µm. **i**, Garment-level integration of fabric-based wearable synthetic biology sensors. Distributed continuous sensing of garment activity can be achieved through multi-bundle imaging. **j**, Connection of fabric-based module to wearable POF spectrometer with wireless connectivity capabilities. The spectrometer electronics consist of a Raspberry Pi Zero W with a camera module (Raspberry Pi Foundation, Cambridge, UK), as well as LED illumination, environmental sensing, and custom-fabricated shields for battery power. Smartphone application for visualization and alarm of wFDCF sensor activation was based on the blynk.io platform (Blynk Inc., New York, NY) which provides support for Raspberry Pi communication. This application allows for wireless recording of experiments, control of device parameters, as well as environmental and geolocation information.

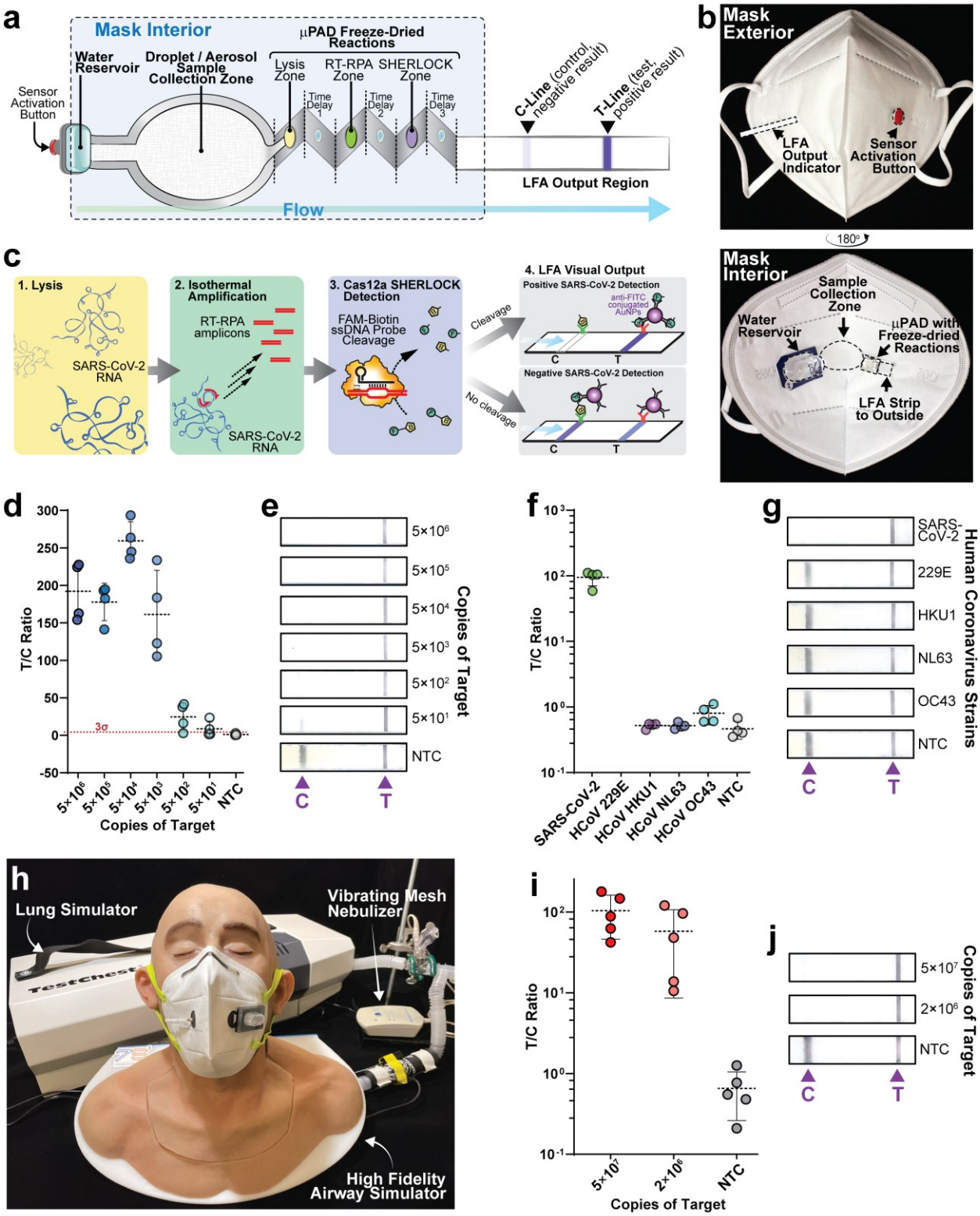

Fig. 4. A face mask-integrated SARS-CoV-2 wearable diagnostic. a, Schematic of the sensor components. Puncture of the water blister reservoir results in flow through wicking material, moving viral particles collected from the wearer's respiration from the sample collection zone to downstream freeze-dried reactions integrated into a μPAD device. The final output is visualized by an LFA strip that is passed externally through the mask. **b**, Photographs of the SARS-CoV-2 sensor integrated into a face mask. An A-version sensor is shown. **c**, Key steps of the freeze-dried reactions, each separated by a PVA time delay. Lysis first releases SARS-CoV-2 vRNA, RT-RPA next targets the S gene for signal

amplification at room temperature, and finally Cas12a detection of the RPA amplicons results in collateral cleavage of FAM-Biotin ssDNA probes. The reaction flows into the LFA where the visual band pattern formation is dependent upon probe cleavage. **d**, Sensitivity of the A-version face mask sensors at various inputs on the sensor zone of IVT-generated SARS-CoV-2 S-gene RNA. The limit of detection threshold, +3 S.D. of the no-template control (NTC), is shown as a red dotted line. **e**, Representative images of LFA outputs from the sensitivity measurements. **f**, Specificity demonstration of A-version face mask sensors show no cross-reactivity with IVT RNA from other commonly circulating human coronaviruses. SARS-CoV-2 RNA was added at 100,000 copies. All other HCoV RNAs were tested at 1,000,000 copies. **g**, Representative images of LFA outputs from the specificity measurements. **h**, Breath emission simulator setup consisting of a lung simulator for spontaneous breathing generation, a vibrating mesh nebulizer for aerosol generation, and a high-fidelity airway simulator for anatomically precise air flow to the face mask. A B-version face mask sensor is shown on the simulator. **i**, On-simulator testing of B-version face mask sensors under conditions simulating physiological respiratory emission of SARS-CoV-2 target and a face mask microclimate. **j**, Representative images of LFA outputs from the on-simulator measurements.

Acknowledgments: We thank Samsara S.R.L - Dreamlux, for aid in the custom fabrication of the wearable fabrics incorporating flexible fiber optics. Our gratitude to Greg Vis from SimVS for providing access and support for the TestChest Lung Simulator. In addition, we thank Troy E. Reihsen from 7-SIGMA, Simulation Systems (7S3) for providing the high-fidelity airway trainer. We are also indebted to Dr. Xiao Tan for consultations on clinical considerations for the SARS-CoV-2 face-mask design. We also acknowledge Thomas Ferrante, for support in the design and fabrication of the optical wearable acquisition device. We further thank Jonathan Gootenberg, Omar Abudayyeh and the Zhang Lab for providing us with Cas13a enzyme. The nanoluciferase plasmid was kindly donated by David Thompson from the Church Lab. The pET28c-F30-2xdBroccoli plasmid was a gift from Samie Jaffrey (Addgene plasmid # 66843). We also thank Jeong Wook Lee for aid in general toehold sensor design, as well as Aaron Dy and Melissa Takahashi for discussions and advice relating to the implementation of cell-free synthetic biology circuits.

Funding: This work was supported by the Defense Threat Reduction Agency grant HDTRA1-14-1-0006, the Paul G. Allen Frontiers Group, the Wyss Institute for Biologically Inspired Engineering, Harvard University (J.J.C, P.Q.N., L.R.S., N.A.M, H.P., N.M.D) and by Johnson & Johnson through the J&J Lab Coat of the Future QuickFire Challenge award 2018. L.R.S. was also supported by CONACyT grant 342369 / 408970, and N.A.M. was supported by an MIT-TATA Center fellowship 2748460.

Author contributions: P.Q.N. and L.R.S. designed and constructed devices, planned and performed experiments, analyzed the data, and wrote the manuscript. N.M.D, N.A.M. and H.P. designed and performed experiments and analyzed the data. A.H. and T.G. performed experiments and edited the manuscript. S.S., T.G., E.M.Z. assisted with aspects of design and construction of sensors or devices. R.L. optimized parts of the freeze-dried reactions. G.L., H.M.S., and J.B.N contributed to concept development of the face mask. J.J.C. directed overall research and edited the manuscript.

Competing interests: The authors have submitted provisional patent applications based on the technology described in this manuscript. J.J.C. is a co-founder and board member of Sherlock Biosciences.

Data and materials availability: All data needed to evaluate the conclusions in the paper can be found in the paper and the Supplementary Materials. Correspondence and requests for materials should be addressed to J.J.C.

Code availability: The custom code developed for this work is provided in the Supplementary Materials.

Additional information:

Supplementary information is available for this paper at: www.nature.com/###########

Supplementary Methods

Supplementary Text

Supplementary Figures S1-S23

Supplementary Tables S1-S4

Supplementary References

Supplementary Information

Wearable Biosensors Enabled by Cell-Free Synthetic Biology

Peter Q. Nguyen[1,2‡], Luis R. Soenksen[1,3,5‡], Nina M. Donghia[1], Nicolaas M. Angenent-Mari[1,4,5], Helena de Puig[1,5], Ally Huang[1,4,5], Rose Lee[1], Shimyn Slomovic[1], Tommaso Galbersanini[6], Geoffrey Lansberry[1], Hani M. Sallum[1], Evan M. Zhao[1], James B. Niemi[1], and James J. Collins[1,4,5,7,8,9*]

[‡] Co-first authors.
[1] Wyss Institute for Biologically Inspired Engineering, Harvard University, Boston, MA 02115.
[2] School of Engineering and Applied Sciences, Harvard University, Cambridge, MA 02138.
[3] Department of Mechanical Engineering, Massachusetts Institute of Technology (MIT), Cambridge, MA 02139.
[4] Department of Biological Engineering, MIT, Cambridge, MA 02139.
[5] Institute for Medical Engineering and Science, MIT, Cambridge, MA 02139.
[6] DREAMLUX, Samsara S.r.l, Milan, MI 20123, Italy.
[7] Synthetic Biology Center, MIT, Cambridge, MA 02139, USA.
[8] Harvard-MIT Program in Health Sciences and Technology, Cambridge, MA 02139, USA.
[9] Broad Institute of MIT and Harvard, Cambridge, MA 02142, USA.

*Corresponding author: James J. Collins
email: jimjc@mit.edu

This PDF file includes:

Materials and Methods
Tables S1 to S4
Figs. S1 to S23

Supplementary Materials and Methods

Fabrication of colorimetric synthetic biology wearable modules

Translucent (Fig.1b top) and opaque (Fig.1b middle/bottom) layers were made using skin-safe Ecoflex® silicone elastomer (Smooth-On, Inc, Macungie, PA), precast overnight and laser-cut on a 75W Epilog Legend 36EXT, according to the layouts shown in Fig. 1b, and Fig. S1a. After laser-cutting, the silicone pieces were placed in a warm wash (45ºC) with Tergazyme® detergent (Alconox, Inc., White Plains, NY) for one hour with agitation, followed by three washes in 18-Ω pure water and a final wash in 70% ethanol, before allowing them to air dry. Layers were aligned and bonded together by depositing freshly made, uncured liquid silicone elastomer and post-curing overnight at 65ºC in a well-ventilated oven to obtain the final assembled prototypes. The final assembled elastomer prototypes were thoroughly sprayed with RNase Away Decontaminant (Thermo Fisher Scientific, Waltham, MA) and washed with 70% ethanol twice before being stored in petri dishes.

For the support matrices housing the cell-free reactions, clean Whatman™ No. 4 filter-paper disks (GE Healthcare Lifesciences Inc., Chicago, IL) (Fig.1b middle) were punched to obtain cellulose discs with dimensions of 8 mm diameter and 0.5 mm thickness. These disks were incubated overnight in 0.01% DEPC, washed 3x with nuclease-free water, then incubated with 5% bovine serum albumin (BSA; MilliporeSigma, St. Louis, MO) in 50 mM Tris buffer, pH 7.5 for one hour with gentle agitation. The prepared BSA blocked discs were frozen at -80°C and subsequently freeze-dried. These lyophilized BSA-blocked discs were used as a scaffold for the deposition of colorimetric wearable synthetic biology reactions in freeze-dried, cell-free (wFDCF) sensors. The saturated reaction disks were finally snap-frozen in liquid nitrogen and freeze-dried for 8-12 hours. in an SP Scientific Freezemobile lyophilizer (SP Industries, Inc., Warminster, PA).

Freeze-dried reaction disks were then inserted through the wicking ports of the elastomer chambers for assembly. The silicone elastomer chambers in the colorimetric device exhibit three 3 x 5 mm curved wicking ports in each of the four wells, which allow routes for fluid entry while delaying evaporation of cell-free reaction (Fig. S1a). The device chamber walls were aligned and bonded using uncured elastomer, to prevent flow or lateral diffusion of the reaction after rehydration. The wicking of contaminated fluid through the entry ports is primarily mediated by capillary action. This event then leads to rehydration of the reaction disk containing the chosen FDCF system (Fig.1a), which marks t = 0 in the validation experiments (Fig.1h-1k). A magnified photograph of an activated reaction well containing an Ebola virus DNA toehold wFDCF sensor is shown in Fig. S1b, whereas the activation of a fabricated wearable bracelet using the same system is depicted in Fig. S1c. All of the colorimetric wFDCF sensors were tested at 30°C and ambient humidity to simulate surface body temperature.

Preparation of optimized colorimetric wearable synthetic biology reactions

Each colorimetric wFDCF reaction used for lyophilization, assuming a 50 μL rehydration volume, was a 75 μL cell-free NEB PURExpress® reaction (New England Biolabs, Inc., Ipswich, MA). Thus, each rehydrated reaction is a 1.5x-concentrated cell-free reaction based on the suggested reaction composition indicated by the manufacturer. Each reaction consisted of: 30

μL of PURExpress Component A, 22.5 μL of PURExpress Component B, 0.6 mg/mL of chlorophenol red-β-D-galactopyranoside (CPRG; MilliporeSigma, St. Louis, MO), 76 U of RNase Inhibitor (Roche GmbH, Mannheim, Germany), and a DNA template encoding the desired artificial genetic circuit at 5 ng/μL. For the TetR transcriptional regulation circuit, FPLC-purified recombinant TetR protein was supplemented in the reaction at a concentration of 120 μg/mL. During activation of the various wFDCF reactions by rehydration, pure nuclease-free H_2O was used for the constitutive LacZ circuit, 25 μg/mL of anhydrotetracycline (aTc) inducer was used for the TetR-regulated circuit, 300 nM of Ebola viral genome trigger was used for the toehold regulated circuit, and 1 mM of theophylline was used for the riboswitch-regulated circuit. The theophylline riboswitch reactions also included 2-phenylethyl β-D-thiogalactoside (MilliporeSigma, St. Louis, MO), a β-galactosidase inhibitor, at a final concentration of 250 μM to suppress the background due to leakiness in these genetic circuits. The Ebola RNA genome trigger was acquired by an *in vitro* transcription reaction utilizing the HiScribe™ T7 Quick High Yield RNA Synthesis Kit (New England Biolabs, Ipswich, MA), using a DNA template as indicated in Table S2. Each wFDCF reaction was applied to a BSA-blocked cellulose disc inserted into a 2 mL microcentrifuge tube. After the reaction was absorbed into the disc, the tubes were submerged in liquid nitrogen to snap-freeze the disc and allowed to lyophilize for 12 hours. All of the colorimetric wFDCF sensors were tested at 30°C and ambient humidity to simulate surface body temperature. The colorimetric wFDCF reactions presented in this work were from distinct sensors, in which each data point is the intensity value of a defined area of the green channel from the color-deconvolution function in ImageJ. The selected area size was kept constant for all sensors. Each data set plotted in Fig. 1e-h are the average of three independently measured wells. Statistical significance values for specific time points were calculated using unpaired parametric Student's t-test (one-sided). In all plots, $*P \leq 0.05$ and $**P \leq 0.01$.

Evaporation and dilution experiments in wearable synthetic biology devices

Evaporation tests were performed by cutting 10 x 10 cm Whatman™ No. 4 filter-paper squares and performing the cleaning and BSA blocking as described above for the discs. Each square was freeze-dried with 100 μL of a 1x PURExpress cell-free reaction with CPRG substrate and a constitutive LacZ plasmid. Various temperature (27-32ºC) and fluid exposure conditions were investigated in combination with different coverage ratios of the rehydrated test squares to assess evaporation reduction. Suitable activity of the rehydrated reactions was assessed by visual inspection of the conversion of the colorimetric substrate from yellow to purple. The port designs shown in Fig. S1a, Fig. S3b and Fig. S9g, were selected empirically due to suitable activation of synthetic biology reactions with reduced evaporation rates (<20% of initial fluid volume in 2 hours) at 30-40% relative humidity.

Kinetic enhancement by freeze-dried concentration of cell-free reaction components

Optimization testing of cell-free component concentrations on the kinetics of the reactions was performed by assembling PURExpress systems, according to the manufacturer's specifications, at various volumes ($V_{initial}$) and then lyophilizing the reactions in PCR tubes overnight (Fig. S2a). Next, the lyophilized pellets were rehydrated using the same sample volume (V_{final}), so that the tested fold-concentration was ($V_{initial}$ / V_{final}). PURExpress concentrations ranging from 1x to

2.5x were tested in replicate by incubation of 10 µL reactions at 30°C for up to 90 minutes, followed by photographic imaging of the colorimetric changes (Fig. S2b) and absorbance measurements at 570 nm (Fig. S2c). The time to half-maximal output signal for each base or concentrated reaction (Fig. S2d) was calculated by a least square fitting of the acquired data.

Screening of textiles for freeze-dried, cell-free synthetic biology reactions

General compatibility of different textiles to freeze-dried, cell-free synthetic biology reactions was tested in 103 different fabrics materials (e.g., silks, cotton, rayon, linen, hemp bamboo, wool, polyester, polyamide, nylon, and combination threads) under activation conditions (Fig. S4). A detailed list of the textiles used for this substrate screening can be found in Table S1. This compatibility of these textiles to FDCF synthetic biology reactions was compared to samples using Whatman™ No. 4 filter paper (GE Healthcare Lifesciences Inc., Chicago, IL) and samples in liquid form without any substrate as seen in Fig. S5. All tests used a T7RNAP-regulated LacZ circuit for constitutive expression. For this evaluation, fabric samples were identified and cut into 2 x 2 cm squares. Visible particles were removed from the fabrics using an adhesive roller. All fabric squares were cut into 1 x 2 cm pairs and washed thoroughly within 1.5 mL Eppendorf tubes with 1mL dd-H_2O for 30 minutes floating in a sonication bath at 80ºC. The washed samples were left to cool to room temperature and then washed with running dd-H_2O for 10 sec. One of each pair of fabric square types was placed in 1.25 mL of a 5% BSA solution for 12 hours. After BSA incubation, the treated fabrics were cleaned with running dd-H_2O for 10 seconds. BSA-blocked and unblocked samples were then placed into fresh Eppendorf tubes with holes in the caps to allow for overnight desiccation of the fabrics at 60ºC. Dried BSA blocked and unblocked fabrics were then cut in triplicate with clean 2 mm diameter disk biopsy punchers and placed in their respective slot in flat 384-well black polystyrene plates with a clear glass bottom (Corning Inc.; Kennebunk ME, Ref#. 3544) for testing. Cell-free PURExpress® *in vitro* protein synthesis solution (New England Biolabs, Inc., Ipswich, MA) was combined with a constitutive LacZ template containing 0.6 mg/mL CPRG and spotted (1.8 µL) on each of the fabric wells. Control wells containing 2 mm disks of Whatman No. 4 filter-paper were also filled with 1.8 µL constitutive LacZ test reactions, whereas 7 µL were spotted on empty wells as liquid controls. A transparent adhesive PCR cover compatible with freezing was then placed over the plate and pressed with a roller to seal chambers. A small opening was pierced in each well with a 25-gauge x 5/8 (0.5 mm x 16 mm) BD PrecisionGlide Needle (Becton, Dickinson and Company; Franklin Lakes, NJ, Ref#305122) to allow for sublimation during lyophilization. Prepared plates were wholly immersed into liquid nitrogen for 1 min. A chilled metallic plate (maintained at -80ºC with dry ice), was immediately put in contact with the bottom of the scored plates with the sealed frozen samples. A single 15 x 17" Kimwipe (Kimtech™, Kimberly-Clark Corp., Irving, TX) was placed on top of the plate humidity openings. Then the 384-well test plate with top Kimwipe and the bottom metallic chiller were wrapped with three layers of aluminum foil. The entire wrapped bundle was then placed inside a sealed glass lyophilization chamber and connected to the freeze-drying machine. Lyophilization was performed for two hours. Freeze-dried paper samples were rehydrated with dd-H_2O to the original reaction volume. The colorimetric change was measured after overnight incubation (12 hours) at 37ºC using a BioTek NEO HTS plate reader (BioTek Instruments, Inc., Winooski, VT) in kinetic absorbance readout mode Fig. S5. Best observed functionality, as measured by the aggregated score shown in Fig. S6, was achieved using a fabric with 85% polyester and 15% polyamide fibers. This substrate

was used for all further fluorescence and luminescence experiments, except for the case for a fluorescence Zika DNA Toehold sensing reaction (Fig. S7), which was also tested on a 100% mercerized cotton thread to validate the possibility of running FDCF reactions at the single-fiber level with this natural material commonly used in wound care.

Fabrication of fluorescence/luminescence synthetic biology wearable textile module

After screening of compatible textiles for freeze-dried, cell-free synthetic biology reactions, the best performing hydrophilic textile substrate (85% polyester / 15% polyamide) was used as weft for a textile inter-woven with a warp made of inert flexible polymeric optic fibers (POF) and polyester support threads. Such POFs were used for distributed optical interrogation of fluorescent or luminescent synthetic biology reactions within this fabric (three fibers per well). Polymeric optic fibers were weaved into this hydrophilic combination fabric using a standard industrial loom (DREAMLUX, Samsara Srl., Milan, IT), according to the design presented in Fig. S8. Once fabric samples were manufactured, three-strip arrangements of this hydrophilic POF fabric were cut to fit the device and laser-etched (5 mm) to disrupt the cladding in the POFs sections within the reaction zones (Fig. S9a-e). Black elastomer layers (top and bottom in Fig. S9b) were precast overnight and laser-cut according to the layout shown in Fig. S9b,e. The silicone elastomer chambers in this device exhibit two 3 x 5 mm curved wicking ports that allow for fluid entry while still delaying evaporation within reaction fabric. Uncured black silicone elastomer was stamp-patterned onto the precast layers as well as into the internal POF fabric strips to be aligned and assembled, preventing air bubble formation between device layers and elastomer wicking in reaction zones. Final assembly of the base three-well sensor "patch" can be seen in Fig. S9b,f,g. Devices were then placed under vacuum for 15 minutes to remove bubbles and were allowed to cure overnight at 65ºC. As with the colorimetric prototypes, the fluorescent POF prototypes were thoroughly sprayed with RNase Away Decontaminant (Thermo Fisher Scientific, Waltham, MA) and washed with 70% ethanol twice before being stored in petri dishes. Once the assembled device was fully cured, POF fibers were separated into excitation and emission bundles and then covered with blackout adhesive fabric as well as black heat shrink tubing (6 mm) to prevent environmental light leakage. Blackout fabric disks (10 mm) made of black polyester knit Item#: 322323 (MoodFabrics Inc. New York, NY) were soaked in RNase Away Decontaminant for 5 minutes, washed thoroughly with 70% ethanol followed by water. The washed blackout fabric was incubated in 0.1% Triton X-100 for 5 minutes (as a wetting agent to enhance the ability of the textile to absorb water) and then excess solution was removed and the fabric pieces allowed to air-dry. The final blackout fabric discs were placed inside the reaction chamber with tweezers to aid in environmental light-blocking over sensing fibers. Finally, quick-turn stainless steel coupling sockets #5194K42 (McMaster-Carr Co., Elmhurst, II) were added to the ends of the sensor device bundles for connection with the wearable spectrometer. The finalized wFDCF sensor device can be seen in Fig. S9f,g.

Hardware / software implementation of wearable POF spectrometer

A custom-made wearable spectrometer with internal processing and wireless connectivity modules was fabricated to provide unsupervised sensing of on-body synthetic biology reactions (Fig. S17). The device electronics were based on a Raspberry Pi Zero W Version 1.3 architecture (Raspberry Pi Foundation, Cambridge, UK) with connection to a custom shield for battery

power, an environmental sensing module, an LED illumination module, and a flexible camera for imaging (Fig. S17a). The Raspberry Pi Zero W was selected as the microprocessor for this application, due to its low cost (<$15.00), small profile/weight (65 x 30 x 5 mm / 12 g), high performance (1 GHz single-core ARM1176JZF-S CPU, 512 MB RAM, VideoCore IV GPU) and on-board wireless connectivity (802.11 b/g/n LAN, Bluetooth(R) 4.1, Bluetooth Low Energy - BLE). Regulated battery power was achieved using a PiZ-UpTime module, which is an uninterruptible power supply shield for Raspberry Pi Zero (Alchemy Power Inc., Santa Clara, CA), that uses rechargeable a Lithium-Ion 14500 battery (Battery & Power management in Fig. S17a), to reliably provide the charge capacity for 48 hrs of intermittent device operation continuously collecting data at a frequency of one measurement per minute. In-device sensing of temperature, humidity, atmospheric pressure, altitude, total Volatile Organic Compound (TVOC) and eCO2 was achieved using an I2C environmental CCS811/BME280 Qwiic-Breakout (SparkFun Electronics®, Niwot, CO). The POF illumination module was achieved using a Saber Z4 Luxeon Z 20 mm Square Quad Color Mixing Array LED Module with aluminum base (Quadica Developments Inc. - Luxeon, Alberta, Canada) connected to a 12-Channel 16-bit PWM TLC59711 LED driver with SPI Interface (Adafruit Industries®, New York, NY). Four Luxeon Star LEDs were installed in the device with wavelengths 447 nm, 470 nm, 505 nm and 6500 K white (LEDs & Driver in Fig. S17a) An 8.6 mm x 8.6 mm Zero Spy Camera with 2" cable (Raspberry Pi Foundation, Cambridge, UK) was connected to the Raspberry Pi Zero W using a flat serial interphase connector to provide POF imaging capabilities to the device. A single 5mm Infinite© aspherical plastic collimator part#: 191-66041G (Quarton Inc., New Taipei City, Taiwan) with numerical aperture (NA): 0.27 and effective focal length (EFL): 4.96 mm, was placed on top of the camera to allow for magnified POF imaging in proximity to the camera. The wearable spectrometer was covered by a two-part case fabricated using black photoreactive resin and a stereolithography 3D printing method using a Form 2 printer (Formlabs Inc., Summerville, MA) as seen in Fig. S17a. A view of the open device is shown in Fig. S17b, while a closed view is shown in Fig. S17c. This case included geometrical features to fit and align the camera/lens arrangement and the removable 3 mm diameter amber acrylic filter for fluorescence readings (slot arrangement in Fig. S17d). Also, the case features a slot for the 4-LED arrangement, a vent for the environmental sensors (Fig. S17d), as well as female Luer connection (Fig. S17a) to fit quick-turn stainless steel coupling sockets #5194K42 (McMaster-Carr Co., Elmhurst, II). A top view of the assembled wearable POF spectrometer is shown in Fig. S17e, while the integration of this device within a wearable garment with wFDCF sensors is shown in Fig. S17f. The final volume of our wearable spectrometer device was approximately 235 cm^3 with a total weight of around 173.8 grams (6.13 ounces), with a total cost of material and consumable supplies under $100 USD. Base data-collection software (test version) implemented in python for control of the Raspberry Pi Zero W within the wearable POF spectrometer is also provided as part of the supplementary information.

Preparation of optimized fluorescence wearable synthetic biology reactions

Constitutive sfGFP expression reactions for wFDCF testing (Fig. 2c) were prepared by combining 50 μL of 1x NEB cell-free PURExpress® in vitro protein synthesis solution with 0.5% Roche Protector RNase Inhibitor and 10 ng/μL constitutive P_{T7}-sfGFP plasmid (+) or without as controls (-). Prepared reactions were quickly deposited in-fabric to be snap-frozen and

then lyophilized for 4-8 hours within the device. Activation of sensors was achieved by rehydration with a fluid splash of dd-H_2O.

The theophylline riboswitch sensor reactions for wFDCF testing (Fig. 2d) were prepared using 1x NEB cell-free PURExpress® supplemented with 10 ng/μL of theophylline riboswitch sensor E mRNA in dd-H_2O. The prepared sensor reactions (50 μL per well) were quickly deposited in-fabric, snap-frozen in LN2, and then lyophilized for 4-8 hours within the device. Activation of sensors was achieved by rehydration with a fluid splash of dd-H_2O spiked with 1 mM theophylline for the positive samples, while 0 mM theophylline was used for controls.

Dimeric Broccoli fluorescent aptamer sensor reactions for wFDCF testing (Fig. 2e) were prepared using 1.5x NEB cell-free PURExpress® with 25 ng/μL of pJL1-F30-2xd-Broccoli aptamer DNA in dd-H_2O. Prepared sensor reactions (50 μL per well) were quickly deposited in-fabric to be snap-frozen and then lyophilized for 4-8 hours within the device. Activation of sensors was achieved by rehydration with a fluid splash of dd-H_2O spiked with 50 μM of the substrate (5Z)-5-((3,5-Difluoro-4-hydroxyphenyl)methylene)-3,5-dihydro-2-methyl-3-(2,2,2-trifluoroethyl)-4H-imidazol-4-one (DFHBI-1T; Tocris Bioscience, Minneapolis, MN) substrate for the positive samples, while 0 μM DFHBI-1T substrate was used for controls.

Zika RNA Toehold switch sensor reactions for wFDCF testing (Fig. S7) were prepared using 1x NEB cell-free PURExpress® with 33 nM Zika DNA toehold sensor 27B in dd-H_2O. Prepared sensor reactions were quickly deposited in a mercerized cotton thread or paper samples to be snap-frozen and then lyophilized for 4-8 hours within a 384-well plate. Activation of sensors was achieved by rehydration with dd-H_2O spiked with 2 μM of freshly made Zika trigger RNA for the positive samples, while 0 μM Zika trigger RNA was used for controls.

For the wearable nerve agent sensor experiments (Fig. 2g), 50 μL reactions consisting of 0.5 U/mL acetylcholinesterase (Type V-S from *E. electricus*, MilliporeSigma, St. Louis, MO), 0.1 U/mL of choline oxidase (recombinant *Arthrobacter sp*., MilliporeSigma, St. Louis, MO), 0.1 mg/mL of freshly prepared horseradish peroxidase (Type VI, MilliporeSigma, St. Louis, MO), and 125 μM of the fluorescent reporter substrate Amplite-IR™ (AAT Bioquest, Sunnyvale, CA) in a final buffer of 10 mM HEPES, pH 8.0 / 1 mg/mL BSA / 1% fish gelatin / 5% trehalose. The reactions were applied to two Whatman™ No. 4 filter-paper 0.8 cm discs, snap frozen in liquid nitrogen, and lyophilized for at least 12 hours. To test in the fluorescent wearable prototype, the paper discs containing the freeze-dried reactions were inserted into the wearable devices and rehydrated with 75 μL of 50 μM acetylcholine (MilliporeSigma, St. Louis, MO) with or without the nerve agent paraoxon-ethyl (MilliporeSigma, St. Louis, MO). The fluorescent wearable device for the nerve agent was altered for the detection of near-infrared fluorescence by replacing the optical components with excitation using a 627 nm red quad-LED array module (Quadica Developments Inc. - Luxeon, Alberta, Canada). Additionally, the emission camera was substituted with a NoIR Zero Spy Camera without infrared filter, on top of which we positioned three gel transmission filters No. 381, 382 and 383 (Rosco Laboratories Inc., Stamford, CT) to form a dedicated emission filtering stack with <1% cutoff at 660nm and peak transmittance at 740nm. All of the fluorescent wFDCF sensors were tested at 30°C and ambient humidity to simulate surface body temperature. All fluorescent wFDCF presented in this work were from distinct sensors, in which each data point is the integrated value of optical fiber signals from one sensor. Any fiber optic fibers that were 1 SD below the mean of all fibers combined were removed from analysis. All of the cell-free and enzymatic wFDCF sensor plots are the average of

three independent wells. Each well contained three separate fiber optic sensors, for a total of 9 fiber outputs presented per variable. Statistical significance values for specific time points were calculated using unpaired parametric Student's t-test (one-sided). In all plots, $*P \leq 0.05$ and $**P \leq 0.01$.

Preparation of optimized luminescence wearable synthetic biology reactions

HIV RNA toehold switch sensor reactions for luminescence wFDCF testing (Fig. 2f and Fig. S12b) were prepared in 50 μL batches using 20 μL of NEB cell-free PURExpress® Component A, 15 μL NEB Component B, 2.5 μL murine RNase inhibitor (New England Biolabs, Inc., Ipswich, MA), 6 ng/μL HIV toehold sensor template with a nano luciferase (nLuc) output, 0.5 μL luciferin substrate (Promega Corp., Madison, WI) in dd-H_2O. Prepared sensor reactions (50 μL per well) were quickly deposited in-fabric to be snap-frozen and then lyophilized for 4-8 hours within the device. Activation of sensors was achieved by rehydration with a fluid splash of dd-H_2O spiked with 10 μM HIV trigger RNA freshly made for the positive samples, while 0 μM HIV trigger RNA was used for controls. The constitutive nLuc control reaction shown as part of Fig. S10b was performed similarly but substituting the toehold switch with a plasmid with a nLuc operon regulated by a T7 promoter.

Borrelia burgdorferi RNA Lyme disease toehold switch sensor reactions for luminescence wFDCF testing (Fig. S10a) were prepared in 50 μL batches using 20 μL of NEB cell-free PURExpress® solution A, 15 μL solution B, 2.5 μL murine RNase inhibitor, 18 nM *B. burgdorferi* toehold DNA with luciferase operon, 2.75 μL luciferin substrate (Promega Corp., Madison, WI) in dd-H_2O. Prepared sensor reactions (50 μL per well) were quickly deposited in-fabric to be snap-frozen and then lyophilized for 4-8 hours within the device. Activation of sensors was achieved by rehydration with a fluid splash of dd-H_2O spiked with 3 μM *B. burgdorferi* trigger RNA freshly made for the positive samples, while 0 μM trigger RNA was used for controls. These wFDCF sensors were tested at 30°C and ambient humidity to simulate surface body temperature.

Preparation of optimized CRISPR Cas12a-based wearable synthetic biology reactions

CRISPR-based sensor reactions for wFDCF testing in Fig. 3b-e,h, Fig. S11, and Fig. S13 were prepared using 100 nM Cas12a (New England Biolabs, Ipswich, MA) and 100 nM gRNA, 1x NEB buffer 2.1, 0.45 mM dNTPs, 500 nM of each RPA primer, 1x RPA liquid basic mix (TwistDx Limited, UK), 14 mM $MgCl_2$, and 5 μM FAM-Iowa Black® FQ quenched ssDNA fluorescent reporter (Integrated DNA Technologies, Coralville, IA) in dd-H_2O. Prepared sensor reactions (50 μL per well) were quickly deposited in-fabric to be snap-frozen and then lyophilized for 4-8 hours within the device. Activation of sensors was achieved by rehydration with a fluid splash of dd-H_2O spiked with 2.7 fM or 100 fM of *mecA*, *spa* or *ermA* DNA trigger depending on the demonstration. In the sensing performed at 2.7 fM *mecA* trigger, the detection limit is 10,000 copies of DNA per μL. These wFDCF sensors were tested at 30°C and ambient humidity to simulate surface body temperature. All of the CRISPR-based wFDCF sensor plots are the average of three independent wells. Each well contained three separate fiber optic sensors, for a total of 9 fiber outputs presented per variable. Statistical significance values for

specific time points were calculated using unpaired parametric Student's t-test (one-sided). In all plots, $*P \leq 0.05$ and $**P \leq 0.01$.

Preparation of optimized CRISPR Cas13a-based wearable synthetic biology reactions

Cas13a CRISPR-based sensor reactions for wFDCF testing (Fig. S12) were prepared using 100 nM Cas13a and 100 nM gRNA, 1x NEB buffer 2.1, 0.45 mM dNTP, 14 mM $MgCl_2$, and 5 μM FAM-Iowa Black® FQ quenched RNA fluorescent reporter (Integrated DNA Technologies, Coralville, IA) in dd-H_2O. Prepared sensor reactions (50 μL per well) were quickly deposited in-fabric to be snap-frozen and then lyophilized for 4-8 hours within the device. Activation of sensors was achieved by rehydration with a fluid splash of dd-H_2O spiked with 20 nM of MRSA RNA trigger.

Preparation of sample lysis-integrated wearable synthetic biology reactions

For wFDCF with integrated lysis reactions, a RNase-free Whatman filter paper disc (8 mm) was filled with concentrated stock solutions that would yield, upon a 50 μL rehydration volume, 5 mM Tris-HCl (pH 7.5), 1% Triton X-100, 1% NP-40, 0.2% CHAPS, 100 μg/mL lysozyme, and 5% sucrose. This was freeze-dried for 4 hours and inserted into the POF wFDCF device below the blackout layer and above a PVA time delay barrier that was sealed around the edges with Ecoflex elastomer to enable an efficient lysis incubation time. All layers containing the lyophilized RPA-Cas12a synthetic biology sensors below the lysis – PVA delay layers were identical to that used in the *mecA* RPA-Cas12a devices shown in Figures 3b-e.

Garment-level integration of colorimetric synthetic biology sensors

After fabrication of colorimetric synthetic biology wearable module, a bracelet "garment" was achieved simply by gluing the module into an elastic band to be placed in the forearm of a mannequin (Fig. S3c).

Garment-level integration of fluorescence/luminescence synthetic biology sensors

After fabrication of at least 12 fluorescence/luminescence synthetic biology wearable modules, a commercially available long-sleeve neoprene wetsuit-type jacket (EYCE Dive & Sail) was modified to integrate an array of wFDCF sensors by sewing these modules in predefined high-splash frequency regions (Fig. 2a, 4a, S17f). Reaction modules were covered in the edges with a blackout fabric border with textile adhesive. POF bundles of these modules were sawn internally and directed to a single multi-bundle arrangement for interrogation via our portable spectrometer device (located in a back pocket within the jacket) as seen in Fig. S17f. Base neoprene fabric used for this jacket was of 3mm thickness and treated with a superhydrophobic coating to prevent fluid absorption in places other than the reaction zones. Fabricated wFDCF jacket prototype was specified to fit a medium-sized male torso 36"(chest) by 31"(waist). In-garment sensors were tested on a mannequin at room temperature.

Construction and preparation of SARS-CoV-2 A-version diagnostic face mask

The SARS-CoV-2 in-mask diagnostic consists of the sensor assembly containing the lyophilized reactions which was then inserted in an N95-equivalent face mask (see Fig. 4a and Supplementary Fig. 21 for fully assembled face masks and Fig. 4b for a schematic of the sensor). First, capillary wicking material (porous HRM (high release media) fiber media #36776, thickness = 0.5 mm, density = 0.07 g/cc, porosity = 92%) was laser-cut into a shape allowing for an elliptical region approximately 50 x 25 mm that serves as the sample collection area, accumulating viral particles from a patient's respiration, vocalization, and/or reflexive tussis. The laser-cut wicking material is then adhered to a white PET double-adhesive backing material (3M Microfluidic Diagnostic Tape, #9965). One end of the wicking material is adhered to a sterile sealed blister pack containing nuclease-free water. The μPAD device is created by wax printing hydrophobic patterns onto Whatman® Grade 1 chromatographic filter paper (Thermo Fisher Scientific, Waltham, MA) using a Xerox Phaser 8560 solid ink printer. The printed μPAD sheets were then wax reflowed by hot pressing for 15 sec at 125°C using a Cricut EasyPress™ (Cricut Inc., Fork, UT), and then left untouched to cool at room temperature. After wax reflow, the reaction zones have an aperture diameter of 5 mm, while the intervening PVA time delays have an aperture diameter of 3 mm. The PVA time delays were placed onto the time-delay zones first, by pipetting 4 μL of 10% ~67,000 MW PVA (Millipore-Sigma, St. Louis, MO) per each delay layer, and allowing it to dry at room temperature overnight. The lysis buffer, RT-RPA reaction, and the Cas12a SHERLOCK reactions as described below were then added to the respective lysis zones.

The lysis reaction added to each sensor lysis zone was 15 μL of 10 mM Tris-HCl (pH 7.5), 1% Triton X-100, 1% NP-40, 0.2% CHAPS, 100 μg/mL lysozyme, and 5% sucrose. The RT-RPA reaction added to the isothermal amplification zone was 15 μL of a single lyophilized TwistAmp® lyophilized RPA pellet (TwistDx Limited, UK) that was rehydrated to 50 μL using a rehydration reaction of 29.6 μL Twist Rehydration Buffer, 9.6 μL of a primer mix (see Table S2; RT-RPA-F4, RT-RPA-R4, RT-RPA-R3 primer in the mix are at a ratio of 10 μM : 10 μM : 20 μM). Roche Protector RNase Inhibitor, TAKARA PrimeScript Reverse Transcriptase, and Ambion RNase H were all added at 1 μL each. Nuclease free water was added at 4.4 μL. Immediately before pipetting onto the reaction zone, 2.5 μL of 280 mM MgOAc was added to the RT-RPA reaction and thoroughly mixed. For the Cas12a SHERLOCK reaction, 15 μL of the following reaction was pipetted onto the SHERLOCK reaction zone: 12.3 μL nuclease-free water, 1.5 μL of NEB Buffer 2.1, 0.3 μL 0.5 M DTT, 0.075 μL of 100 μM NEB EnGen® Lba Cas12a, 0.26 μL of 40 μM coronavirus S-gene gRNA. Immediately before pipetting onto the reaction zone, 1 pmol of the 6-FAM/TTATTATT/Biotin oligo (FB probe, from Integrated DNA Technologies, Inc., Coralville, Iowa) was added to the Cas12a reaction and thoroughly mixed. Sequences for all primers, RNA targets, and the gRNA are presented in Supplementary Table S2.

All reactions are pipetted onto the reaction zones and the wax-printed sheet is then dipped into liquid nitrogen to freeze all of the embedded reactions, and then immediately wrapped in foil and placed on a lyophilizer. After lyophilization for 4-24 hours, the wax arrays are removed from the lyophilizer. Cutting of the arrays into individual μPAD strips can be performed before or after the lyophilization process. Each strip is folded using sterilized tweezers into an overlapping accordion arrangement (see Figure 4b), overlapping the reaction zones and time delays to form a μPAD device. The output end of the laser-cut Porex sample collection section was carefully inserted on top of the lysis zone, while the input end of a Milenia HybriDetect-1 Universal

Lateral Flow Assay (TwistDx Limited, UK) was inserted on top of the last PVA time delay. The entire μPAD section was carefully sandwiched and taped together to compress all of the layers. The entire blister-pack water reservoir – Porex sample collection area – μPAD – LFA test strip is secured using the double-sided backing to the inside of an N95 equivalent mask, positioning the sample collection area in the region directly in front of the mouth and nose. The LFA test strip is routed to the outside of the mask through a small slit in the mask and the indicator has been oriented to hide the results from external viewing, to ensure patient confidentiality. To access the results, the test strip must be bent over to view the results (see Supplementary Fig. S21g). Lastly, a button is affixed to the outside of the mask directly over the water blister reservoir. The button contains a small spike embedded in a compressible foam double-sided adhesive material. When pressed down, the button pierces the foil on the blister, allowing the nuclease-free water to flow through the same collection zone, the μPAD reaction zones and time delays, and finally into the LFA indicator strip. The modular design of the sensor components allows elements such as the water reservoir, μPAD or LFA strip to be adjusted for different orientations or placement on the inside or outside of the mask. Only the sample collection pad module has strict orientation and positional requirements.

Benchtop testing of A-version SARS-CoV-2 diagnostic face-mask sensors

For Figures 4d,f, each data point consisted of a face-mask sensor in which a defined amount of synthetic SARS-CoV-2 RNA fragment containing the specific gRNA targeting region of the SARS-CoV-2 spike gene was generated by in vitro transcription using the HiScribe™ T7 Quick High Yield RNA Synthesis Kit (NEB, Ipswitch, MA) using synthetic DNA templates with a T7 promoter (Integrated DNA Technologies, Inc., Coralville, Iowa, and Twist Bioscience, San Francisco, CA). Corresponding homologous regions to the spike gene for the commonly circulating human coronavirus strains 229E, HKU1, NL63, and OC43, were determined by sequence homology alignment of the respective spike genes (see Fig. S21a) and the RNA targets were generated using the same method described above. All SARS-CoV-2 face-mask sensors were tested at room temperature at ambient humidity. After activation and LFA output formation (~20-30 min), the LFA strips were digitized using the scanner function on a Ricoh MP C3504 on default contrast settings. This ensured equal brightness and contrast across all strips in comparison to photography. Each “T” and “C” output line from each strip was quantified in ImageJ from the 32-bit converted raw scanned images without any adjustments to brightness or contrast.

Fabrication of B-version face-mask sensors

The following optimizations to the A-version sensors were implemented, resulting in the improved B-version. Wax-printed μPAD templates were prepared as described above for the A-version sensors. To prevent failure from flow leakage between different layers of the folded μPAD, unwaxed borders were rendered hydrophobic by drawing over the area with a Super PAP Pen (ThermoFisher, Inc., Waltham MA) and allowed to air dry for at least one hour. The sample collection pads for the B-version sensors were laser-cut from sheets of Porex high release media #36776 with the dominant fiber direction along the long axis of the pad to allow faster flow of the hydration front. The pad geometry was adjusted to enhance water flow by moving the reservoir puncture point to the distal end of the water blister, increasing the pad area in contact with the water reservoir, and reducing the sample collection region. Approximately 2 mm of the

outer border of the sample pad was rastered during laser-cutting to heat seal the Porex material to the PET backing material, preventing delamination. Before assembly, approximately 1 cm of the backing material was peeled away and cut off from the end of the sample pad region that is to be in contact with the reservoir.

Prior to the addition of the reagents to the μPAD, each reaction zone area was blocked with 5 mL of 1% BSA + 0.02% Triton X-100 and allowed to air dry for 12 hours to prevent nonspecific adsorption of the biochemical reaction components to the filter paper matrix. PVA at a concentration of 18% (w/v) at a volume of ~5 μL was applied to each time delay zone and allowed to air dry for 24 hours. The lysis buffer for the B-version sensors was reformulated to 10 mM Tris-HCl (pH 7.5), 5% Sucrose, 0.02% NP-40, and 2% CHAPS. The amount of non-ionic surfactants in the lysis buffer were reduced to prevent observed degradation of the wax barrier, an observation we had made during design and testing of the A-version μPADs. The CHAPS concentration was increased as it was not found to degrade the wax and this zwitterionic detergent has previously been shown to be effective in lysing coronavirus particles[1]. A volume of 10 μL of this lysis buffer was added to the μPAD lysis zone. The RT-RPA and Cas12a SHERLOCK reaction compositions, volumes, and lyophilization parameters were unchanged. During final assembly of the B-version sensor, both the sample pad::μPAD and the μPAD::LFA contact regions were fully sealed using precut sterile aluminum PCR foil seals (#60941-076, VWR Intl., Radnor, PA) to improve contact transfer and prevent any fluidic short-circuiting that may occur from undesired droplet contact to the folded μPAD edges. To facilitate unimpeded sample flow, venting holes were introduced into the water-containing blister mold to prevent vacuum buildup inside the blister during flow. Three venting holes were punched into the blister surface using an 18-gauge needle and then sealed with a 6-mm adhesive disc of a single-sided rayon breathable hydrophobic porous film (#60941-086 VWR Intl., PA). This allows venting of vacuum while preventing leakage and contamination of the nuclease-free water. For all B-version face-mask-integrated sensors, the water reservoir module was positioned on the exterior of the mask to minimize unwanted contact pressure on the blister pack during wearing of the mask. The sensor activation mechanism is the same as the A-version sensors. To integrate the sensors into the face masks, 1 cm slits were cut into KN-95 masks through which the sensor ends were threaded and subsequently sealed using adhesive.

Breathing simulator apparatus assembly

Our face-mask sensor testing platform consisted of four modules that performed the following functions: spontaneous breath generation, aerosol production, heating control, and physiologic airway and head simulation. For the breath generation, we employed the TestChest® lung simulator (Organis GmbH, Switzerland), a highly accurate artificial lung that uses an actuated dual bellows design to replicate lung mechanics such as lung vial capacity and tidal volume. The TestChest® was connected through ventilator tubing to all other downstream modules for simulated spontaneous breathing. Directly downstream of the TestChest®, we placed an in-line Aerogen® Solo nebulizer (Aerogen, Inc., Ireland). The Aerogen® Solo is a medical-grade vibrating-mesh nebulizer for the administration of lung inhalation therapeutics. Previous studies have demonstrated that the nebulizer generates aerosol droplets that are similar in diameter to those that occur naturally from human lung emissions[2]. Furthermore, previous work has used the Aerogen® system to deliver therapeutic RNA in an animal model[3], showing that it can be used to produce transmissible RNA-laden aerosols. The tubing is next wrapped in a temperature-regulated heat pad (Zoo Med Laboratories, Inc., San Luis Obispo, CA) that maintains the output

temperature at 35°C. The tubing is connected to a lung input tube in a high-fidelity airway manikin (7-SIGMA Simulation Systems, Minneapolis, MN) that faithfully replicates pulmonary and nasopharyngeal structures as well as head movement ranges. The other simulated lung and the simulated esophagus are clamped shut to direct breath output only through the oral cavity.

On-simulator testing of face-mask integrated B-version sensors

For all simulator-based testing, a SARS-CoV-2 B-version sensor-containing face mask was fitted onto the 7-SIGMA airway manikin and the TestChest® was set to the "Normal Stable" setting, which generates a spontaneous breathing rate of 12 breaths per minute. The entire breathing simulator assembly was then checked for leaks. Temperature regulation was set to maintain an outflow temperature of 35°C. A 5 mL solution of SARS-CoV-2 F5R11 vRNA IVT target was then pipetted into the Aerogen® Solo reservoir and the controller unit activated. The simulated breath was allowed to collect in the face mask and sensor for a period of 30 minutes, then the sensor was activated on the manikin for processing while maintaining the breathing and heating. The LFA outputs for all sensors were scanned using a Ricoh MP C3504 printer system using default settings.

The total amount of aerosolized vRNA collected after 30 minutes on each mask sensor for a given concentration of vRNA IVT target solution was estimated by RT-qPCR analysis of a 6 mm filter paper disc affixed to the sample pad area. After the 30 minutes of the breathing simulation, the disc was removed and frozen immediately in nuclease-free microcentrifuge tubes at -80°C for later analysis. Replicate disc collections were then repeated using the same procedure. For analysis, the discs were thawed and resuspended in 100 µL nuclease-free water supplemented with Protector RNase Inhibitor (Roche AG, Switzerland). RNA was extracted by repeated vortexing for 20 second burst intervals with resting on ice. This extracted sample was used as template in RT-qPCR reactions to obtain the total accumulated target RNA copy number on the 6 mm sampling disc. The mean collection values (in copies per mm^2) are then multiplied by the exposed surface area of the sample collection pad (2,513 mm^2) to estimate the total aerosolized vRNA target collected on the sensor. For a stock solution of 16.7 fM vRNA IVT target, the estimated total collected copies per sensor is $2.3x10^6$ copies. For a stock solution of 1.67 pM vRNA IVT target, the estimated total collected copies per sensor is $5x10^7$ copies. These values are reported in Figs. 4i,j. The scatter plots for each target concentration shows the T/C ratio from five independently measured sensors.

Sensor and reporter sequences

Tables S2 and S3 contain the DNA and RNA sequences of sensors and reporters used in this study. The plasmid construct used for the Zika 27B toehold sensor has been previously described elsewhere[4]. The Lyme disease and HIV toehold sensors with a nanoluciferase output were cloned into the pBW121 plasmid backbone (Addgene plasmid #68779). All other plasmid constructs utilized the pJL1 backbone that has been previously described[5, 6]. The F30 dimeric Broccoli fluorescent aptamer was subcloned into pJL1 from pET28c-F30-2xdBroccoli which was a gift from Samie Jaffrey (Addgene plasmid #66843; http://n2t.net/addgene:66843; RRID: Addgene_66843). The sequence for the pJL1-sfGFP plasmid can be found on Addgene (Plasmid #69496).

Table S1: List of tested fabrics for wFDCF synthetic biology reactions in this study

ID	Supplier	Supp. ID	Material	Type	Name	Manufacturer Description	Mode	Price Per Bolt ($/yd)
0	-	N/A	-	No substrate (control)	No substrate (control)	-	-	-
1	Whatman GE	1442-042	Cellulose Paper	42.5mm filter papers	42.5mm filter papers	Ashless filter papers with 0.2mm thickness and 42.5mm diameter.	100 Disk box	+$300/yd
2	Dharma Trading Co. (DTC)	SBC45	Silk	Spun Silk Broadcloth 45" wide	Spun Silk Broadcloth 45" wide	100% spun silk 23mm, mid-weight flat woven fabric with a crisp hand and slight sheen, drapes nicely.	-	$13.39/yd
3	DTC	SD	Silk	Silk Dupion 19mm 45" wide	Silk Dupion 19mm 45" wide	Picture shimmery silk with lots of texture - raised silk slubs - intermittent shiny threads - similar to Shantung. Makes outstanding jackets, suits, coats, etc.	50 yd bolts	$10.75/yd.
4	DTC	SG36	Silk	Silk Gauze 3mm	Silk Gauze 3mm 36" wide	Wide weave. Very light, very sheer, very beautiful.	50 yd bolts	$2.32/yd.
		SG45	Silk		Silk Gauze 3mm 45" wide	Wide weave. Very light, very sheer, very beautiful.		$2.72/yd.
		SG55	Silk		Silk Gauze 3mm 55" wide	Wide weave. Very light, very sheer, very beautiful.		$3.79/yd
5	DTC	SVEL45	Silk	Silk Velvet	Silk Velvet 45" wide	Standard silk, 82% rayon. Dyes and paints super. The ultimate! Use for the Devore technique.	30 yd bolts.	$11.09/yd.
		SVEL55	Silk		Silk Velvet 55" wide	Standard silk, 82% rayon. Dyes and paints super. The ultimate! Use for the Devore technique.	33 yd bolts	$13.69/yd.
6	DTC	STCH ARM	Silk / Spandex	Stretch Charmeuse 12mm 45" wide	Stretch Charmeuse 12mm 45" wide	All die softness and sheen of silk with the comfort of a Stretch fabric. 95% silk & 5% spandex. The low amount of spandex will not the dyeing process.	50 yd bolts	$13.15/yd.
7	DTC	ST	Silk	Silk Twill 12mm 45" wide	Silk Twill 12mm 45" wide	A very utilitarian durable silk. Great for shirts, handkerchiefs, pillow cases, lamp shades, screens, etc.	50 yd bolts	$8.48/yd.

8	DTC	SRS45	Silk	Smooth Raw Silk 31.5mm	Smooth Raw Silk 31.5mm	100% Silk 45" width	-	$6.59/yd.
9	DTC	SG4545	Silk	Silk Gauze 4.5MM 45" wide	Silk Gauze 4.5MM 45" wide	Some like it a bit heavier. Beautiful flowing fabric, great for sewing and gifts.	50 yd bolts	$4.09/yd.
10	DTC	SK45	Silk	Silk Knit 45" wide	Silk Knit 45" wide	100% Silk Jersey, 3oz/square yard approx. 100 g/m2, 22" wide tube (44" wide), soft hand with a nice drape, great for silk underwear garments and scarves.	-	$15.79/yd.
11	DTC	ORG45	Silk	Organza 5.5 mm	Organza 5.5 mm 45" wide	Very sheer, transparent, stiff, gauze-like fabric.	50 yd bolts	$4.59/yd.
		ORG55	Silk		Organza 5.5 mm 55" wide	Very sheer, transparent, stiff, gauze-like fabric.		$5.75/yd.
12	DTC	CBSS36	Silk	Crepe Back Silk Satin (Charmeuse)	Crepe Back Silk Satin (Charmeuse) 19.5mm 36" wide	It has a firm feel to the hand and a luxuriously heavy drape. Dyes and paints will show an intensity of color and richness on this fiber.	-	$10.29/yd
		CBSS45	Silk		Crepe Back Silk Satin (Charmeuse) 19.5mm 45" wide	It has a firm feel to the hand and a luxuriously heavy drape. Dyes and paints will show an intensity of color and richness on this fiber.		$10.65/yd.
		CBSS55	Silk		Crepe Back Silk Satin (Charmeuse) 19.5mm 55" wide	It has a firm feel to the hand and a luxuriously heavy drape. Dyes and paints will show an intensity of color and richness on this fiber.		$13.95/yd.
13	DTC	VRS	Rayon / Silk	Vicose Rayon / Silk Blend	Vicose Rayon / Silk Blend	75% Rayon / 25% Silk blend. Weight equivalent to 18mm. Although fabric is semi-sheer when white. when dyed it is mostly opaque. 58"wide	-	$6.59/yd.
14	DTC	TAF55	Silk	Silk Taffeta - 14.5mm	Silk Taffeta - 14.5mm	100% Silk 55" width	-	$20.37/yd.
15	DTC	SWSC	Silk	Sand Washed (Sueded) Charmeuse 19.5mm 15" w	Sand Washed (Sueded) Charmeuse 19.5mm 15" wide	Beautiful & desirable! people here are taking up sewing because of it.	11/50 yd bolts	$19.01/yd.

16	DTC	SWCDC	Silk	Stone wash Crepe de Chine	Stone wash Crepe de Chine	By stone (sand) washing this heavier weight of Crepe de Chine, one gets a matte silk with a soft, luxurious drape. This is a great weight for any almost article of clothing items like pillows, curtains and such.	-	$12.69/yd.
17	DTC	SWF	Silk / Wool	Silk / Wool blend 63% silk, 37% wool	Silk / Wool blend 63% silk, 37% wool	Slightly sheer with a diagonal weave almost like a chiffon but sturdier. We also have scarves made out of this fabric. It's softer than wool warmer than silk 12.5mm 55" wide.	-	$10.95/yd.
18	DTC	CHIF16	Silk	Silk Double Chiffon 16mm 45"	Silk Double Chiffon 16mm 45"	With a crepey texture and a low subtle sheen, this is a perfect weight and drape for blouses. dressy slacks, or skirts. Takes dye beautifully	-	$10.35/yd.
19	DTC	CHIF10	Silk	Silk Chiffon 10 mm, 54"	Silk Chiffon 10 mm, 54"	An elegant, sheer fiber with a soft beautiful drape and a crepe like texture. Heavier and wider than the 8mm.	-	$7.35/yd.
20	DTC	CHIF44	Silk	Silk Chiffon 8mm	Silk Chiffon 8mm 44"	An elegant. sheer fiber with a soft drape and a crepe like texture.	50 yd bolts	$5.05/yd.
		CHIF55	Silk		Silk Chiffon 8mm 55"	An elegant. sheer fiber with a soft drape and a crepe like texture.		$6.89/yd.
21	DTC	CDC1236	Silk	Crepe de Chine	Crepe de Chine 12mm 36" wide	Soft luxurious crepe texture with great draping quality. Comes in 36"/45"/55" Width	-	$7.29/yd.
		CDC1245	Silk		Crepe de Chine 12mm 45" wide	Soft luxurious crepe texture with great draping quality. Comes in 36"/45"/55" Width		$7.49/yd.
		CDC1255	Silk		Crepe de Chine 12mm 55" wide	Soft luxurious crepe texture with great draping quality. Comes in 36"/45"/55" Width		$9.55/yd.
22	DTC	CDC45	Silk	Crepe de Chine	Crepe de Chine 16mm 45"	Slightly crinkled texture with a gentle, graceful drape and very soft hand. Has a smooth surface that lends itself well to all types of painting styles. Ideal for all types of clothing and decorating.	50 yd bolts	$8.90/yd.
		CDC55	Silk		Crepe de Chine 16mm 55"	Slightly crinkled texture with a gentle, graceful drape and very soft hand. Has a smooth surface that lends itself well to all types of painting styles. Ideal for all types of clothing and decorating.		$11.69/yd.
23	DTC	CCDC45	Silk	Crepe de Chine	Crepe de Chine	100% Silk, Optically Whitened — 16mm, 45" width	-	$8.90/yd.
24	DTC	CBSSL36	Silk	Crepe Back Silk Satin '	Crepe Back Silk Satin 36"	100% Silk 12mm lightweight satin with a nice sheen on one side, matte texture on the other side, drapes nicely and feels fabulous.	-	$7.65/yd.

		CBSSL 45	Silk		Crepe Back Silk Satin 45"'	100% Silk 12mm lightweight satin with a nice sheen on one side, matte texture on the other side, drapes nicely and feels fabulous.		$7.99/yd.
		CBSSL 55	Silk		Crepe Back Silk Satin 55"	100% Silk 12mm lightweight satin with a nice sheen on one side, matte texture on the other side, drapes nicely and feels fabulous.		$10.29/yd.
25	DTC	HS16	Silk	Silk Habotai	Silk Habotai 16mm 45" wide	The basic "China Silk" but even heavier	-	$9.35/yd.
26	DTC	HCJ	Hemp / Cotton	Hemp/Cotton Jersey	Hemp/Cotton Jersey	55% Hemp, 45% Cotton — 50z, 61" width	-	$7.22/yd.
27	DTC	HS1036	Silk	Habotai Silk	Habotai Silk 36"-103"	Heavier weight. Great for pillows, jackets, banners.	50 yd bolts	$5.65/yd.
		HS1045	Silk		Habotai Silk 36"-103"	Heavier weight. Great for pillows, jackets, banners.		$7.09/yd.
		HS1055	Silk		Habotai Silk 36"-103"	Heavier weight. Great for pillows, jackets, banners.		$7.49/yd.
		HS1070	Silk		Habotai Silk 36"-103"	Heavier weight. Great for pillows, jackets, banners.		$13.15/yd.
28	DTC	HS12	Silk	Silk Habotai	Silk Habotai 45" wide	The basic China Silk, but heavier	-	$7.79/yd.
29	DTC	HS836	Silk	Habotai Silk	Habotai Silk 8mm 36" wide	When they say China Silk this is What they mean. Light Weight and sheer. The 8mm is the one most seen, and of which our Habotai scarves are made. Great for pillows, linings for jackets, etc.	50 yd bolts	$4.75/yd.
		HS845	Silk		Habotai Silk 8mm 45" wide	When they say China Silk this is What they mean. Light Weight and sheer. The 8mm is the one most seen, and of which our Habotai scarves are made. Great for pillows, linings for jackets, etc.		$5.05/yd.
		HS855	Silk		Habotai Silk 8mm 55" wide	When they say China Silk this is What they mean. Light Weight and sheer. The 8mm is the one most seen, and of which our Habotai scarves are made. Great for pillows, linings for jackets, etc.		$6.35/yd.
30	DTC	HS536	Silk	Habotai Silk	Habotai Silk 5mm 36" wide	When they say China Silk this is What they mean. Light Weight and sheer.	50 yd bolts	$2.77/yd.
		HS545	Silk		Habotai Silk 5mm 45" wide	When they say China Silk this is What they mean. Light Weight and sheer.		$3.56/yd.
		HS555	Silk		Habotai Silk 5mm 55" wide	When they say China Silk this is What they mean. Light Weight and sheer.		$3.65/yd.

31	DTC	FCR4S	Silk	Flat Crepe	Flat Crepe 8mm 45" Wide	A fibric that looks like a combination of the texture and drape of crepe and luster of habotai. It is easy to dye and paint and accepts readily all types of painting techniques.	50 yd bolts	$9.19/yd.
32	DTC	DSAT45	Rayon / Silk	Devore Satin (30% Silk / 70% Rayon)	Devore Satin (30% Silk / 70% Rayon)	19 mm 45" wide. Silky, shiny beautiful fabric for "burn-out" (apply "Fiber-Etch" to remove the Rayon threads in a design leaving a lace of silk).	-	$6.79/yd.
33	DTC	HCDC	Silk	Heavy Crepe de Chine	Heavy Crepe de Chine 30mm 45"	Like our 16mm crepe de chine, only heavy enough to take dye with great depth and intensity. With a dull sheen and a soft drape it is perfect for pants, jackets, etc.	-	$18.49/yd.
34	DTC	JAC9702	Silk	Inkjet Printable Silk fabric	Inkjet Printable Silk fabric	Inkjet silk fabric sheets 1.5"x11" comes with detachable paper support	-	$17.12/yd.
35	DTC	JAC9703	Silk	Semi-transparent Inkjet Printable Silk fabric	Semi-transparent Inkjet Printable Silk fabric	Thin and semi-transparent inkjet silk fabric sheets 1.5"x11" comes with detachable paper support	-	$13.95/yd.
36	DTC	PWFC	Wool	Pure Wool Gauze Twill Fabric	Pure Wool Gauze Twill Fabric 45"	100% wool, lightweight with a subtle twill weave, 45" wide, 3.2 oz / linear yard	-	$18.19/yd.
37	DTC	PWFA	Wool	Pure Wool Gauze Fabric	Pure Wool Gauze Fabric 45"	100% wool, lightweight and semi-sheer, 45" wide, 3.2 oz / linear yard	-	$14.32/yd.
38	DTC	PHC	Hemp	Hemp Canvas	Hemp Canvas	100% Hemp - 11 oz, 53" width, optically whitened	-	$14.17/yd.
39	DTC	HWM	Hemp	Hemp Woven Mid-weight	Hemp Woven Mid-weight	100% Hemp - 5.4 oz, 53" width, optically whitened	-	$8.99/yd.
40	DTC	HSCH	Hemp / Silk	Hemp Silk Charmeuse	Hemp Silk Charmeuse	60% hemp, 40% silk. Silk lends a beautiful shine to one side, while the hemp lends strength to the body. 57" wide	-	$22.38/yd.
41	DTC	HS	Hemp / Silk	60% Hemp / 40% Silk	60% Hemp / 40% Silk	Natural. 57" wide. A spectacular fabric. Beautiful, soft and interesting. If this fabric was human you would want to marry it. The elegance of silk and the strength of hemp. Vertical textured grain., 2.6 oz/yd	30 yd bolts	$18.49/yd.
42	DTC	HR	Hemp / Rayon	55% Hemp / 45% Rayon	55% Hemp / 45% Rayon	Natural, 59" wide. Soft and smooth, great for dresses and other clothing items. It washes well. 5.5 oz/yd	-	$14.9/yd.

43	DTC	HM	Hemp	Hemp Summer Cloth	Hemp Summer Cloth	100% Hemp - 70z, 53" width. Optically whitened	-	$8.98/yd.
44	DTC	HCM	Hemp / Cotton	Hemp Cotton Muslin	Hemp Cotton Muslin	55% Hemp, 45% Cotton - 4.15z. 53" width. Optically whitened	-	$5.51/yd.
45	DTC	PTC45/ 58	Cotton	Pimatex Cotton - PFD	Pimatex Cotton - PFD	High quality, great for sewing fine clothing. For that special occasion blouse, dress shirt or heirloom item. Dyes as well or better than mercerized cotton 133x72 thread count, 45" wide, 3.7 oz/yd.	30 yd bolts	$5.75/yd.
46	DTC	POP60	Cotton	Poplin	Poplin	100% Cotton tightly woven, medium weight fabric 6 oz pet yard Wide. Thread count is 108 threads per inch x 50 threads per inch.	-	$5.8/yd.
47	DTC	WJ242	Rayon	Rayon Satin, Heavyweig ht	Rayon Satin, Heavyweight 58"	Satin refers to a particular type of weave which results in a fabric with a very solid, tightly woven look. Optically whitened. 58" wide.	-	$9.65/yd.
48	DTC	VRL	Rayon	Vicose Rayon Light	Vicose Rayon Light	100% rayon, Optically whitened, 4 oz per sq yd, 45" wide threads per inch x 38 threads per inch.	-	$3.36/yd.
49	DTC	VCI	Rayon	Viscose (Rayon) Challis (Import)	Viscose (Rayon) Challis (Import)	Often seen in hawaiian shirts and ladies' wrap skirts. Because rayon is pure cellulose, it allows dyes to give very brilliant colors. 58" wide, 4 oz/yd, 90x60 threads.	30 yd bolts	$5.78/yd.
50	DTC	SCVO	Cotton	Silky Cotton Voile	Silky Cotton Voile	Similar to our Cotton Voile, but with a tighter weave and a nice sheen this fabric has a very smooth silky 1.9 oz/yd sq. 52" wide	-	$6.33/yd.
51	DTC	SCN	Cotton	Slubby Cotton Knit	Slubby Cotton Knit	100% cotton - 30z. 58"width	-	$3.24/yd.
52	DTC	BBF	Bamboo Rayon	Bamboo Rayon	Bamboo Rayon	100% bamboo rayon. It's beautiful, soft and luxurious. 3.2 oz /sq yd, 60" wide. Thread count is 76x76 threads per inch.	-	$7.15/yd.
53	DTC	BAMF	Bamboo Rayon	100% Bamboo Rayon Fleece	100% Bamboo Rayon Fleece	This fabric is really soft. One side is a smooth knit while the flip side is a soft fleece. 14oz per square yd, 60" wide.	-	$17.25/yd.
54	DTC	SOCJ	Soy Cotton	Soy Organic	Soy Organic Cotton Jersey	58% Soy, 37% Organic cotton, 5% Spandex. This is a lovely and extremely soft jersey with a wonderful drape. 6.3oz per square yd, 60"wide.	-	$12.99/yd.

				Cotton Jersey				
55	DTC	RSAT45	Rayon	Rayon Satin	Rayon Satin	Satin refers to a particular type of weave which results in a fabric with a very solid, tightly woven look. 45" wide. Optically Whitened.	-	$8.95/yd.
56	DTC	RV045	Rayon	Rayon Voile	Rayon Voile	Gorgeous sheen and a soft smooth hand. Weave is loose, somewhat sheer, and drapes well. 45" wide Optically Whitened.	-	$6.65/yd.
57	DTC	RT55	Rayon	Rayon Twill	Rayon Twill	Has perhaps the nicest drape of any of our fabrics, including silks. Strong twill weave that will last. 55" Wide. Optically Whitened.	-	$8.67/yd.
58	DTC	RL55	Rayon	Rayon Lawn	Rayon Lawn	100% rayon very smooth and has a fine weave. 2.5 oz per square yard, 54/55" wide. Thread count is 90 threads per inch x 88 threads per inch.	-	$4.47/yd.
59	DTC	RCK	Rayon	Rayon Crinkle	Rayon Crinkle	Beautiful, light crinkled rayon - great fabric for all kinds of clothing. 86 x 44, 4.5 oz. / sq. yd. approx.	30 yd bolts	$6.65/yd.
60	DTC	QCS	Cotton	Cotton Sateen	Cotton Sateen	Sateen has a smooth finish on one side, kind of a sheen. This softer, finely woven fabric is used for lots more than quilts.	20 yd bolts	$7.65/yd.
61	DTC	JER40	Cotton	Jersey Cotton	Jersey Cotton	100% Cotton slightly stretchy fabric with a smooth flat face. It's what basic t-shirts are made of. 6.50z per linear yd 58/60" wide.	-	$2.85/yd.
62	DTC	MUS5B	Cotton	Premier Muslin Bleached	Premier Muslin 60" Bleached	Bleached midweight muslin. 100% Cotton, 3.2 oz per square yard, 60" wide, Thread count is 68 threads per inch x 68 threads per inch	-	$3.75/yd.
63	DTC	NF	Nylon	Nylon	Nylon 58" wide	Untreated dye able nylon. Prepared for printing. Perfect tor banners or flags. Stronger outdoors than natural fibers.	-	$2.95/yd.
64	DTC	NET48	Cotton	Cotton Net Fabric	Cotton Net Fabric 48"	100% cotton, slight stiffness disappears when washed, 33yd bolt comes pre-folded in a bag, 48" wide.	-	$3.75/yd.
65	DTC	NPF	Nylon	Nylon 'Puppet Skin' Fleece	Nylon 'Puppet Skin' Fleece	100% Nylon - 120z, 54"/56" width.	-	$17.89/yd.
66	DTC	NVEL	Rayon / Nylon	Rayon/Nylon Velvet	Rayon/Nylon Velvet	80% Rayon, 20% Nylon - 4.20z, 45" width.	-	$8.55/yd.
67	DTC	OCDT	Cotton	Organic Cotton Denim Twill	Organic Cotton Denim Twill	This denim is strong and versatile. Anywhere you might use denim or twill. 70z per square yd, 56" wide.	-	$12.38/yd.

68	DTC	MJ60	Rayon	Modal Rayon Jersey	Modal Rayon Jersey	95% Rayon, Lycra. Rayon jersey is extremely popular in ready to wear at all the best retail stores. 100z / linear yard. 60" wide.	-	$6.49/yd.
69	DTC	MCCB 45	Cotton	Mercerized Combed Cotton Broadcloth	Mercerized Combed Cotton Broadcloth 45" wide	Very finely Woven, 133 x 72 threads per inch. Mercerized to take dyes and paints better. 60" Wide. For batik and fine painting. 3.5 oz/yd sq.	50 yd bolts	$4.85/yd.
		MCCB 60	Cotton		Mercerized Combed Cotton Broadcloth 60" wide	Very finely Woven, 133 x 72 threads per inch. Mercerized to take dyes and paints better. 60" Wide. For batik and fine painting. 3.5 oz/yd sq.		$6.35/yd.
70	DTC	LR	Linen / Rayon	55% Linen / 45% Rayon	55% Linen / 45% Rayon	Want the soft drape of rayon and cool comfort of linen? This is the one fabric for you. The linen look is heavy enough for pant, drapey enough for tops and dresses, 52" wide.	30 yd bolts	$4.49/yd.
71	DTC	LIN21	Linen	Linen-100% Bleached Linen	Linen-100% Bleached Linen	Beautiful soft bleached fabric. We sell in three different weights. This one is 3.8 oz per square yard with 52x53 Thread Count, 54" wide.	-	$6.59/yd.
72	DTC	LIN6	Linen	Linen	Linen	100% Linen, Optically Whitened — 6,80z, 54" width.	-	$7.42/yd.
73	DTC	LIN	Linen	Linen-100% Bleached Linen	Linen-100% Bleached Linen	Beautiful soft bleached fabric. We sell in three different weights. This one is 4.70z per square yard with 50x54 Thread Count, 54" wide.	-	$6.59/yd.
74	DTC	KC118	Cotton	Kona Premium Muslin	Kona Premium Muslin 118"	Midweight cotton sheeting. 100% cotton, 4.2 oz per square yard, 118" wide, Thread count is 130 threads per inch x 70 threads per inch.	-	$9.63/yd.
75	DTC	mac	Cotton	Kona Cotton - PFD	Kona Cotton - PFD 45" wide	A quilter's dream fabric. also good for soft children's clothing, comfy shirts and dresses. The 60x60 thread count gives this even weave fabric a soft luscious feel and great durability. 45" wide. 44 oz/yd.	30 yd bolts	$5.39/yd.
		KC60	Cotton		Kona Cotton - PFD 60" wide	A quilter's dream fabric. also good for soft children's clothing, comfy shirts and dresses. The 60x60 thread count gives this even weave fabric a soft luscious feel and great durability. 45" wide. 44 oz/yd.		$8.35/yd.
76	DTC	CVEL	Cotton	Cotton Velveteen - PFD	Cotton Velveteen - PFD	Our Velveteen is a woven ICO% cotton with a short close weft pile in imitation Of velvet. Stronger and denser than our rayon Silk velvet and the pile is shorter. 220g/sq meter, 44" wide.	-	$11.28/yd.

77	DTC	CVO55	Cotton	Cotton Voile	Cotton Voile	Soft, gauzy cotton with a silky wonderful feel. Glides over your fingers and floats on air. Fantastic For all your Arabian night fantasies. 55" wide 1.9 oz/yd. 80x72 thread count, 30yd bolts.	-	$5.82/yd.
78	DTC	CST57	Cotton	Cotton Sateen	Cotton Sateen 57"	100% Cotton, mercerized, very soft sheen, 144x66 thread count, 60yd bolts, 57" wide.	-	$5.99/yd.
79	DTC	CS	Cotton	Cotton Sheeting	Cotton Sheeting	Good quality fabric soft and nice mid-weight. Suitable for all clothing types. 4.20z/sq yd. 55"-58" wide. 60x60 Thread count.	-	$4.91/yd.
80	DTC	CPOP57	Cotton	Cotton Poplin	Cotton Poplin 57"	100% cotton, mercerized, crisp fabric with a tight weave, 144x68 thread count, 57" wide, bolts are 60 yards.	-	$5.37/yd.
81	DTC	CPC	Cotton	Cotton Print Cloth Mercerized	Cotton Print Cloth Mercerized	Our Best selling cotton fabric. For eyers, dyers, quilters and painters with great quality for finished items (80x80 thread count). Takes dyes and paints particularly well. 45" wide. 3.1 oz/yd	100 yd bolts	$3.85/yd.
82	DTC	CLF	Cotton	Cotton Lycra PFD	Cotton Lycra PFD	Cotton, Lycra. This is the fabric We use to make our cotton/lycra bike shorts and tights. It's PFD (prepared for dyeing) so it dyes up brilliantly. 60" before shrinkage, 6.3 oz/yd.	50 yd bolts	$5.76/yd.
83	DTC	CL55	Cotton	Cotton Lawn	Cotton Lawn	100% Cotton, Optically Whitened, 2.0 oz per Square yard. 56/57" wide, thread count 90 threads per inch x 88 threads per inch.	-	$4.36/yd.
84	DTC	MUS2B	Cotton	Cotton Muslin Bleached	Cotton Muslin 36" - Bleached	Bleached lightweight muslin, with tiny slubs throughout the weave. 100% cotton, oz per square yard, wide. Thread count 68"x68".	-	$1.98/yd.
85	DTC	7CDB60	Cotton	7 oz Duck, Bleached	7 oz Duck, Bleached 60"	Grade "A" Duck. 84 x 29 threads. A little lighter weight. Drapes better than the 10 oz. All dye well. but the natural dyes darker.	-	$4.98/yd.
		7CDN63	Cotton		7 oz'Duck,Natural 60"	Grade "A" Duck. 84 x 29 threads. A little lighter weight. Drapes better than the 10 oz. All dye well. but the natural dyes darker.		$4.72/yd.
86	DTC	BD-N	Cotton	Bull Denim Natural	Bull Denim Natural	Soft feel and tough as nails. Dyes great. Hats, pants, shorts, bags anywhere you use denim. 60" wide. 10 oz/yd. 50 yard bolts.	-	$4.39/yd.
		BD-B	Cotton		Bull Denim bleached	Soft feel and tough as nails. Dyes great. Hats, pants, shorts, bags anywhere you use denim. 60" wide. 10 oz/yd. 50 yard bolts.		$4.68/yd.
87	DTC	CCL	Cotton	Combed Cotton Lawn	Combed Cotton Lawn	This is a soft, high quality semi-sheer lawn suitable for blouses. christening gowns, lingerie, and all your fine sewing needs.	20 yd bolts	$6.95/yd.

88	DTC	CC110	Cotton	Combed Cotton	Combed Cotton 110"	100% Mercerized Soft Cotton, oz per square yard, 110-112" wide. Thread count is 92 threads per inch x 88 threads per inch.	-	$6.69/yd.
89	DTC	HCG	Cotton	Heavier Cotton Gauze	Heavier Cotton Gauze	Optically whitened, Soft lightly textured. A heavier weight than our cotton bubble gauze. 3.7 oz per square yd, 50" wide, 48 x48 Thread Count.	-	$5.26/yd.
90	DTC	FT60	Cotton	French Twill	French Twill 60"	Midweight cotton with a tight diagonal weave, 100% cotton, 4.5 oz per square yard. 60" wide, thread count is 132x61	-	$5.99/yd.
91	DTC	ESS	Cotton	Essex Linen-PFD	Essex Linen-PFD	Linen 145% Cotton Blend. Slightly textured with a linen look. Optically whitened. 5.5 oz per square yd, 52" wide. 51x49 Thread Count.	-	$4.75/yd.
92	DTC	CVS55	Cotton	Cotton Voile	Cotton Voile	100% Fully Combed Cotton, Optically whitened, 1.4oz per square yard, 57-58" wide, Thread count is 70 x 70 threads per inch.	-	$4.19/yd.
93	DTC	CJ60	Cotton	Cotton Jersey PFD	Cotton Jersey 60" PFD	100% cotton jersey. PFD ready to dye. 9.5 oz per linear yd. 6 oz./yd. That is a little heavier than the average T-shirt. We use it for skirts, dresses, tops and kids' clothing. 60" wide.	30 yd bolts	$3.55/yd.
94	DTC	CIL	Cotton	Cotton Interlock	Cotton Interlock	Very warm and soft a little stretchy. Perfect for baby wear. Double knit construction makes it thicker & heavier than single knit. 60z/sq. yd, 62" wide.	-	$5.19/yd.
95	DTC	CG	Cotton	Cotton Bubble Gauze	Cotton Bubble Gauze	Beautiful white all cotton fabric. like a crinkle gauze. Very neat for skirts, tops, anywhere you want it light and airy. We have a heavier gauze. 50" wide, 22oz/sq yd.	50yd bolts	$4.98/yd.
96	DTC	CF60	Cotton	Combed Cotton Fleece	Combed Cotton Fleece	100% Cotton - 8.70z, 60" width	-	$11.79/yd.
97	DTC	10CDB 60	Cotton	Cotton Duck, Bleached	Cotton Duck, Bleached. 10 oz. 45/60"	Grade "A" duck. 76 x 28 threads. Almost has the weight and texture of canvas but the flex and drape of a heavy jacket weight cotton. For strong use. It dyes well, but the natural dyes darker.	-	$5.69/yd.
		10CDB 63	Cotton		Cotton Duck, Natural. 10 oz. 63"	Grade "A" duck. 76 x 28 threads. Almost has the weight and texture of canvas but the flex and drape of a heavy jacket weight cotton. For strong use. It dyes well, but the natural dyes darker.	-	$5.55/yd.
98	Jacquard, Rupert, Gibbon & Spider	JAC97 01	Cotton	Jackard Inkjet Printable	Inkjet Printable Cotton fabric	Inkjet fabric sheets 1.5"x11" comes with detachable paper support	-	$100/yd

	Inc. (JRGSI)			Cotton fabric				
99	Silhouette of America Inc.	CTNFAB	Cotton	Silhouette Inkjet Printable Cotton fabric	Inkjet Printable Cotton fabric	Inkjet fabric sheets 1.5"x11" comes with detachable paper support	-	$150/yd
100	LumiGram SARL	LUMW01	Polyester	Lumigram optic fiber fabric (white)	Lumigram optic fiber fabric (white)	Lumigram optic fiber fabric (white). Optic fiber diameter is 0.25mm, with a spacing pitch of 1.2mm, horizontally oriented in a matrix of polyester based synthetic fabric (85% PL,15% PA6)	-	$35/yd
5101	Wilton Industries Inc.	5005230240	Sucralose/Dextrose	Inkjet Printable Sugar sheets	Inkjet Printable Sugar sheets	Dried inkjet sheets made of food starch-modified (corn), maltodextrin, glycerin, sugar, water, food starch-modified (potato), dextrose, cellulose gum, gum arabic, titanium dioxide (color), polysorbate 60, mono and diglycerides of fatty acids, sorbitan monostearate, potassium sorbate (preservative), artificial flavor, citric acid, sucralose.	-	+$300/yd
102	JRGSI	JAC9702	Silk	Dirty Inkjet Printable Silk fabric	Dirty Inkjet Printable Silk fabric	Inkjet silk fabric sheets 1.5"x11" comes with detachable paper support	-	+$300/yd
103	JRGSI	JAC9703	Silk	Dirty Semi-transparent Inkjet Printable Silk fabric	Dirty Semi-transparent Inkjet Printable Silk fabric	Thin and semi-transparent inkjet silk fabric sheets 1.5"x11" comes with detachable paper support	-	+$300/yd
104	JRGSI	JAC9701	Cotton	Dirty Inkjet Printable Cotton fabric	Dirty Inkjet Printable Cotton fabric	Inkjet fabric sheets 1.5"x11" comes with detachable paper support	-	+$300/yd
105	Silhouette of America Inc.	CTNFAB	Cotton	Dirty Inkjet Printable Cotton fabric	Dirty Inkjet Printable Cotton fabric	Inkjet fabric sheets 1.5"x11" comes with detachable paper support	-	+$300/yd

Table S2: DNA and RNA sensor sequences used in this study.

Name	Sequence (5' to 3')	Fig.	Notes
tetO	TCCCTATCAGTGATAGAGATTGACATCCCTATCAGTGATAGAG ATCTAGAAATAATTTTGTTTAACTTTAAGAAGGAGATATACAT	1	TetR operator region. sfGFP coding region immediately follows.
Zaire Ebola Virus Toehold Switch Sensor (ZD)[7]	AAGCTGTTGGATATTGTATCAGTCCTTGCTCTGCATGTTATAG TTATGAACAGAGGAGACATAACATGAACATGCAGAACCATGTT AACCTGGCGGCAGCGCAAAAG*ACCATGATTACGGATTCA…*	1, S3	Zaire Strain Ebola Toehold Sensor. DNA template is shown. The start of the LacZ coding sequence is shown in italics.
Zaire Ebola Virus RNA trigger (ZD)[7]	AUGCAGAGCAAGGACUGAUACAAUAUCCAACAGCUU	1, S3	RNA gene fragment trigger of the VP30 gene of Zaire ebolavirus
Theophylline Riboswitch Sensor E (Sensor E)[8]	GGTGATACCAGCATCGTCTTGATGCCCTTGGCAGCACCCTGCT AAGGAGGTAACAACAAGatgagcaaaggtgaagaa*ATGACCAT GATTACGGATTCA…*	1,2	Theophylline riboswitch E sequence. DNA template is shown. Coding sequence begins with a 6-aa sfGFP fragment. The start of the LacZ coding sequence is shown in italics.
F30-2xdBroccoli Aptamer[9]	TTGCCATGTGTATGTGGGAGACGGTCGGGTCCATCTGAGACGG TCGGGTCCAGATATTCGTATCTGTCGAGTAGAGTGTGGGCTCA GATGTCGAGTAGAGTGTGGGCTCCCACATACTCTGATGATCCA GACGGTCGGGTCCATCTGAGACGGTCGGGTCCAGATATTCGTA TCTGTCGAGTAGAGTGTGGGCTCAGATGTCGAGTAGAGTGTGG GCTGGATCATTCATGGCAAG	2, S14	F30-dimeric RNA broccoli aptamer sequence. DNA template is shown. Subcloned from Addgene plasmid #66843 (pET28c-F30-2xdBroccoli).
HIV RNA Toehold switch Sensor (#8)	CCCUUUUCUUUUAAAAUUGUGAAUGAAUACUGCCAUGGACUUU AGAACAGAGGAGAUAAAGAUGAUGGCAGUAUUAAACCUUGCGG CAGCGCAAAAG	2, S10	RNA HIV Toehold Sensor
HIV Virus RNA trigger	AUGGCAGUAUUCAUUCACAAUUUUAAAAGAAAAGGG	2, S10	RNA gene fragment trigger of the HIV retrovirus
Lyme Disease RNA Toehold switch Sensor	GUUGCAGAUGUAUUCCCAUCUUUCCCUGAAUUAUUACGGACUU UAGAACAGAGGAGAUAAAGAUGGUAAUAAUUCAGAACCUGGCG GCAGCGCAAAAG	S10	RNA Lyme Toehold Sensor
Lyme Disease (*B. burgdorferi*) *ospC* RNA trigger	GGCAAUAUUAAUGACUUUAUUUUUAUUUAUAUCUUGUAAUAAU UCAGGGAAAGAUGGGAAUACAUCUGCAAAUUCUGCUGAUGAGU CUGUUAAAGGGCCUAAUCUUACAGAAAUAAGUAAAAAAAUUAC GGAUUCUAA	S10	RNA gene fragment trigger from *B. burgdorferi* bacterium (Lyme's Disease)
CRISPR-Cas12a *mecA* gRNA	GGGUAAUUUCUACUAAGUGUAGAUUUAAAGAAGAUGGUAUGUG G	3, S11, S13	Cas12a guide RNA targeting single *mecA* gene fragment, was synthesized by in vitro T7 transcription.
CRISPR-Cas12a *mecA* dsDNA trigger	TTTAATTTTGTTAAAGAAGATGGTATGTGGAAGTTAGATT	3, S11, S13	Double stranded trigger sequence for Cas12a using *mecA* gRNA.
mecA RPA primer1 (F)	CATTGATCGCAACGTTCAATTTAATTTTGTTAAAG	3, S11, S13	Forward primer for RPA reaction for Cas12a *mecA* experiments
mecA RPA primer2 (R)	TACGATCAATATGTATGCTTTGGTCTTTCTGCATTCCTG	3, S11, S13	Reverse primer for RPA reaction for Cas12a *mecA* experiments
CRISPR-Cas12a *ermA* gRNA	GGGUAAUUUCUACUAAGUGUAGAUCUAUUAAUGGUGGAGAUGG A	3, S13	Cas12a guide RNA targeting single *ermA* gene fragment, was synthesized by in vitro T7 transcription.
CRISPR-Cas12a *ermA*-dsDNA trigger	GCTTTGGGTTTACTATTAATGGTGGAGATGGATATAAAAA	3, S13	Double stranded trigger sequence for Cas12a using *ermA* gRNA.
ermA RPA primer1 (F)	TCGTTGAGAAGGGATTTGCGAAAAGATTGC	3, S13	Forward primer for RPA reaction for Cas12a *ermA experiments*
ermA RPA primer2 (R)	GGATGAAAATATAGTGGTGGTACTTTTTTGAGC	3, S13	Reverse primer for RPA reaction for Cas12a *ermA experiments*
CRISPR-Cas12a *spa* gRNA	GGGUAAUUUCUACUAAGUGUAGAUUGGUAAUGCUUGAGCUUUG U	3, S13	Cas12a guide RNA targeting single *spa* gene fragment, was synthesized by in vitro T7 transcription.
CRISPR-Cas12a *spa* dsDNA trigger	TTCACCAGTTTCTGGTAATGCTTGAGCTTTGTTAGCATCT	3, S13	Double stranded trigger sequence for Cas12a using *spa* gRNA.
spa RPA primer1 *(F)*	AAGAAGCAACCAGCAAACCATGCAGATGC	3, S13	Forward primer for RPA reaction for Cas12a *spa* experiments
spa RPA primer2 *(R)*	ACCTAACGCTAATGATAATCCACCAAATAC	3, S13	Reverse primer for RPA reaction for Cas12a *spa* experiments
CRISPR-Cas13a MRSA crRNA	GAUUUAGACUACCCCAAAAACGAAGGGGACUAAAACACTCATG CCATACATAAATGGATAGACG	S12	Cas13a guide RNA (crRNA) targeting single MRSA gene

			fragment, was synthesized by in vitro T7 transcription.
CRISPR-Cas13a MRSA Trigger	CGUCUAUCCAUUUAUGUAUGGCAUGAGU	S12	Single stranded RNA trigger sequence for Cas13a using MRSA crRNA.
Fluorophore-quencher (FQ) reporter	5'-6FAM/TTATT/IowaBlackFQ	3, 4, S11, S13, S16	Substrate for Cas12a CRISPR-based sensors. When trans-cleaved by cis-activated Cas12a it generates a fluorescent signal.
Zika Toehold switch 27B sensor[4]	TTTCGCTCTATTCTCATCAGTTTCATGTCCTGTGTCGGACTTTAGAACAGAGGAGATAAAGATGGACACAGGACACAACCTGGCGGCAGCGCAAAAGCTGCGTAAACT*Gagc…*	S7	RNA Zika Toehold Sensor. The start of the sfGFP coding sequence is shown in italics.
Zika Virus RNA trigger[4]	GGGCCAGCACAGUGGGAUGAUCGUUAAUGACACAGGACAUGAAACUGAUGAGAAUAGAGCGAAAGUUGAGAUAACGCCCAAUUCACCAAGAGCCGAAGCCACCCUGGGGGGGUUUGGAAGCCUAGGACUUGAUUGUGAACCGAGGACAGG	S7	RNA gene fragment trigger of the Zika single-stranded RNA flavivirus
SARS-CoV-2 S-gene Cas12a gRNA Sensor	GGGUAAUUUCUACUAAGUGUAGAUCAGGCUGCGUUAUAGCUUGGAAUU	4	gRNA targeting region in SARS-CoV-2 Spike gene
RT-RPA-F4	gcaaactggaaagattgctgattataattataaattacc	4	Primer for SARS-CoV-2 RT-RPA
RT-RPA-R4	cctgatagatttcagttgaaatatctc	4	Primer for SARS-CoV-2 RT-RPA
RT-RPA-R3	ccttcaacaccattacaaggtgtgctacc	4	Primer for SARS-CoV-2 RT-RPA
SARS-Cov-2 IVT RNA Target	GGUGAUGAAGUCAGACAAAUCGCUCCAGGGCAAACUGGAAAGAUUGCUGAUUAUAAUUAUAAAUUACCAGAUGAUUUUACAGGCUGCGUUAUAGCUUGGAAUUCUAACAAUCUUGAUUCUAAGGUUGGUGGUAAUUAUAAUUACCUGUAUAGAUUGUUUAGGAAGUCUAAUCUCAAACCUUUUGAGAGAGAUAUUUCAACUGAAAUCUAUCAGGCCGGUAGCACACCUUGUAAUGGUGUUGAAGGUUUUAAUUGUUACUUUCCUUUACAAUCAUAUGGUUUCCAACCCACUAAUGGUGUUGGUUACCAACCA	4	S gene RNA fragment trigger for SARS-CoV-2 generated by in vitro transcription from a DNA template
HCoV-229E IVT RNA Target	GGGGUUAAUGUGUCACAAACCUCUAUUGCUAAUAUAAUUUAUUGCAACUCUGUUAUUAACAGACUGAGAUGUGACCAGUUGUCCUUUGAUGUACCAGAUGGUUUUUAUUCUACAAGCCCUAUUCAAUCCGUUGAGCUACCUGUGUCUAUUGUGUCGCUACCUGUUUAUCAUAAACAUACGUUUAUUGUGUUGUACGUUGACUUCAAACCUCAGAGUGGCGGUGGCAAGUGCUUUAACUGUUAUCCUGCUGGUGUUAAUAUUACACUGGCCAAUUUUAAUGAAACUAAAGGGCCUUUGUGUGUUGACACAUCACACUUCACUACCAAAUACGUUGCUGUUUAUGCCAAUGUUGGUAGGUGGAGUGCUAGUAUUAACACGGGAAAUUGCCCUUUUUCUUUUGGCAAAGUUAAUAACUUUGUUAAAUUUGGCAGUGUAUGUUUUUCGCUAAAGGAUAUACCCGGUGGUUGCGCAAUGCCUAUAGUGGCUAAUUGGGCUUAUAGUAAGUACUAUACUAUAGGCUCAUUGUAUGUUUCUUGGAGUGAUGGUGAUGGAAUUACUGGCGUCCCACAA	4	Homologous S gene RNA fragment trigger from human coronavirus strain 229E, generated by in vitro transcription from a DNA template
HCoV-HKU1 IVT RNA Target	GGGGUUACUAUUAAUAAUUAUAAUCCUUCUUCUUGGAAUAGAAGGUAUGGUUUUAAUAAUUUUAAUUUGAGCUCUCAUAGUGUUGUUUACUCACGUUAUUGUUUUUCUGUUAAUAAUACUUUUUGUCCUUGUGCUAAACCUUCUUUUGCUUCAAGUUGCAAGAGUCAUAAACCACCUUCUGCUUCCUGUCCUAUUGGUACUAAUUAUCGUUCUUGUGAGAGUACUACUGUACUCGACCACACUGACUGGUGUAGGUGUUCUUGUUUACCUGAUCCUAUAACUGCUUAUGACCCUAGGUCUUGUUCUCAAAAAAAGUCUCUGGUUGGUGUUGGUGAACAUUGUGCAGGGUUCGGUGUUGAUGAAGAAAAGUGUGGUGUAUUGGAUGGAUCAUAUAAUGUUUCUUGUCUUUGUAGUACUGAUGCCUUUCUAGGUUGGUCUUAUGACACUUGCGUCAGUAACAACCGUUGUAAUAUUUUUUCUAAUUUUAUUUUAAAUGGUAUCAAUAGUGGUACCACUUGUUCUAAUGAUUUAUUGCAGCCUAAUACUGAAGUUUUUACUGAUGUUUGUGUUGAUUACG	4	Homologous S gene RNA fragment trigger from human coronavirus strain HKU1, generated by in vitro transcription from a DNA template

HCoV-NL63 IVT RNA Target	GGGGUUAAUGUUAGUGCAACUAACAUUCAAAACUUACUUUAUU GCGAUUCUCCAUUUGAAAAGUUGCAGUGUGAGCACUUGCAGUU UGGAUUGCAGGAUGGUUUUUAUUCUGCAAAUUUUCUUGAUGAU AAUGUUUUGCCUGAGACUUAUGUUGCACUCCCCAUUUAUUAUC AACACACGGACAUAAAUUUUACUGCAACUGCAUCUUUUGGUGG UUCUUGUUAUGUUUGUAAACCACACCAGGUUAAUAUAUCUCUU AAUGGUAACACUUCAGUGUGUGUUAGAACAUCUCAUUUUUCAA UUAGGUAUAUUUAUAACCGCGUUAAGAGUGGUUCACCAGGUGA CUCUUCAUGGCACAUUUAUUUAAAGAGUGGCACUUGUCCAUUU UCUUUUUCUAAGUUAAAUAAUUUUCAAAAGUUCAAGACUAUUU GUUUCUCAACCGUCGAAGUGCCUGGUAGUUGUAAUUUUCCGCU UGAAGCCACCUGGCAUUACACUUCUUAUACUAUUGUUGGUGCU UUGUAUGUUACUUGGUCUGAAGGUAAUUCUAUUACUGGUGUAC CUUA	4	Homologous S gene RNA fragment trigger from human coronavirus strain NL63, generated by in vitro transcription from a DNA template
HCoV-OC43 IVT RNA Target	GGGGCAGGUUUAAUCCUUCUACUUGGAAUAGGAGAUUUGGUUU UACAGAACAAUCUGUUUUUAAGCCUCAACCUGUAGGUGUUUUU ACUCAUCAUGAUGUUGUUUAUGCACAACAUUGUUUUAAAGCUC CCACAAAUUUCUGUCCGUGUAAAUUGGAUGGGUCUUUGUGUGU AGGUAAUGGUCCUGGUAUAGAUGCUGGUUAUAAAAAUAGUGGU AUAGGCACUUGUCCUGCAGGUACUAAUUAUUUAACUUGCCAUA AUGCUGCCCAAUGUGAUUGUUUGUGCACUCCCGACCCCAUUAC AUCUAAAUCUACAGGGCCUUACAAGUGCCCCCAAACUAAAUAC UUAGUUGGCAUAGGUGAGCACUGUUCGGGUCUUGCUAUUAAAA GUGAUUAUUGUGGAGGUAAUCCUUGUACUUGCCAACCACAAGC AUUUUUGGGUUGGUCUGUUGACUCUUGUUUACAAGGGGAUAGG UGUAAUAUUUUUGCUAAUUUUAUUUUGCAUGAUGUUAAUAGUG GUACUACUUGUUCUACUGAUUUACAAAAAUCAAACACAGACAU AAUUCUUGGUGUUUGUGUUAAUUAU	4	Homologous S gene RNA fragment trigger from human coronavirus strain OC43, generated by in vitro transcription from a DNA template
Fluorophore-Biotin (FB) reporter	5'-6FAM/TTATTTTATT/Biotin	4	Reporter molecule used for the SARS-CoV-2 face mask sensor SHERLOCK Reaction. Upon cis-activation, Cas12a collateral activity will cleave the ssDNA linker, separating the 6-carboxyfluorescein from the biotin moiety.

Notes:

1. All toehold sensors and corresponding trigger RNAs for were in vitro transcribed from DNA templates containing the T7 RNA polymerase promoter: TAATACGACTCACTATA
2. The sequence GGG was added to the 5' end of all toehold sensor RNA and target RNA fragment sequences for efficient expression by T7 RNA polymerase. The Ebola ZD toehold sensor only contains a GG after the T7 promoter. If the RNA sequence began with G or GG, only GG or G, respectively, was added to the 5' end of the sequence.
3. The GGG prefix is not shown in the sensor sequences so that the target RNA binding site can be readily identified, but GGG was always added to the start of each RNA to encourage efficient transcription by the polymerase.
4. The coding sequences of the reporter protein LacZ in the colorimetric sensors were added immediately after the 21-nt linker in the toehold switch RNA sequences starting with the second codon (Threonine) of the wild-type beta-Galactosidase enzyme.
5. Considered Zika virus strains (KU312312, AY632535) have sufficient sequence homology to be detected using the same toehold switch sensors (27B).

Table S3: Reporter sequences used in this study.

Name (Fig.#)	Sequence (5' to 3')
LacZ Colorimetric Reporter DNA Sequence (Fig.1, S1-S5)	**ATG**ACCATGATTACGGATTCACTGGCCGTCGTTTTACAACGTCGTGACTGGGAAAACCCTGGCGTTACCCAACTTAATCGCCTTGCAGCACATCCCCCTTTCGCCAGCTGG CGTAATAGCGAAGAGGCCCGCACCGATCGCCCTTCCCAACAGTTGCGCAGCCTGAATGGCGAATGGCGCTTTGCCTGGTTTCCGGCACCAGAAGCGGTGCCGGAAAGCTGG CTGGAGTGCGATCTTCCTGAGGCCGATACTGTCGTCGTCCCCTCAAACTGGCAGATGCACGGTTACGATGCGCCCATCTACACCAACGTGACCTATCCCATTACGGTCAAT CCGCCGTTTGTTCCCACGGAGAATCCGACGGGTTGTTACTCGCTCACATTTAATGTTGATGAAAGCTGGCTACAGGAAGGCCAGACGCGAATTATTTTTGATGGCGTTAAC TCGGCGTTTCATCTGTGGTGCAACGGGCGCTGGGTCGGTTACGGCCAGGACAGTCGTTTGCCGTCTGAATTTGACCTGAGCGCATTTTTACGCGCCGGAGAAAACCGCCTC GCGGTGATGGTGCTGCGCTGGAGTGACGGCAGTTATCTGGAAGATCAGGATATGTGGCGGATGAGCGGCATTTTCCGTGACGTCTCGTTGCTGCATAAACCGACTACACAA ATCAGCGATTTCCATGTTGCCACTCGCTTTAATGATGATTTCAGCCGCGCTGTACTGGAGGCTGAAGTTCAGATGTGCGGCGAGTTGCGTGACTACCTACGGGTAACAGTT TCTTTATGGCAGGGTGAAACGCAGGTCGCCAGCGGCACCGCGCCTTTCGGCGGTGAAATTATCGATGAGCGTGGTGGTTATGCCGATCGCGTCACACTACGTCTGAACGTC GAAAACCCGAAACTGTGGAGCGCCGAAATCCCGAATCTCTATCGTGCGGTGGTTGAACTGCACACCGCCGACGGCACGCTGATTGAAGCAGAAGCCTGCGATGTCGGTTTC CGCGAGGTGCGGATTGAAAATGGTCTGCTGCTGCTGAACGGCAAGCCGTTGCTGATTCGAGGCGTTAACCGTCACGAGCATCATCCTCTGCATGGTCAGGTCATGGATGAG CAGACGATGGTGCAGGATATCCTGCTGATGAAGCAGAACAACTTTAACGCCGTGCGCTGTTCGCATTATCCGAACCATCCGCTGTGGTACACGCTGTGCGACCGCTACGGC CTGTATGTGGTGGATGAAGCCAATATTGAAACCCACGGCATGGTGCCAATGAATCGTCTGACCGATGATCCGCGCTGGCTACCGGCGATGAGCGAACGCGTAACGCGAATG GTGCAGCGCGATCGTAATCACCCGAGTGTGATCATCTGGTCGCTGGGGAATGAATCAGGCCACGGCGCTAATCACGACGCGCTGTATCGCTGGATCAAATCTGTCGATCCT TCCCGCCCGGTGCAGTATGAAGGCGGCGGAGCCGACACCACGGCCACCGATATTATTTGCCCGATGTACGCGCGCGTGGATGAAGACCAGCCCTTCCCGGCTGTGCCGAAA TGGTCCATCAAAAAATGGCTTTCGCTACCTGGAGAGACGCGCCCGCTGATCCTTTGCGAATACGCCCACGCGATGGGTAACAGTCTTGGCGGTTTCGCTAAATACTGGCAG GCGTTTCGTCAGTATCCCCGTTTACAGGGCGGCTTCGTCTGGGACTGGGTGGATCAGTCGCTGATTAAATATGATGAAAACGGCAACCCGTGGTCGGCTTACGGCGGTGAT TTTGGCGATACGCCGAACGATCGCCAGTTCTGTATGAACGGTCTGGTCTTTGCCGACCGCACGCCGCATCCAGCGCTGACGGAAGCAAAACACCAGCAGCAGTTTTTCCAG TTCCGTTTATCCGGGCAAACCATCGAAGTGACCAGCGAATACCTGTTCCGTCATAGCGATAACGAGCTCCTGCACTGGATGGTGGCGCTGGATGGTAAGCCGCTGGCAAGC GGTGAAGTGCCTCTGGATGTCGCTCCACAAGGTAAACAGTTGATTGAACTGCCTGAACTACCGCAGCCGGAGAGCGCCGGGCAACTCTGGCTCACAGTACGCGTAGTGCAA CCGAACGCGACCGCATGGTCAGAAGCCGGGCACATCAGCGCCTGGCAGCAGTGGCGTCTGGCGAAAACCTCAGTGTGACGCTCCCCGCCGCGTCCCACGCCATCCCGCAT CTGACCACCAGCGAAATGGATTTTTGCATCGAGCTGGGTAATAAGCGTTGGCAATTTAACCGCCAGTCAGGCTTTCTTTCACAGATGTGGATTGGCGATAAAAAACAACTG CTGACGCCGCTGCGCGATCAGTTCACCCGTGCACCGCTGGATAACGACATTGGCGTAAGTGAAGCGACCCGCATTGACCCTAACGCCTGGGTCGAACGCTGGAAGGCGGCG GGCCATTACCAGGCCGAAGCAGCGTTGTTGCAGTGCACGGCAGATACACTTGCTGATGCGGTGCTGATTACGACCGCTCACGCGTGGCAGCATCAGGGGAAAACCTTATTT ATCAGCCGGAAAACCTACCGGATTGATGGTAGTGGTCAAATGGCGATTACCGTTGATGTTGAAGTGGCGAGCGATACACCGCATCCGGCGCGGATTGGCCTGAACTGCCAG CTGGCGCAGGTAGCAGAGCGGGTAAACTGGCTCGGATTAGGGCCGCAAGAAAACTATCCCGACCGCCTTACTGCCGCCTGTTTTGACCGCTGGGATCTGCCATTGTCAGAC ATGTATACCCCGTACGTCTTCCCGAGCGAAAACGGTCTGCGCTGCGGGACGCGCGAATTGAATTATGGCCCACACCAGTGGCGCGGCGACTTCCAGTTCAACATCAGCCGC TACAGTCAACAGCAACTGATGGAAACCAGCCATCGCCATCTGCTGCACGCGGAAGAAGGCACATGGCTGAATATCGACGGTTTCCATATGGGGATTGGTGGCGACGACTCC TGGAGCCCGTCAGTATCGGCGGAATTCCAGCTGAGCGCCGGTCGCTACCATTACCAGTTGGTCTGGTGTCAAAAA**TAA**
GFPmut3B Fluorescent Reporter DNA Sequence (Fig. S7)	**ATG**CGTAAAGGAGAAGAACTTTTCACTGGAGTTGTCCCAATTCTTGTTGAATTAGATGGTGATGTTAATGGGCACAAATTTTCTGTCAGTGGAGAGGGTGAAGGTGATGCA ACATACGGAAAACTTACCCTTAAATTTATTTGCACTACTGGAAAACTACCTGTTCCGTGGCCAACACTTGTCACTACTTTCGGTTATGGTGTTCAATGCTTTGCGAGATAC CCAGATCACATGAAACAGCATGACTTTTTCAAGAGTGCCATGCCCGAAGGTTACGTACAGGAAAGAACTATATTTTTCAAAGATGACGGGAACTACAAGACACGTGCTGAA GTCAAGTTTGAAGGTGATACCCTTGTTAATAGAATCGAGTTAAAAGGTATTGATTTTAAAGAAGATGGAAACATTCTTGGACACAAATTGGAATACAACTATAACTCACAC AATGTATACATCATGGCAGACAAACAAAAGAATGGAATCAAAGTTAACTTCAAAATTAGACACAACATTGAAGATGGAAGCGTTCAACTAGCAGACCATTATCAACAAAAT ACTCCGATTGGCGATGGCCCTGTCCTTTTACCAGACAACCATTACCTGTCCACACAATCTGCCCTTTCGAAAGATCCCAACGAAAAGAGAGACCACATGGTCCTTCTTGAG TTTGTAACCGCTGCTGGGATTACACATGGCATGGATGAACTATACAAAAGGCCTGCAGCAAACGACGAAAACTACGCTTTAGTAGCT**TAA**
sfGFP Fluorescent Reporter DNA Sequence (Fig. 2, 3)	**ATG**AGCAAAGGTGAAGAACTGTTTACCGGCGTTGTGCCGATTCTGGTGGAACTGGATGGCGATGTGAACGGTCACAAATTCAGCGTGCGTGGTGAAGGTGAAGGCGATGCC ACGATTGGCAAACTGACGCTGAAATTTATCTGCACCACCGGCAAACTGCCGGTGCCGTGGCCGACGCTGGTGACCACCCTGACCTATGGCGTTCAGTGTTTTAGTCGCTAT CCGGATCACATGAAACGTCACGATTTCTTTAAATCTGCAATGCCGGAAGGCTATGTGCAGGAACGTACGATTAGCTTTAAAGATGATGGCAAATATAAAACGCGCGCCGTT GTGAAATTTGAAGGCGATACCCTGGTGAACCGCATTGAACTGAAAGGCACGGATTTTAAAGAAGATGGCAATATCCTGGGCCATAAACTGGAATACAACTTTAATAGCCAT AATGTTTATATTACGGCGGATAAACAGAAAAATGGCATCAAAGCGAATTTTACCGTTCGCCATAACGTTGAAGATGGCAGTGTGCAGCTGGCAGATCATTATCAGCAGAAT ACCCCGATTGGTGATGGTCCGGTGCTGCTGCCGGATAATCATTATCTGAGCACGCAGACCGTTCTGTCTAAAGATCCGAACGAAAAAGGCACGCGGGACCACATGGTTCTG CACGAATATGTGAATGCGGCAGGTATTACGTGGAGCCATCCGCAGTTCGAAAAA**TAA**
eforRed Fluorescent Reporter DNA Sequence (Fig. 2, S15)	**ATG**AGCGTGATTAAACAGGTGATGAAAACCAAACTGCATCTGGAAGGCACCGTTAATGGTCATGATTTCACCATTGAAGGTAAAGGTGAAGGCAAACCGTATGAAGGTCTG CAGCATATGAAAATGACCGTTACCAAAGGTGCACCGCTGCCGTTTAGCGTTCATATTCTGACCCCGAGCCATATGTATGGTAGCAAACCGTTTAACAAATATCCGGCAGAT ATCCCGGATTATCACAAACAGAGCTTTCCGGAAGGTATGAGCTGGGAACGTAGCATGATTTTTGAAGATGGTGGTGTTTGTACCGCAAGCAATCATAGCAGCATTAATCTG CAAGAAAACTGCTTCATCTACGACGTGAAATTCCATGGTGTTAATCTGCCTCCGGATGGTCCGGTTATGCAGAAAACCATTGCAGGTTGGGAACCGAGCGTTGAAACCCTG TATGTTCGTGATGGTATGCTGAAAAGCGATACCGCCATGGTTTTTAAACTGAAAGGTGGTGGTCATCATCGTGTGGATTTCAAAACCACCTACAAAGCAAAAAAACCGGTT AAACTGCCGGAATTCCATTTTGTTGAACATCGTCTGGAACTGACCAAACACGATAAAGATTTTACCACCTGGGATCAGCAAGAAGCAGCAGAAGGTCATTTTAGTCCGCTG CCGAAAGCACTGCCG**TAA**
dTomato Fluorescent Reporter DNA Sequence (Fig. 2, S15)	**ATG**GTGAGCAAGGGCGAGGAGGTCATCAAAGAGTTCATGCGCTTCAAGGTGCGCATGGAGGGCTCCATGAACGGCCACGAGTTCGAGATCGAGGGCGAGGGCGAGGGCCGC CCCTACGAGGGCACCCAGACCGCCAAGCTGAAGGTGACCAAGGGCGGCCCCCTGCCCTTCGCCTGGGACATCCTGTCCCCCCAGTTCATGTACGGCTCCAAGGCGTACGTG AAGCACCCCGCCGACATCCCCGATTACAAGAAGCTGTCCTTCCCCGAGGGCTTCAAGTGGGAGCGCGTGATGAACTTCGAGGACGGCGGTCTGGTGACCGTGACCCAGGAC TCCTCCCTGCAGGACGGCACGCTGATCTACAAGGTGAAGATGCGCGGCACCAACTTCCCCCCCGACGGCCCCGTAATGCAGAAGAAGACCATGGGCTGGGAGGCCTCCACC GAGCGCCTGTACCCCCGCGACGGCGTGCTGAAGGGCGAGATCCACCAGGCCCTGAAGCTGAAGGACGGCGGCCACTACCTGGTGGAGTTCAAGACCATCTACATGGCCAAG AAGCCCGTGCAACTGCCCGGCTACTACTACGTGGACACCAAGCTGGACATCACCTCCCACAACGAGGACTACACCATCGTGGAACAGTACGAGCGCTCCGAGGGCCGCCAC CACCTGTTCCTGTACGGCATGGACGAGCTGTACAAG**TAA**
Nanoluciferase Luminescent Reporter DNA Sequence (Fig. 2, S10)	**ATG**GGTCATCACCACCACCATCACGGTGGCGCTAGCGTGTTCACATTGGAGGACTTTGTAGGGGACTGGCGCCAGACAGCGGGCTACAACCTTGATCAGGTTCTGGAGCAG GGAGGTGTAAGTTCACTTTTCCAGAATTTGGGTGTGAGTGTCACCCCGATCCAACGTATCGTGCTTTCCGGAGAAAATGGGCTGAAGATCGACATCCATGTTATTATTCCT TATGAAGGGCTTAGCGGAGATCAAATGGGCCAAATCGAAAAGATTTTCAAAGTGGTATATCCTGTTGACGACCATCATTTTAAGGTCATTCTGCATTACGGAACTTTAGTC ATCGACGGCGTCACACCTAACATGATTGACTATTTTGGCCGTCCGTATGAGGGCATCGCAGTGTTTGACGGAAAAAAAATCACCGTGACAGGGACACTGTGGAACGGCAAT AAGATTATCGACGAGCGCCTTATTAACCCAGATGGGTCGCTTTTATTCCGTGTCACTATTAATGGTGTCACTGGCTGGCGTTTGTGCGAACGCATCCTGGCA**TAA**

5

Table S4: Technology Comparison

Table S4a. Comparison to other related technology categories.

	Wearable Synthetic Biology (This work)	Current Wearable Devices	Point-of-Care Diagnostics
Wearable Form Factor	YES	YES	NO
Autonomously Functioning	YES	YES	NO
Synthetic Biology Reactions	YES	NO	YES
Molecular Sensing	YES	NO	YES
Pathogen Sensing	YES	NO	YES
Rapid Modular Programmability of Components	YES	NO	YES
Portable Instrumentation	YES	YES	YES

5

Table S4b. Detailed comparison with other synthetic biology sensor-embedded materials.

	Stretchable Hydrogel-Elastomer Devices with Encapsulated Programmed Cells (Liu, X. et al 2017) [4]	3D Printing of Living Responsive Materials and Devices (Liu, X. et al 2017) [5]	Engineered Bacteria Deposited onto Textiles, Ceramics, and Plastic (Moser, F. et al 2019) [6]	Harnessing the Hygroscopic and Biofluorescent Behaviors of Genetically Tractable Microbial Cells to Design Biohybrid Wearables (Wang, W. et al. 2017) [7]	Programmable CRISPR-Responsive Smart Materials (English, et al. 2020) [13]	wFDCF (This Work)
LOD	100 nM	100 nM	25 μM	n/a	11 aM	17 aM
Sensor Format	Living Cells	Living Cells	Living Cells	Living Cells	Cell-free Freeze-dried Reactions	Cell-free Freeze-dried Reactions
Matrix Material	Hydrogel	Hydrogel	Textiles, Ceramics, Polymer	Polymer	Hydrogel, paper	Textiles, polymer, paper
Shelf-stable	NO	NO	NO	NO	YES	YES
Detection target	Small Molecules	Small Molecules	Small Molecules, Light	Atmospheric Humidity	dsDNA	Hydration, Small Molecules, Proteins, RNA and DNA.
Output	Fluorescent	Fluorescent	Fluorescent	Fluorescent	Fluorescent, Colorimetric, Conductivity	Fluorescent, Colorimetric, Luminescent
Detection time	2 hrs	2-4 hrs	3-18 hrs	minutes	45 min – 24 hrs	6 min – 2 hrs
System Complexity	Simple	Moderate	Moderate	Moderate (Additional Wash Steps)	Moderate	Moderate
Wearable Format	NO	NO	YES	YES	NO	YES

Table S4c. Detailed comparison with point-of-care diagnostic technologies.

Variable	qPCR	Microarrays/ Fluorescent barcodes	Next Generation Sequencing (NGS)	Fluorescence In Situ Hybridization (FISH)	Toehold switches	SHERLOCK / DETECTR	wFDCF (This work)
Cost (USD)	$0.85	$250.00	$23.00	Expensive	Low-Cost	Low-Cost	Low-Cost (~$100 USD for reusable portable spectrophotometer + ~$1 USD per sensor)
Ease of Use	Trained Specialist	Trained Specialist	Trained Specialist	Trained Specialist	Trained Specialist	Trained Specialist	Autonomous Functioning
Readout	Fluorescence	Fluorescence	Fluorescence	Fluorescence	Visual/ Fluorescence	Visual/ Fluorescence	Visual, Fluorescence, Luminescence and Digital
Sensitivity	aM	aM	aM	aM	fM	aM	aM
Time	~3 Hour	1 Day	>1 Day	4-16 Hour	1-4 Hour	~1-3 Hour	6 min - 2 Hour
Multiplex	YES	YES	YES	YES	YES	YES	YES
Wearable Format	NO	NO	NO	NO	NO	NO	YES

5

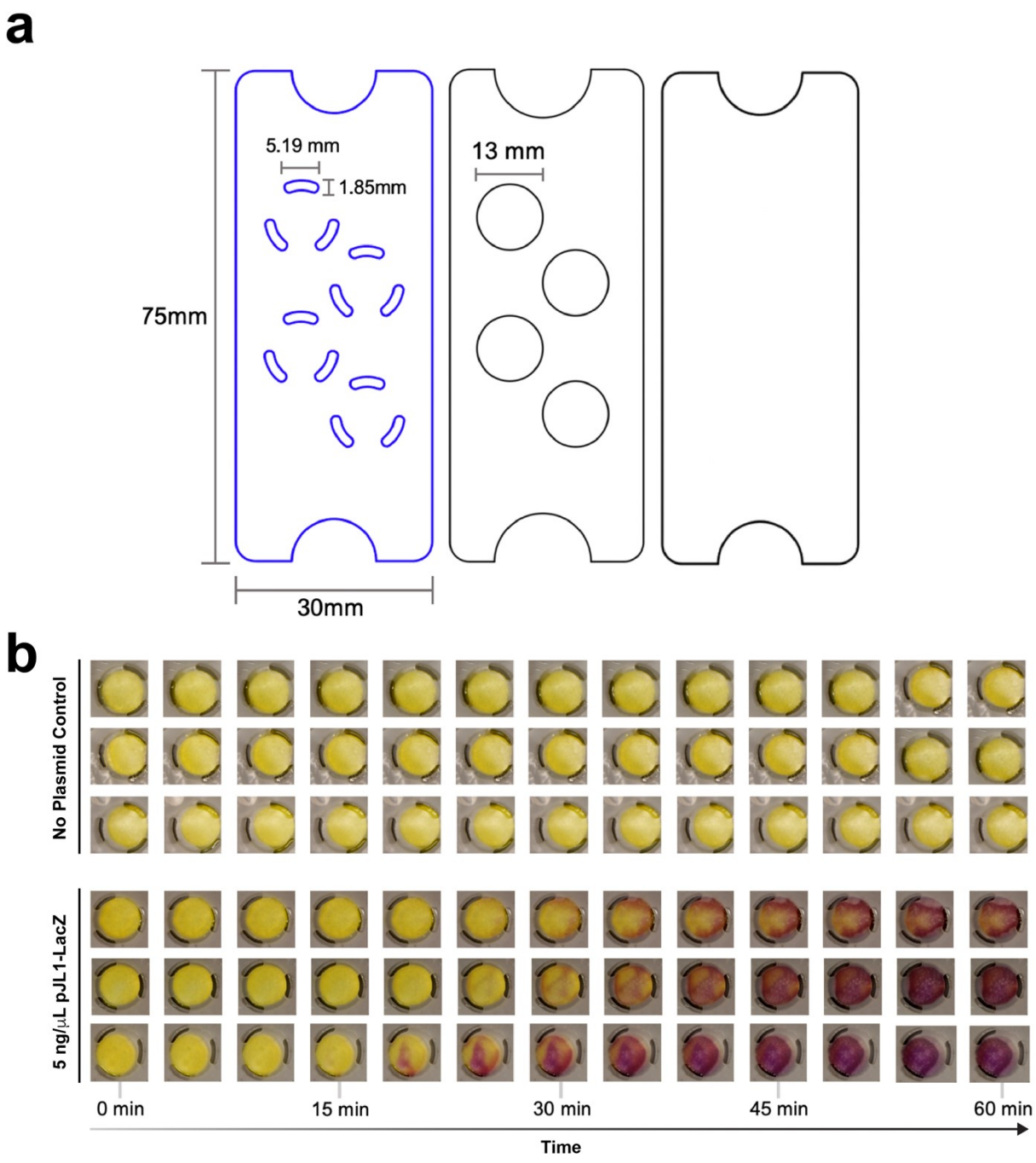

Fig. S1. Assembly layers and sample activation of colorimetric wFDCF reactions with constitutive P_{T7}::LacZ module. a, The layout of elastomer layers in the colorimetric wFDCF device. **b,** Activation of colorimetric prototype wells using 40 ng/μL constitutive LacZ-T7 plasmid in a 50 μL rehydration splash as compared to rehydration with no plasmid. After complete rehydration, PURExpress reactions were conducted at 1.5x concentration. All the reactions were incubated at 30°C and were exposed to the ambient environment. Images were taken every 5 minutes. Each row shows a representative single-well reaction.

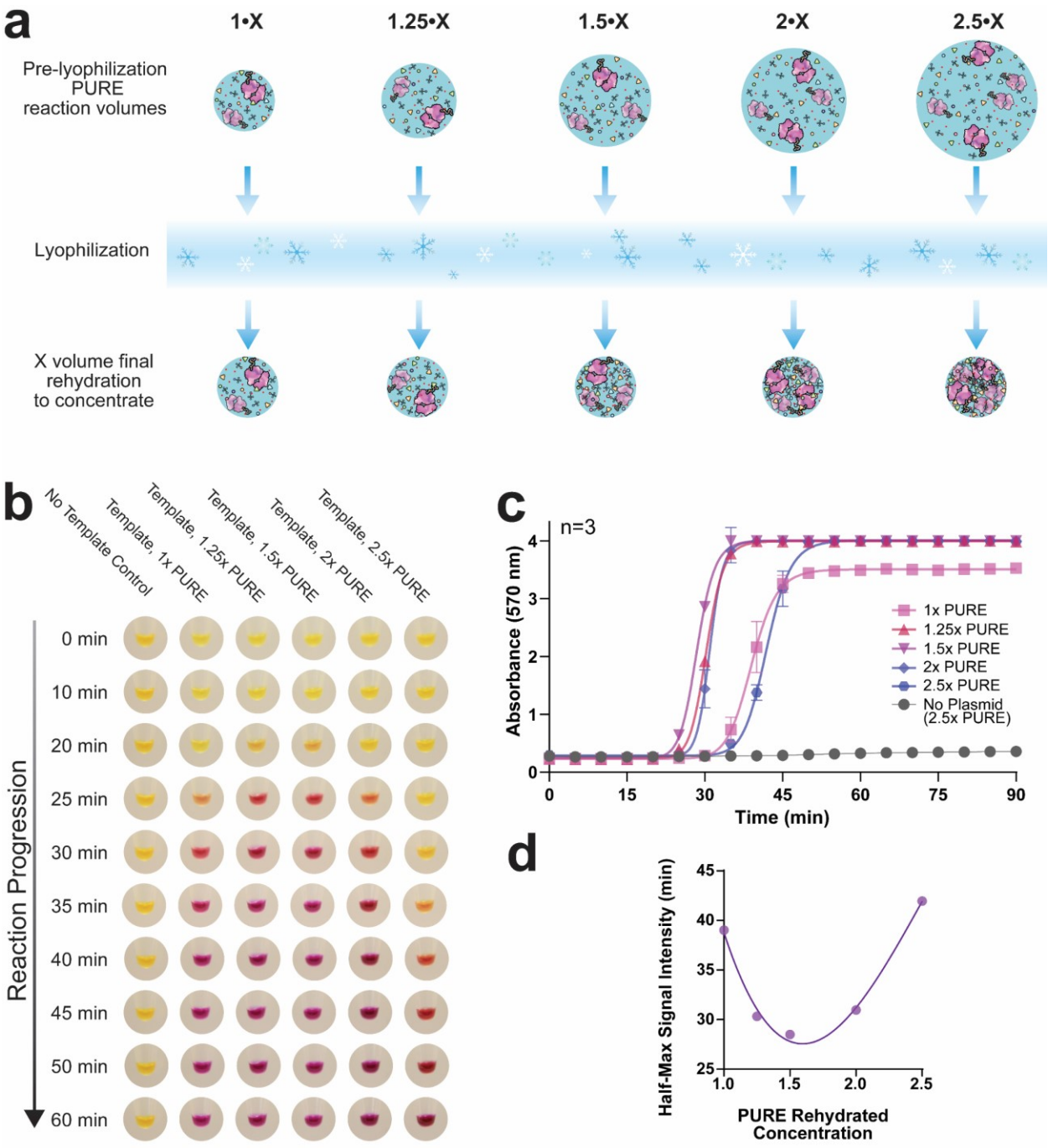

Fig. S2. Concentrating PURE cell-free reactions increases reaction kinetics. a, Schematic of reaction concentration through the lyophilization of PURExpress reactions at varying volumes followed by rehydration at a set volume. Using this method, synthetic biology reactions can be concentrated to enhance kinetics through molecular crowding effects or greater density of cell-free components per volume. **b,** Representative images of PURE reactions with a LacZ output over one hour, at various concentrations. **c,** Quantified PURExpress reactions with a LacZ output in triplicate; the error bars denote standard deviation. **d,** The half-maximal values from curve fitting the data shown in S2c indicate that the 1.5x concentrated PURE reaction accelerates the signal output by more than 10 minutes. Error bars are smaller than the data points.

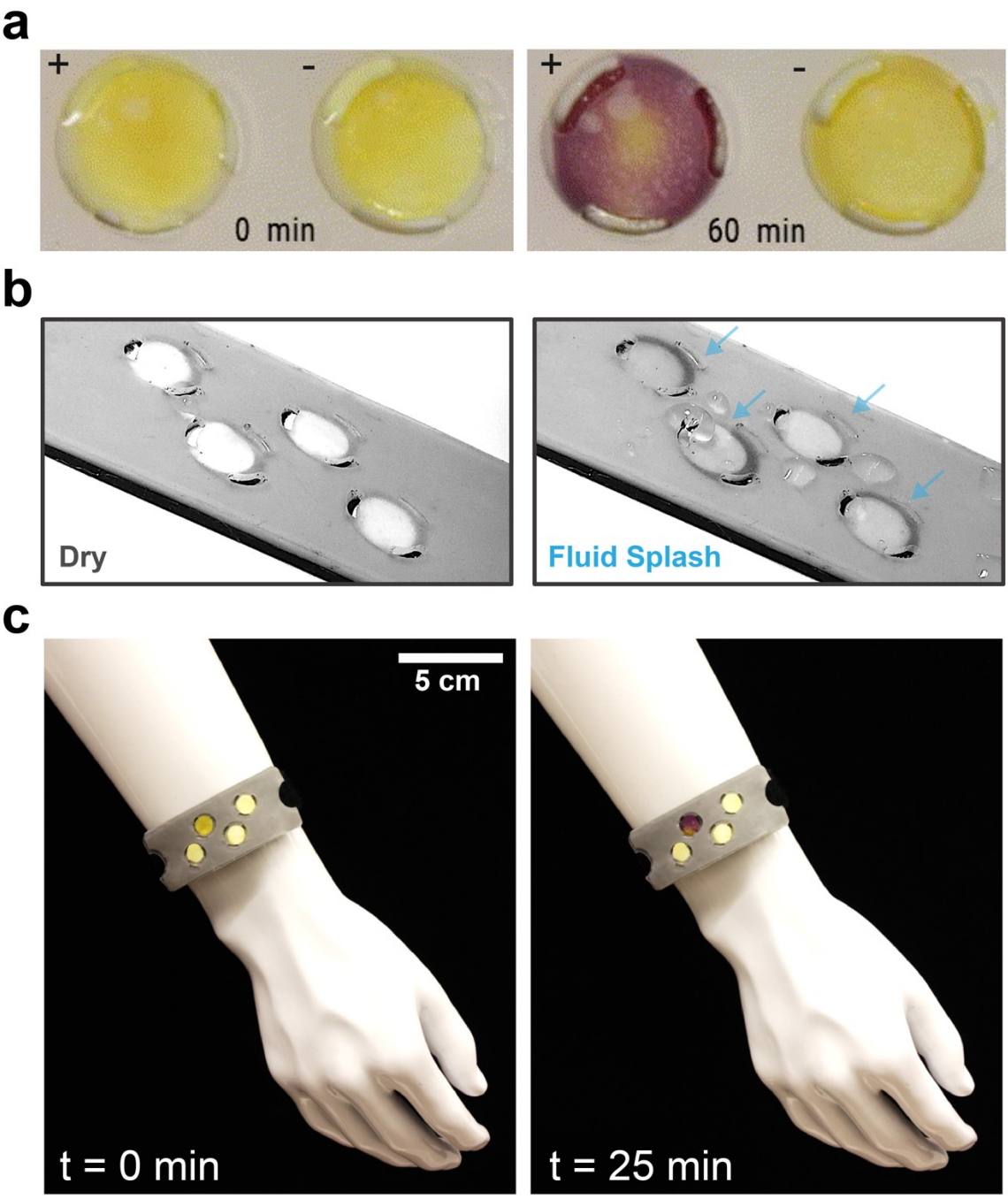

Fig. S3. Sample activation of wFDCF colorimetric devices and bracelet for detection of Ebola virus RNA. a, Activation of colorimetric Ebola virus DNA toehold wFDCF sensor using a 50 μL splash of dd-H_2O sample containing 300 nM Ebola RNA trigger as compared to control (t = 60 min). **b,** Port wicking into sachets containing reaction disks using dd-H_2O fluid splash. Rehydrated paper disks are visibly darker after fluid entry and wicking into the substrate (t = 1 sec after splash). **c,** Activation of the wearable colorimetric bracelet with four independent Ebola virus DNA toehold sensors (t = 25 min). Color change in activated sensor disk is distinguishable within 25-60 min after rehydration, as compared to surrounding controls.

Fig. S4. Textile substrate compatibility testing using synthetic biology reactions and sample colorimetric reaction. a, Samples of eight fabric types selected as part of the textile screening for wFDCF compatibility. Bottom icons indicate the environmental and hydration conditions that were monitored over time for analysis. **b,** A sample wFDCF colorimetric activation in a 1 x 1 cm cellulose matrix square containing 75 µL of NEB cell-free PURExpress® in vitro protein synthesis solution (New England Biolabs, Inc., Ipswich, MA) with 40 ng/µL constitutive pJL1-LacZ plasmid.

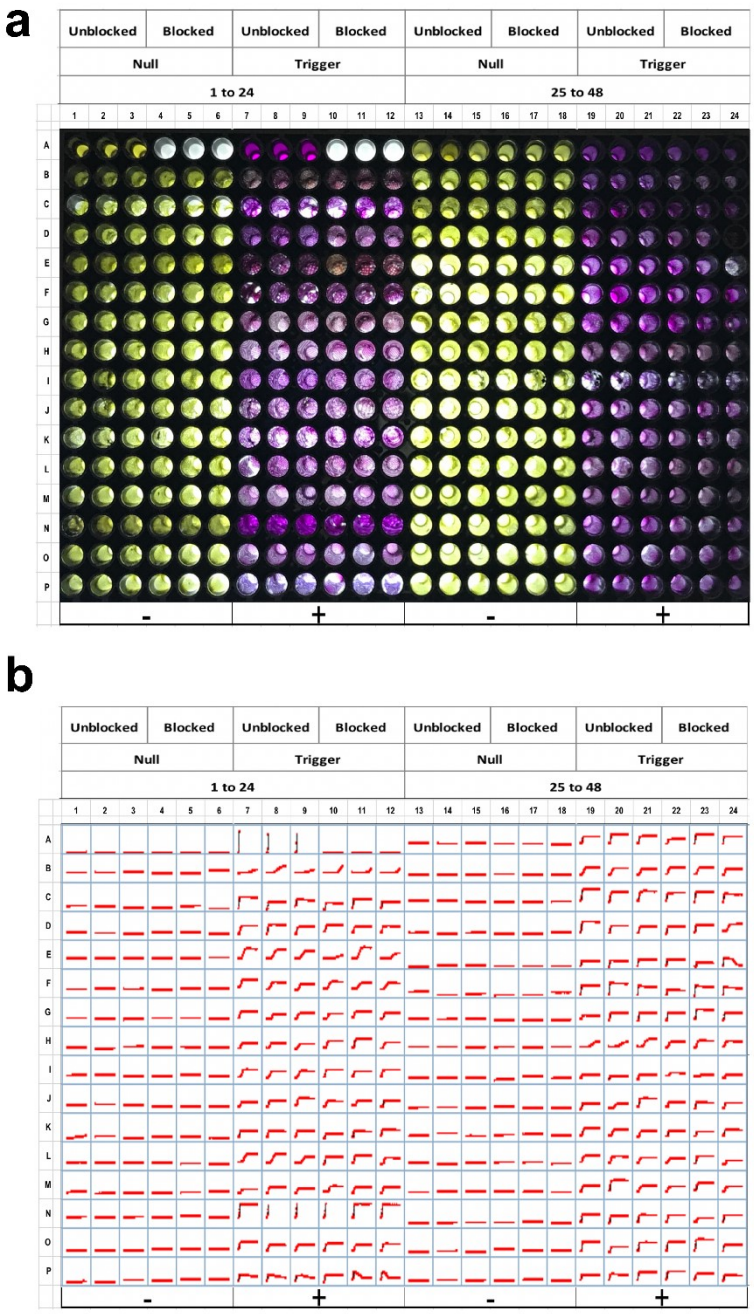

Fig. S5. Textile screening using model constitutive P_{T7}::LacZ assay. a, A sample 384-well plate containing triplicates of BSA blocked and unblocked 2 mm discs of 30 different textile types after constitutive P_{T7}::LacZ expression following a 12-hour run for reactions containing 1.8 µL of NEB cell-free PURExpress® in vitro protein synthesis solution (New England Biolabs, Inc., Ipswich, MA) with 40 ng/µL constitutive pJL1-pLacZ plasmid (+) or without plasmid as controls (-). **b,** Examples of qualitative traces of colorimetric signals for these different fabric disks using a plate spectrophotometer (420 nm absorbance). While the traces shown here are not normalized across all samples, the increase in signal per cell indicates a color change from yellow to purple. Normalized absorbance values were calculated and used for subsequent analyses.

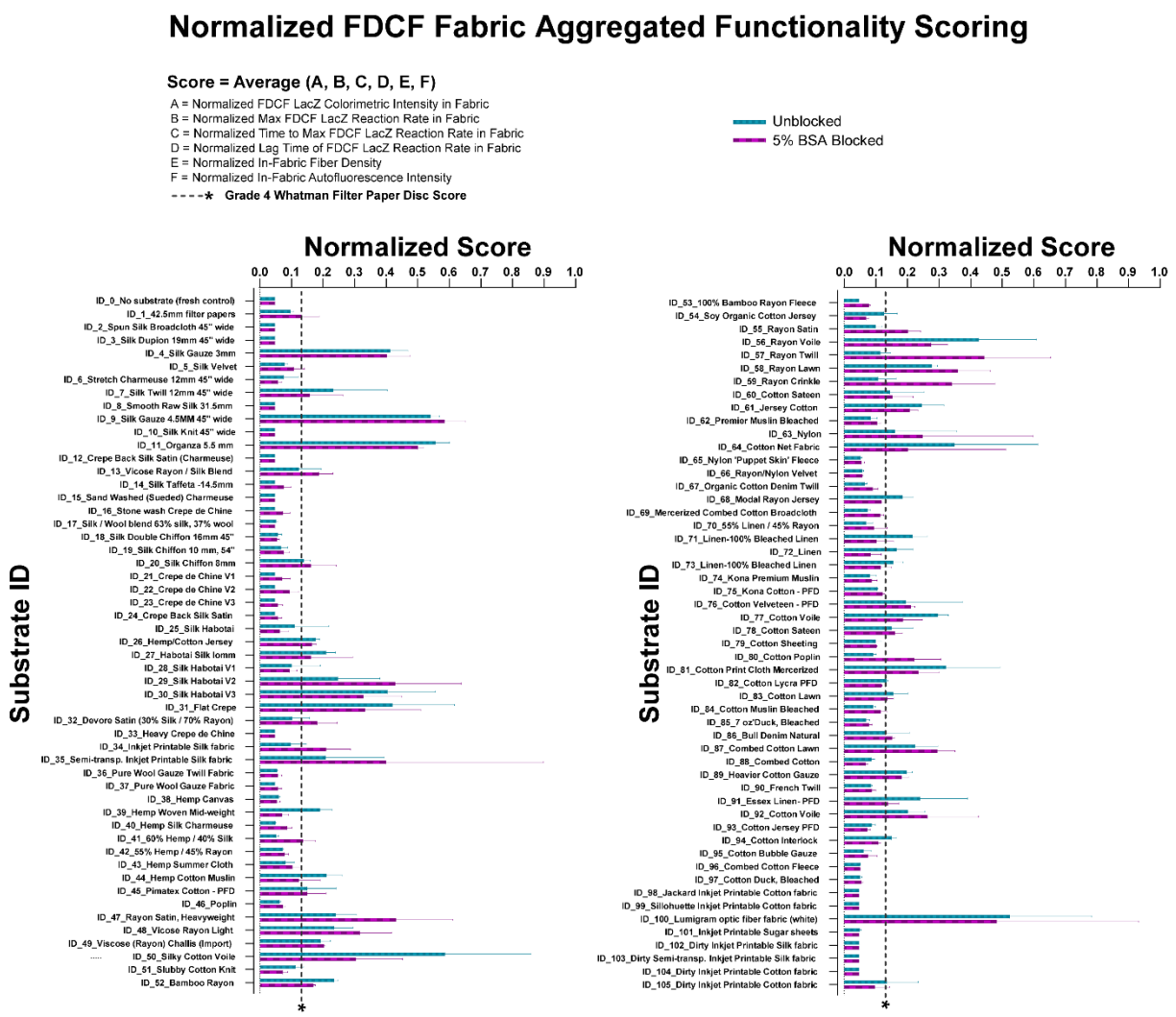

Fig. S6. Compilation of normalized functional scoring for colorimetric wFDCF textile screening. A normalized functionality score was calculated for each of the 103 evaluated fabrics tested for compatibility with freeze-dried PURExpress reaction generating a LacZ output. This score was generated by measuring six key parameters: peak absorbance intensity at 420 nm, reaction rate, time to maximum signal, lag-time, fabric fiber density and in-fabric autofluorescence, and then multiplying normalized scores for each of these measurements, penalizing longer times to maximum signal, long lag-times and high autofluorescence. Dotted line indicates aggregated score value for Whatman No. 4 filter paper. The highest average score was observed in fabric ID#:100 containing 85% Polyester / 15% Polyamide fibers.

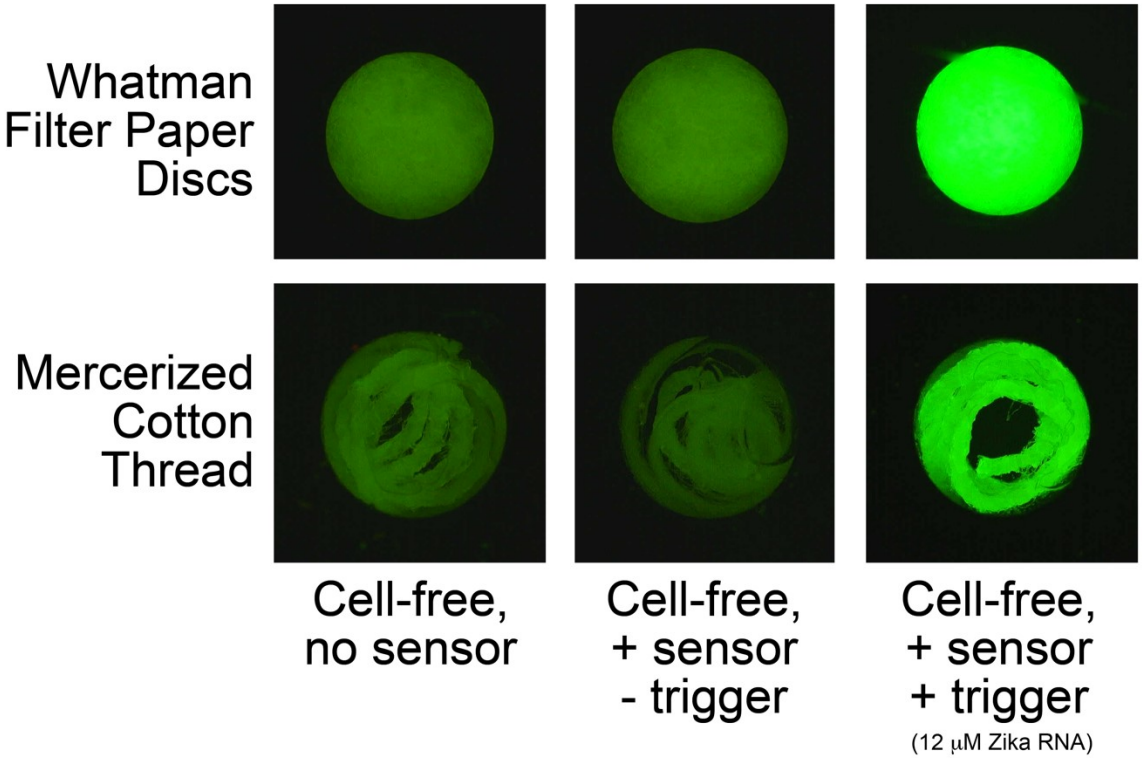

Fig. S7. Zika DNA toehold sensor activation in single mercerized cotton thread. a, Sterile mercerized cotton threads (d = 0.2 mm, L = 1 cm) taken from a Dukal™ Gauze pad (Dukal Corp., Ronkonkoma, NY) were coiled and deposited into single wells of a flat 384-well black polystyrene plate with a clear glass bottom (Corning Inc., Kennebunk ME). Thread samples were wicked with 2 μL of a solution containing 1x Cell-free PURExpress® in vitro protein synthesis solution (New England Biolabs, Inc., Ipswich, MA), adding 33 nM Zika DNA toehold sensor 27B (sfGFP) for sensing. Samples were frozen using liquid nitrogen and lyophilized for 4 hours. For testing, 2 μL of dd-H_2O with 1.2 μM of freshly made Zika RNA trigger was added to each of the freeze-dried samples, and fluorescence was assessed after 60 minutes under a fluorescence digital microscope Dino-Lite Edge AM4115T-GFBW (Dunwell Tech, Inc., Torrance, CA). These reactions were compared to those occurring in 2 mm disks of Whatman™ No. 4 filter paper (GE Healthcare Lifesciences Inc., Chicago, IL). Zika RNA trigger appears to produce a higher fluorescent signal as compared to PURExpress reactions containing no template and reactions with sensor template but with no trigger.

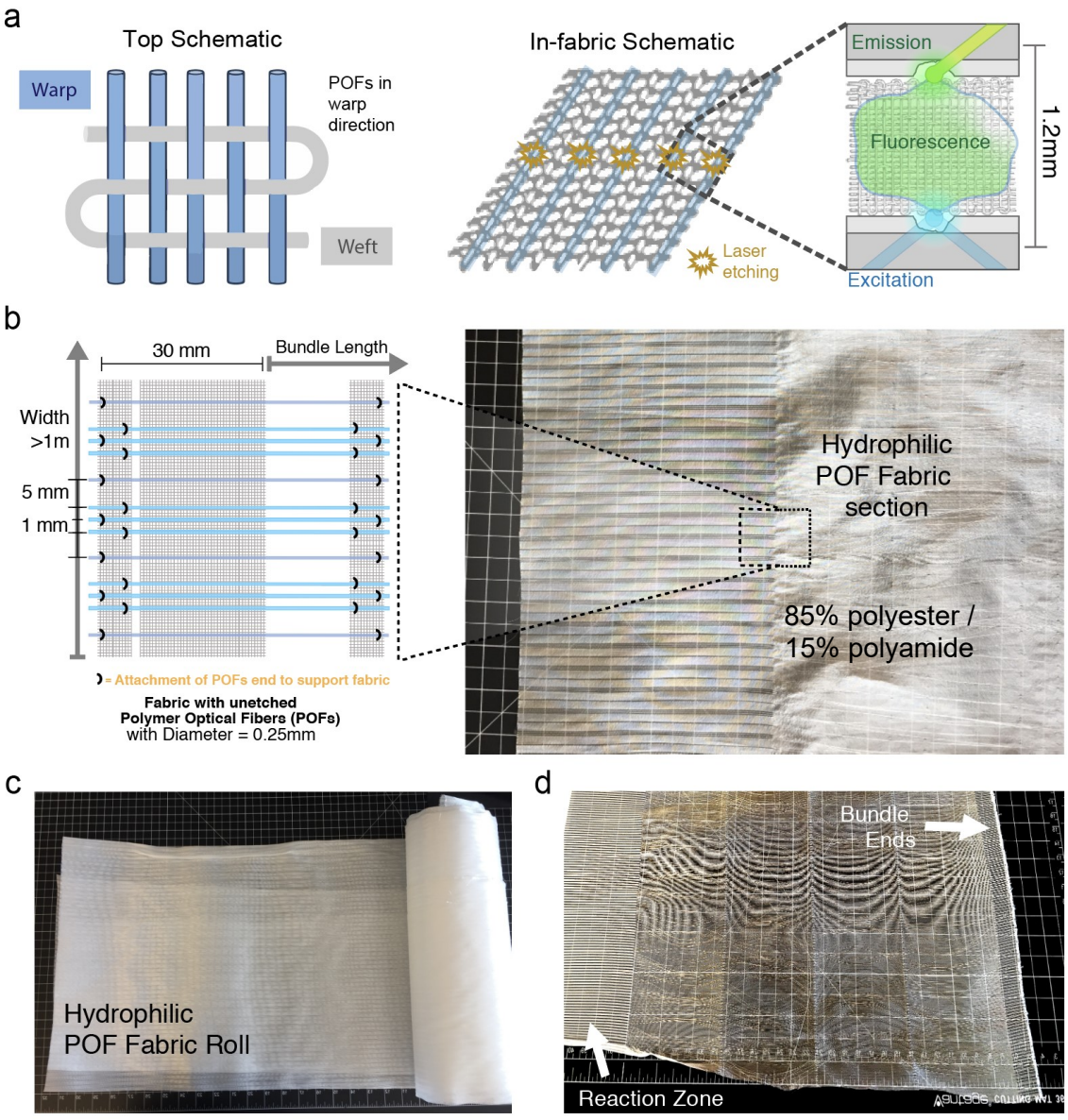

Fig. S8. Fabrication of polymeric optic fiber (POF) fabric for wFDCF. a, Clean 0.2 mm hydrophilic yarns made of 85% polyester and 15% polyamide were weaved in VELO style along the weft in combination with 0.25 mm un-etched poly(methyl methacrylate) POFs as warp using a standard industrial loom via Dreamlux's process (Samsara S.R.L., Milan, IT). When etched in specific regions, the cladding of POFs can be disrupted to allow for efficient excitation and emission signal collection from fluorescent or luminescent samples rehydrated within the hydrophilic fibers of the fabric. **b,** A three-fiber multi-strip design was achieved with a POF pitch of ~1 mm and intermediate POFs at 5 mm from the strip center for easy cutting. The reaction zone was cut to be ~30 mm in length. The width of the fabric roll was arbitrary, usually above 1 m depending on the used loom. Free POFs can then be detached from the un-weaved side to be bundled together. **c,** A roll of the hydrophilic POF fabric after weaving. **d,** A cut section of the hydrophilic POF fabric with indications in reaction zone and bundle ends.

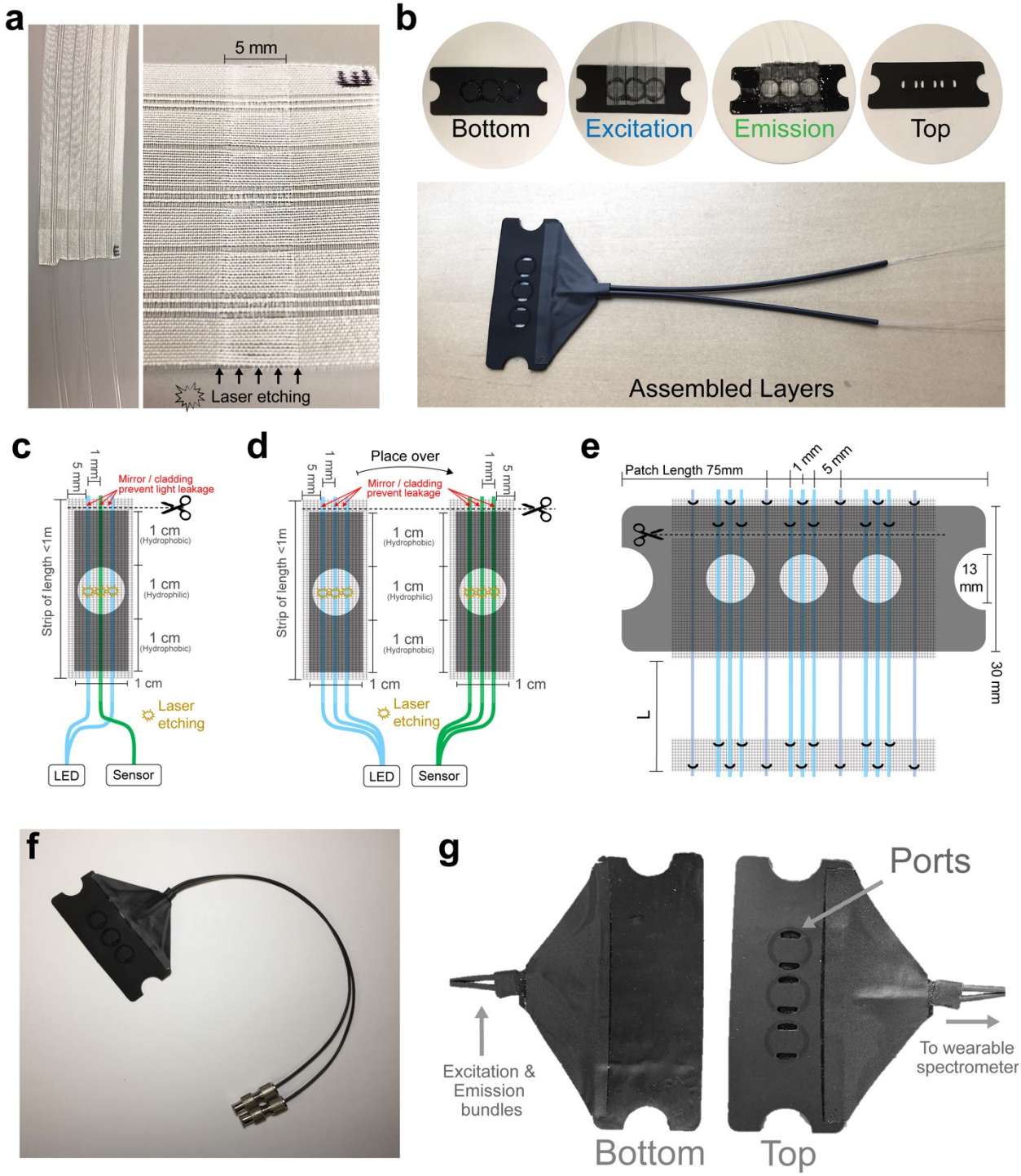

Fig. S9. Fabrication of textile-based wFDCF sensor patch. a, A cut strip of hydrophilic POF fabric was laser-etched (5 mm) to disrupt the POF outer cladding in the POFs sections closest to the reaction zone. **b,** Examples of prepared wFDCF fabric-elastomer layers and final assembly into a three-well sensor for garment integration. POFs in these devices were covered with black heat shrink tubing (6 mm). Top elastomer cover features two 5.19 x 1.85 mm curved sample ports instead of three as in the colorimetric prototypes to reduce direct light leakage on top of the POFs that may cause background light detection. **c,** Schematic of a POF-fabric-elastomer strip

for sensing in a single textile layer including two excitation fibers on the sides of an emission fiber. **d,** Schematic of a double POF-fabric-elastomer strip for sensing with dedicated excitation and emission layers. This design was the one selected for further experiments due to higher hydrophilic fiber content and capacity to immobilize fluid for lyophilization. **e,** Schematic of a single excitation or emission POF-fabric-elastomer layer overlaid on an applied elastomer pattern for creating the impermeable reaction wells. **f**, A finalized three-well sensor wFDCF device with heat shrunk POF covers and Luer connectors for interface with a portable spectrometer device. **g,** Top and bottom views of a final three-well sensor wFDCF device. The blackout fabric can be seen through the sample wicking ports and serve to prevent environmental light penetration into reaction wells.

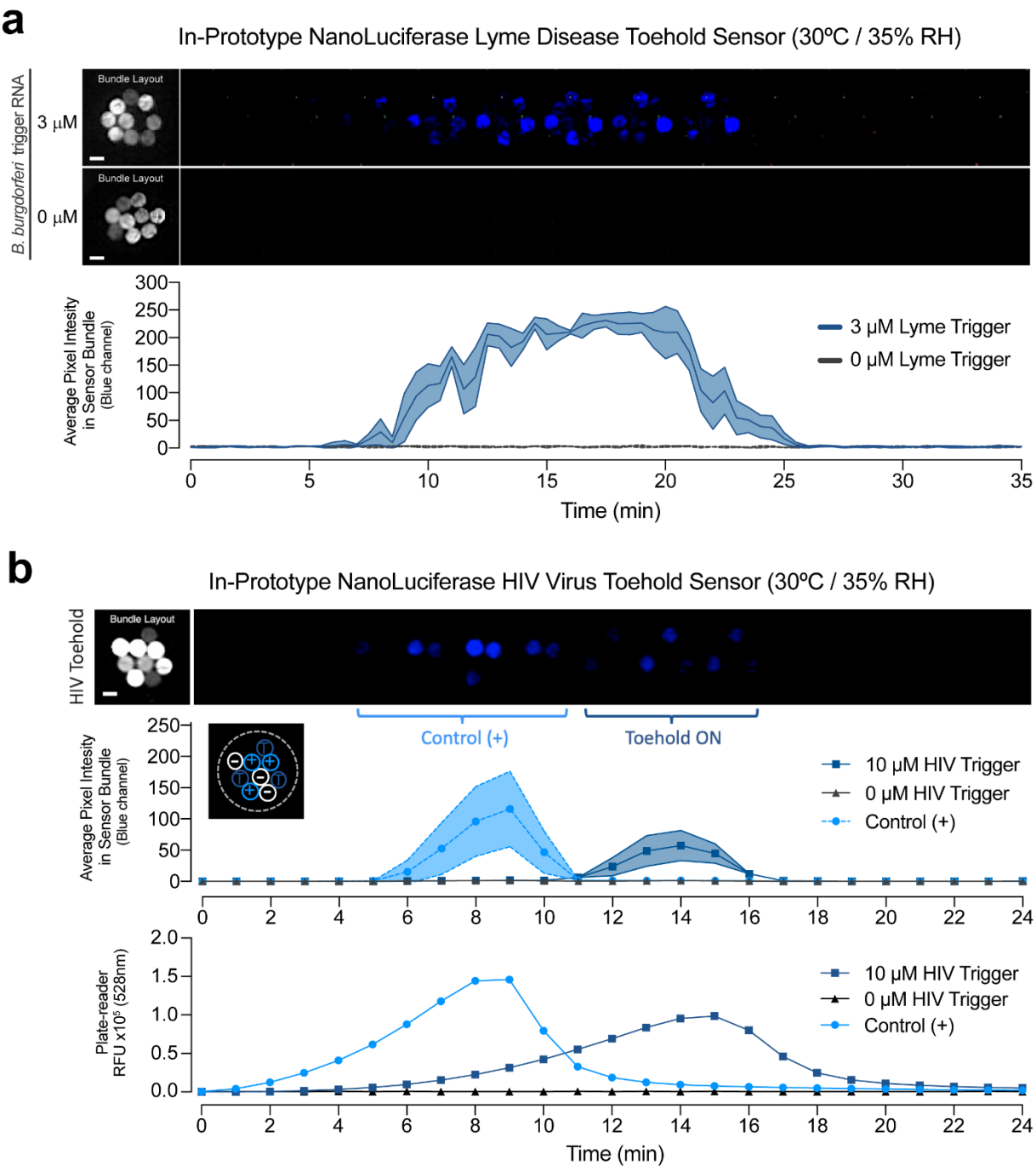

Fig. S10. Additional Nanoluciferase (nLuc) luminescence experiments. a, Dynamic response of a wFDCF Lyme disease RNA toehold switch sensor with luminescence output. In this experiment, 50 µL reactions consisting of 20 µL of NEB cell-free PURExpress® Component A, 15 µL NEB Component B, 2.5 µL NEB murine RNase inhibitor, 19 µL Lyme disease toehold sensor DNA with nLuc reporter (6 ng/µL), 0.5 µL luciferin substrate (Promega Corp., Madison, WI) and 19 µL dd-H_2O. Prepared sensor reactions (50 µL per well) were quickly deposited in-

fabric to be snap-frozen and then lyophilized for 4-8 hours within the device. Activation of sensors was achieved by rehydration with a fluid splash of dd-H_2O spiked with 3 μM *B. burgdorferi* trigger RNA freshly made for the positive samples, while 0 μM trigger RNA was used for controls. Luminescence signal from toehold sensor in-device is statistically distinguishable from the control after 13 minutes ($P<0.05$). **b,** Dynamic response of a wFDCF HIV RNA toehold switch sensor with luminescence output in comparison to constitutive P_{T7}::nLuc expression as a positive control (+), which was statistically distinguishable from the negative condition after 8 minutes ($P<0.05$). The HIV toehold reaction was prepared in 50 μL batches using 20 μL of NEB cell-free PURExpress® Component A, 15μL NEB Component B, 2.5 μL NEB murine RNase inhibitor, 19 μL HIV toehold sensor DNA template with a nanoLuciferase reporter (6 ng/μL), 0.5 μL luciferin substrate (Promega Corp., Madison, WI) and 19 μL dd-H_2O. Prepared sensor reactions (50 μL per well) were quickly deposited in-fabric to be snap-frozen and then lyophilized for 4-8 hours within the device. Activation of sensors was achieved by rehydration with a fluid splash of dd-H_2O spiked with 10 μM HIV trigger RNA freshly made for the positive samples, while 0 μM HIV trigger RNA was used for controls. The constitutive P_{T7}::nLuc positive control reaction shown was also prepared similarly, but substituting the toehold switch in the plasmid with a T7 promoter. Results were compared to the same reactions run in a 384-well plate and analyzed using a BioTek NEO HTS plate reader (BioTek Instruments, Inc., Winooski, VT) in luminescence mode. Activation of constitutive reaction peaked at ~8 minutes, whereas toehold with 10 μM trigger produced its peak signal at ~15 minutes. Both the wFDCF device tests and the plate reader profiles appeared to be temporally aligned and exhibit analogous signal amplitude differences among reactions.

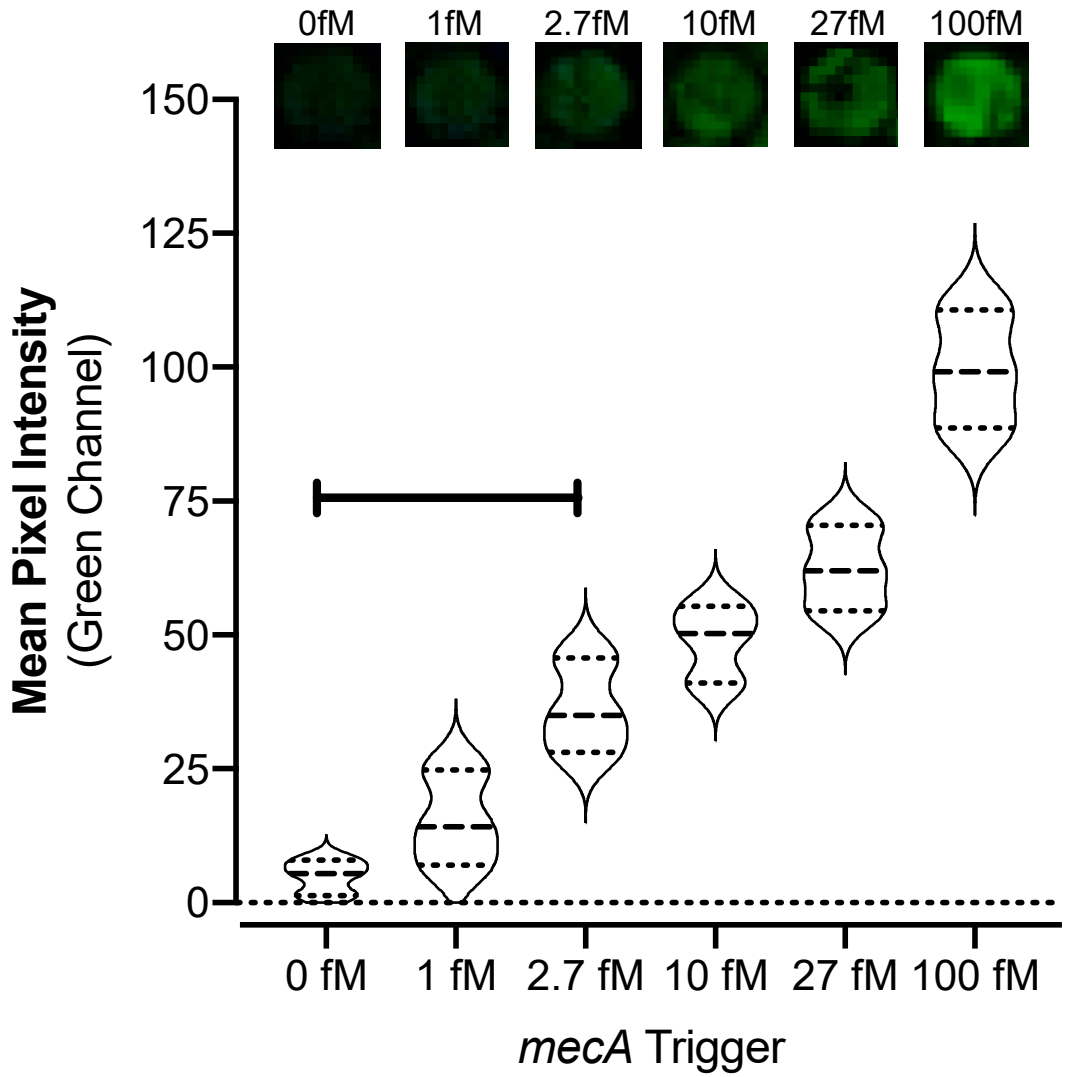

Fig. S11. Limit of detection of wFDCF CRISPR-Cas12a based sensor activated in-fabric. Our wFDCF *mecA* CRISPR-based sensor was exposed to various trigger concentrations containing 100, 27, 10, 2.7 and 1 fM *mecA* trigger, to assess in-fabric reaction fluorescence at t = 90 min after fluid entry as compared to controls with a scrambled trigger. Increasing concentrations of trigger lead to an increase in fluorescence signal at the evaluation timepoint as denoted by the recorded mean pixel intensity from POF regions (n=3). A statistically significant difference between the negative control and trigger presence was observed at 90 min only for concentrations equal and above that of 2.7 fM of trigger ($P<0.05$), which can be considered a limit of detection for this specific trigger, device configuration and evaluation timepoint.

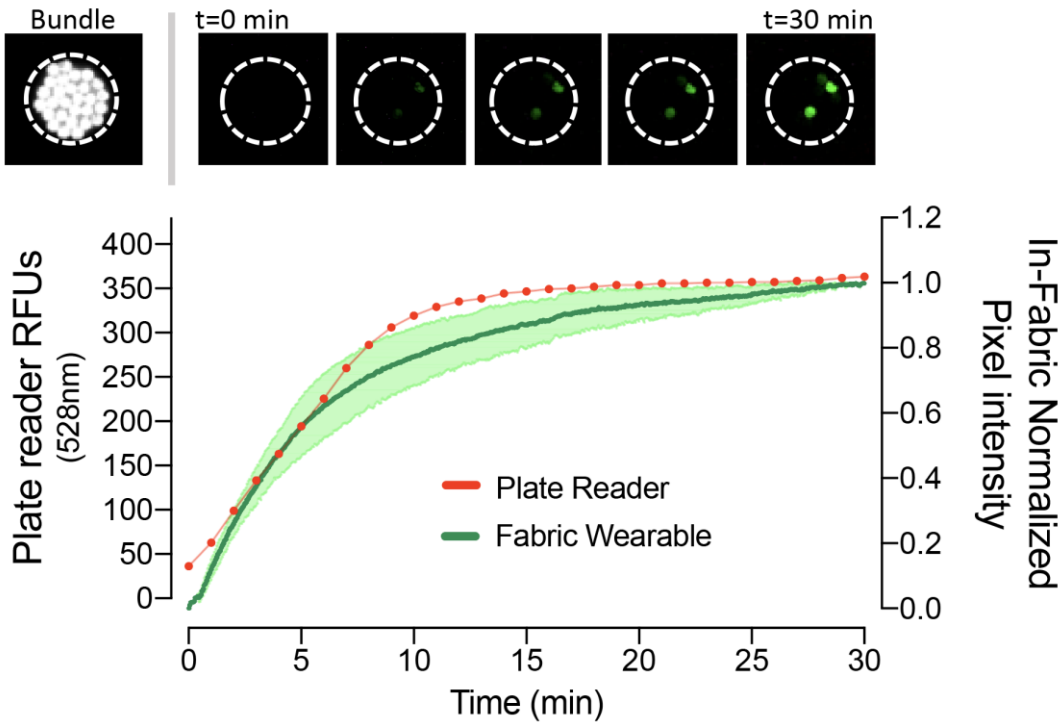

Fig. S12. Comparison of Cas13a-based SHERLOCK MRSA RNA-sensing in wFDCF in-fabric prototype against signal in a standardized plate reader. A CRISPR-Cas13a based MRSA SHERLOCK RNA sensor was prepared and freeze-dried over a wearable textile device for testing. This reaction contained Cas13a for ssRNA detection instead of Cas12a for dsDNA detection as reported for our other CRISPR-based sensors. Cell-free reactions were freeze-dried in the wearable devices for 4-8 hours and also freeze-dried in a 384-well plate for comparison in 4 µL reaction aliquots. All reactions contained RNaseAlert substrate, a quenched fluorophore probe that is cleaved by activated Cas13a (Integrated DNA Technologies, Coralville, IA). The wearable sensor was activated with a fluid splash of dd-H_2O containing 20 nM *mecA* RNA trigger, while the plate samples were rehydrated with the same trigger concentrations to the originally deposited reaction volume (4 µL). Reactions were monitored at 30ºC for 30 minutes using the wearable optical device or and a BioTek NEO HTS plate reader (BioTek Instruments, Inc., Winooski, VT) in fluorescence mode (Ex. 470 nm / Em. 510 nm). Normalized pixel intensity in the wearable device is comparable in behavior to the results of the kinetic run conducted in the plate reader.

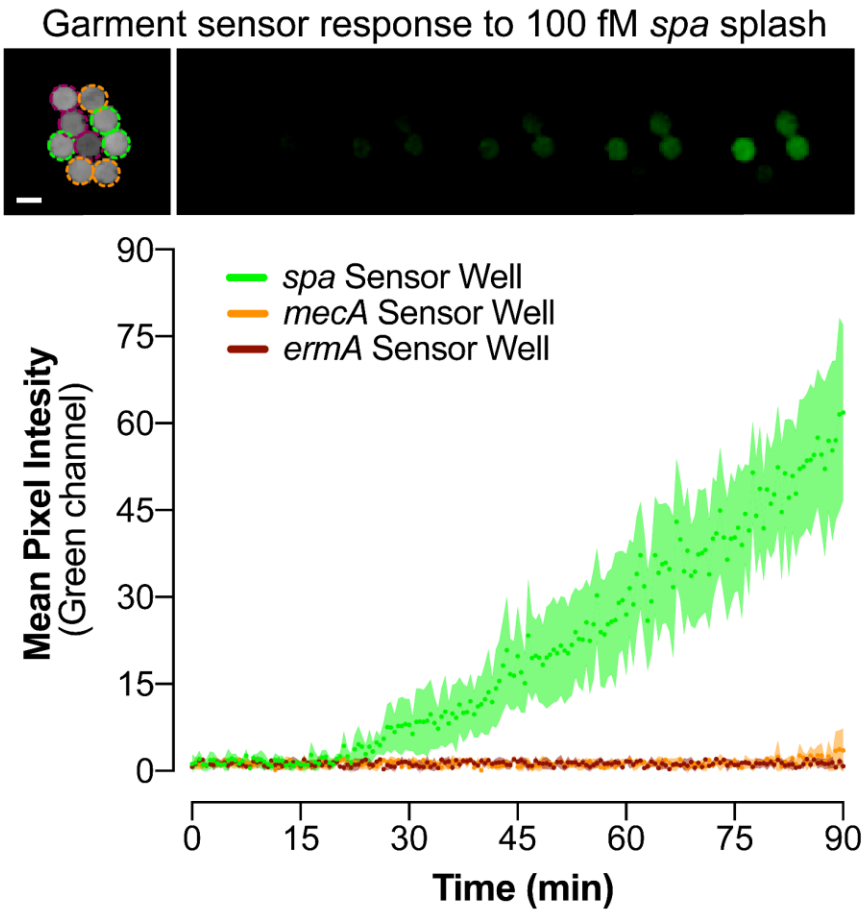

Fig. S13. Antibiotic resistance sensors for *spa*, *ermA* and *mecA* genes using in-wearable sensor demonstrate specific orthogonality. Only reaction chambers with a Cas12a sensor targeting the *S. aureus* virulence factor-encoding *spa*-gene generates a detectable signal within 30 min.

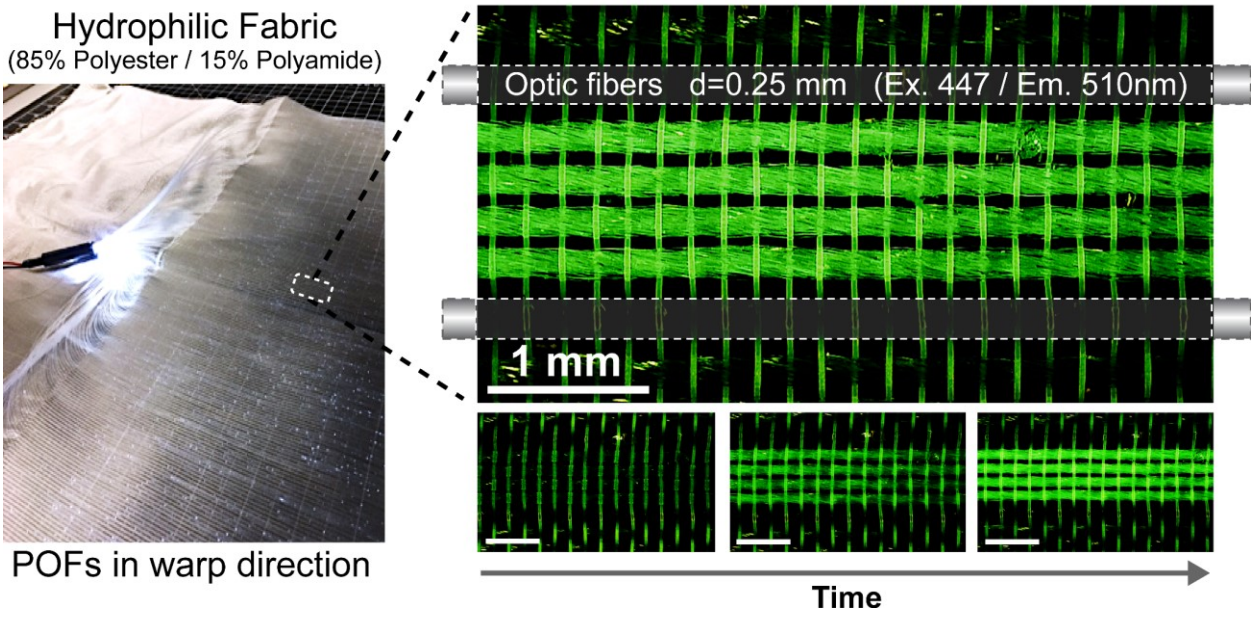

Fig. S14. POF fabric compatibility with lyophilized transcription-only fluorescent aptamer reactions. POF fabric treated to eliminate RNases was lyophilized with a fluorescent aptamer reaction containing pJL1-F30-2xd-Broccoli aptamer template and an in vitro transcription reaction (HiScribe™ T7 Quick High Yield RNA Synthesis Kit; NEB, Ipswich, MA). The lyophilized in-fabric sensors were activated by rehydration with a fluid splash of dd-H_2O spiked with 50 μM of the substrate (5Z)-5-((3,5-Difluoro-4-hydroxyphenyl)methylene)-3,5-dihydro-2-methyl-3-(2,2,2-trifluoroethyl)-4H-imidazol-4-one (DFHBI-1T; Tocris Bioscience, Minneapolis, MN). Upon rehydration, the in vitro transcription reaction generates an RNA aptamer that binds to the DFHBI-1T substrate, generating fluorescence.

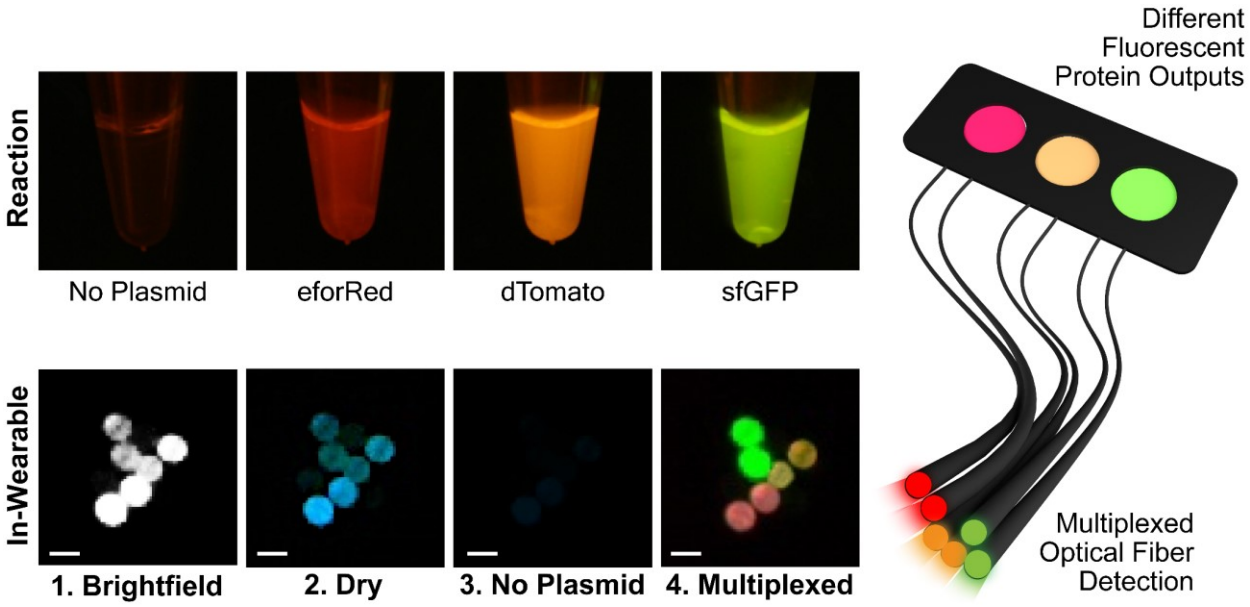

Fig. S15. Sensor multiplexing using different fluorescent proteins can be detected in a single device. Top row, cell-free reactions demonstrating different fluorescent protein outputs generated after 30 min at 30°C. All tubes were photographed with illumination using an Invitrogen Safe Imager 2.0 G6600 Blue Light Transilluminator (Carlsbad, CA). Bottom row, sensor images of fiber topic bundles in (1) brightfield (intense light is placed over the sensor regions to spatially locate each fiber), (2) image when the sensor is dry, (3) image when wFDCF reaction is hydrated but without plasmid (30 min incubation at 30°C), and (4) image when wFDCF reaction is hydrated but with FP plasmids (30 min incubation at 30°C).

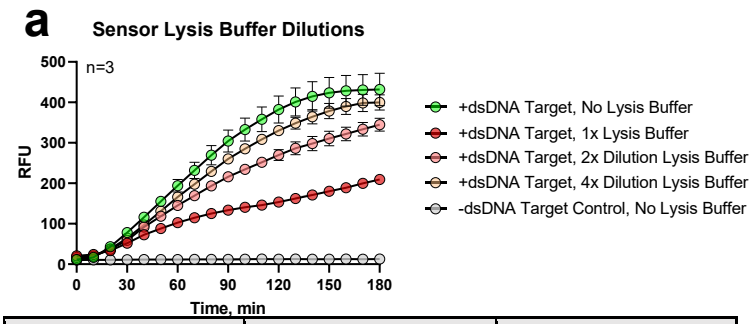

1x	2x dilution	4x dilution
20 mM Tris-HCl, pH 7.5	10 mM Tris-HCl, pH 7.5	5 mM Tris-HCl, pH 7.5
2% Triton X-100	1% Triton X-100	0.5% Triton X-100
2% NP-40	1% NP-40	0.5% NP-40
0.4% CHAPS	0.2% CHAPS	0.1% CHAPS

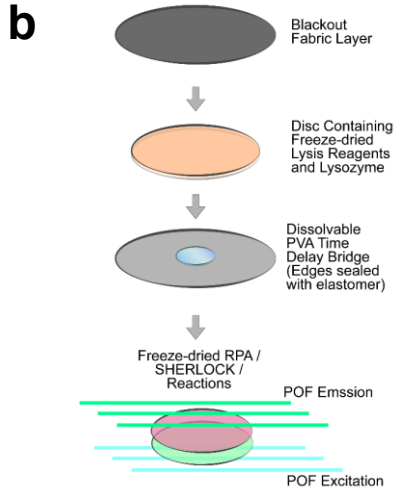

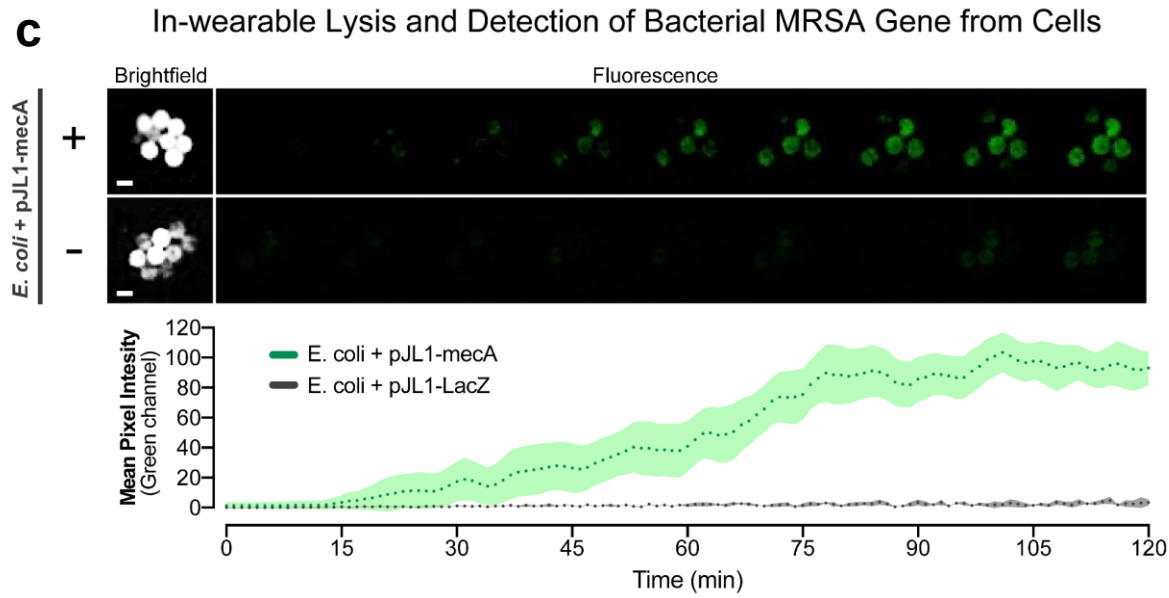

Fig. S16. Integrated wFDCF sample lysis. a, Detergent combinations for cellular lysis were tested against CRISPR-Cas12a SHERLOCK reactions. Shown are reactions for the SARS-CoV-2 SHERLOCK sensor tested in various detergent dilutions. Based on these results, the 2x dilution was chosen as the optimal lysis buffer. For bacterial samples, the lysis buffer was supplemented with 100 µg/mL of lysozyme for dissolving peptidoglycan and 5% sucrose to create a hyperosmotic environment. **b**, In-wearable wFDCF mecA sensors containing a lyophilized lysis buffer were challenged with intact *E. coli* cells either containing the target *mecA* gene (+, top images) or a negative control plasmid (-, bottom images).

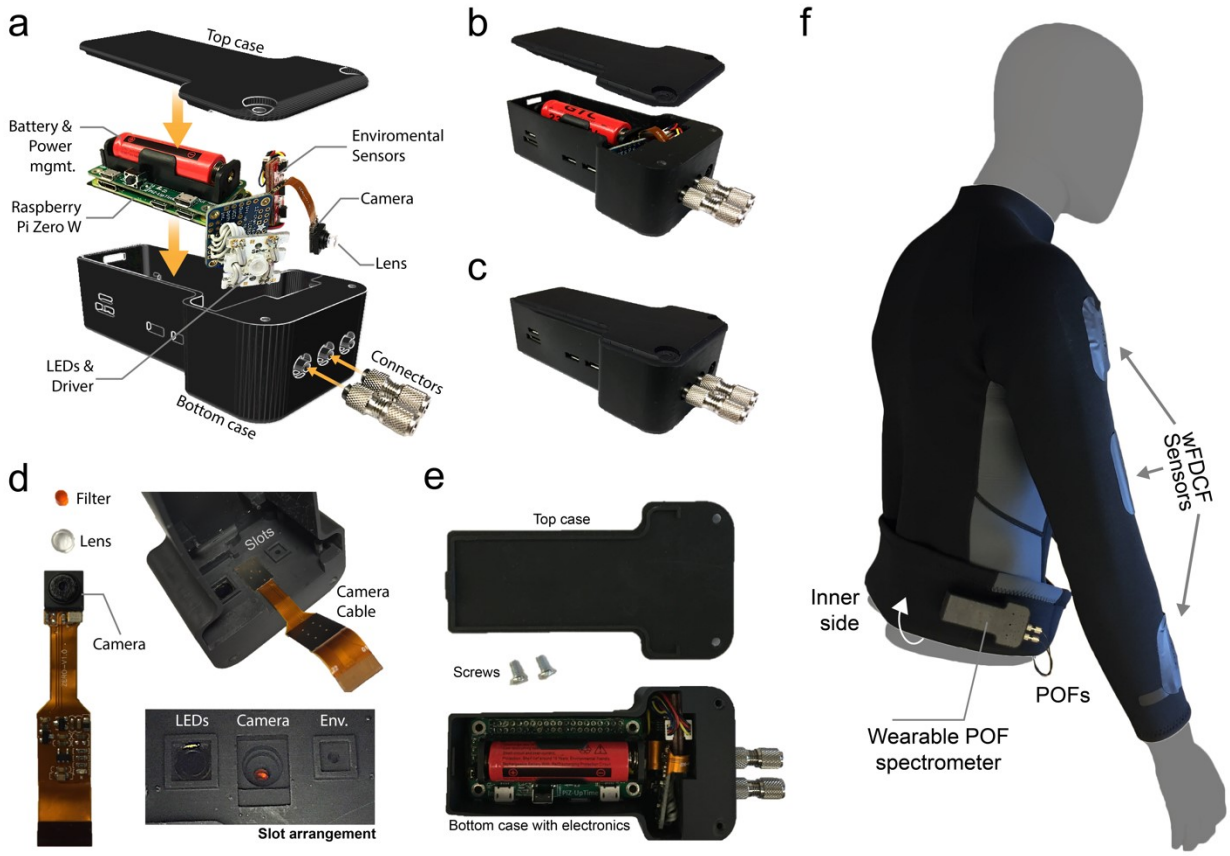

Fig. S17. Fabrication of wearable microcontroller system with LED illumination and spectrometric capabilities. a, Exploded isometric view of wearable POF spectrometer components with case and electronics. The device electronics are based on a Raspberry Pi Zero W Version 1.3 (Raspberry Pi Foundation, Cambridge, UK), assembled with a PiZ-UpTime battery power board (Alchemy Power Inc., Santa Clara, CA), an environmental sensing module, an LED illumination module, and a flexible camera for imaging. **b,** Photograph of an open assembled device. **c,** Photograph of a fully assembled device ready for imaging. **d,** Details of camera used in the device as well as the amber fluorescence emission filter and lens for magnification. Slots at the front of the bottom case fit the camera end, the LED arrangement and a vent for the environmental sensors. **e,** Top view of an assembled device to provide detail of compact electronics arrangement. **f,** Arrangement of wearable POF spectrometer with wireless connectivity in-garment for wFDCF reaction testing.

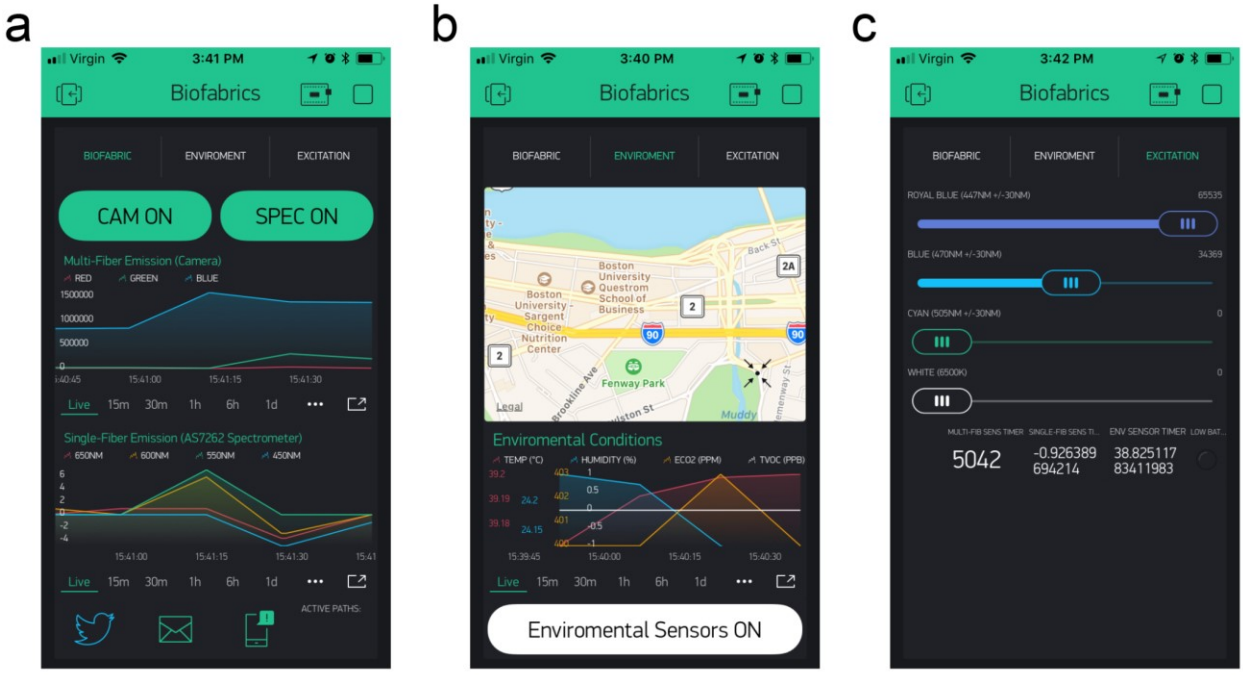

Fig. S18. Custom mobile application software. a, Main window of the developed wFDCD sensor mobile application "Biofabrics" where spectrographic measurements are continuously recorded. Display graphs show independent color channels and bottom icons alert features such as Twitter, email, or messaging as a method of alarm in case of sensor activation. **b,** Environmental window of the mobile application shows geolocation information as well as recorded measurements of temperature (ºC), humidity (%) and CO2 (PPM). **c,** Excitation window of the application allows on-the-fly user adjustment of the LED illumination parameters of the four Luxeon Star LEDs installed in the wFDCF device using a Saber Z4 Color Mixing Array (Quadica Developments Inc., Lethbridge, Alberta). LEDs included in the current device were: 447nm, 470nm, 505nm, and 6500K white. This mobile application was developed using blynk.io (Blynk Inc., New York, NY) and the Raspberry Pi communication module. All generated data were recorded in the internal local memory of the wearable device and this application for analysis.

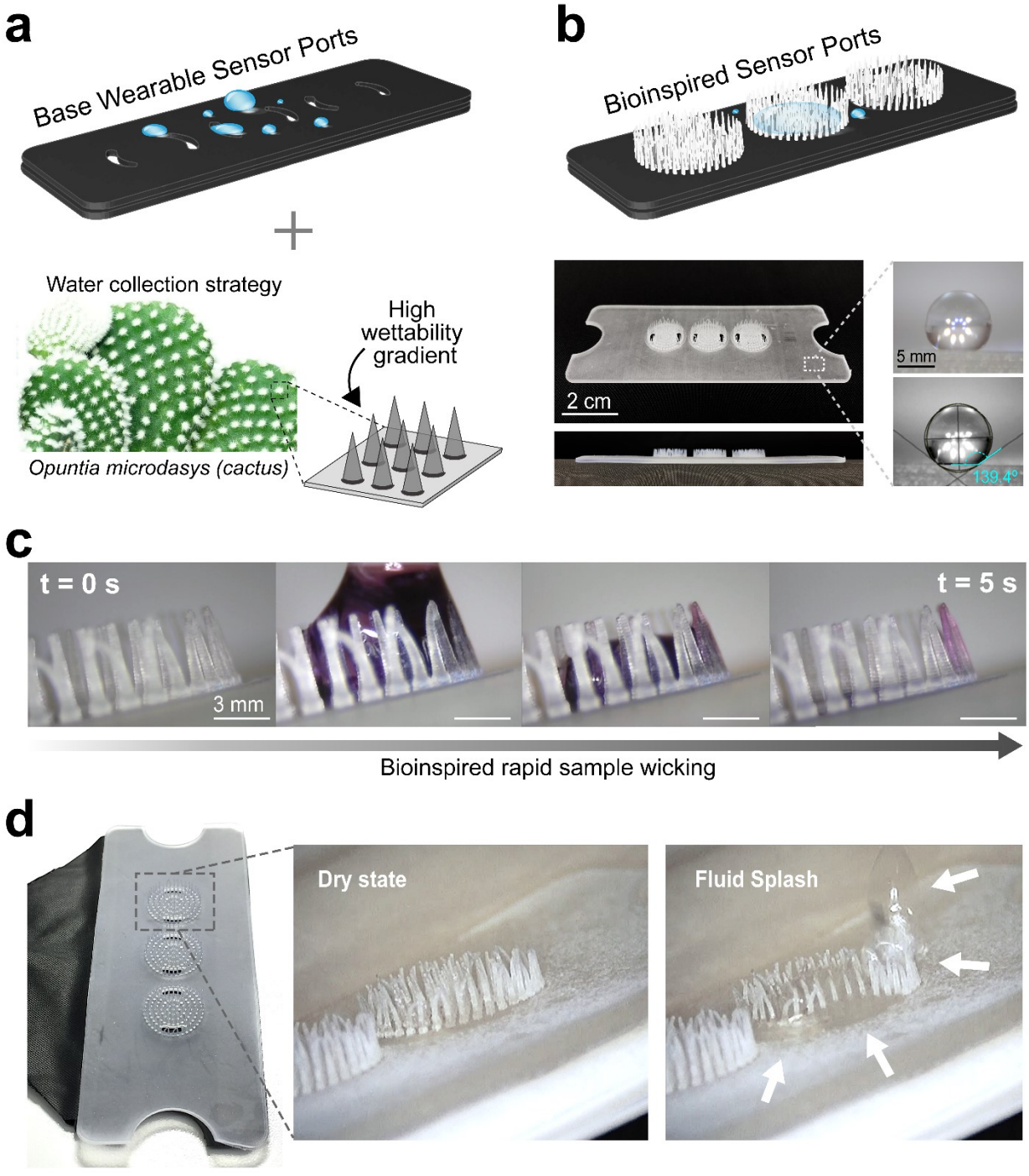

Fig S19. Bioinspired sample-wicking for textile-based wFDCF synthetic biology devices. a, Schematic of the base cover presented for the textile-based wFDCF synthetic biology devices, as well as the underlying biomechanical mechanism of water collection at the areoles of the bunny ears cactus, *Opuntia microdasys*[10, 11]. The high aspect ratio and agglomeration of spikes in these

areoles, known as glochids, provide a high wettability gradient, which pins fluid for rapid absorption. **b,** Modified cover for our textile-based wFDCF synthetic biology devices with *Opuntia*-inspired wicking ports. The cover features 3D-printed conical spikes (1 mm base diameter) with an aspect ratio of 1:5 arranged concentrically with 1 mm spacing. The cover was fabricated using an elastic photoreactive resin and a stereolithography 3D-printing method using a Form 2 printer (Formlabs Inc., Sommerville, MA), coated with NeverWet© superhydrophobic coating (NeverWet LLC., Lancaster, PA). Contact angle measurements to confirm hydrophobicity of cover surfaces is also shown. **c,** Five-second time-lapse of the fluid pinning and port wicking exhibited by the device. This demonstration shows that upon fluid splash over the device, fluid rolls through superhydrophobic regions until they encounter the bioinspired ports, which readily pin the fluid, drawing it down into the underlying absorbent fabric layers inside the reaction chamber. **d,** A photograph of an assembled textile-based wFDCF synthetic biology device including the bioinspired port. Images before and after fluid splash are also shown to evince behavior.

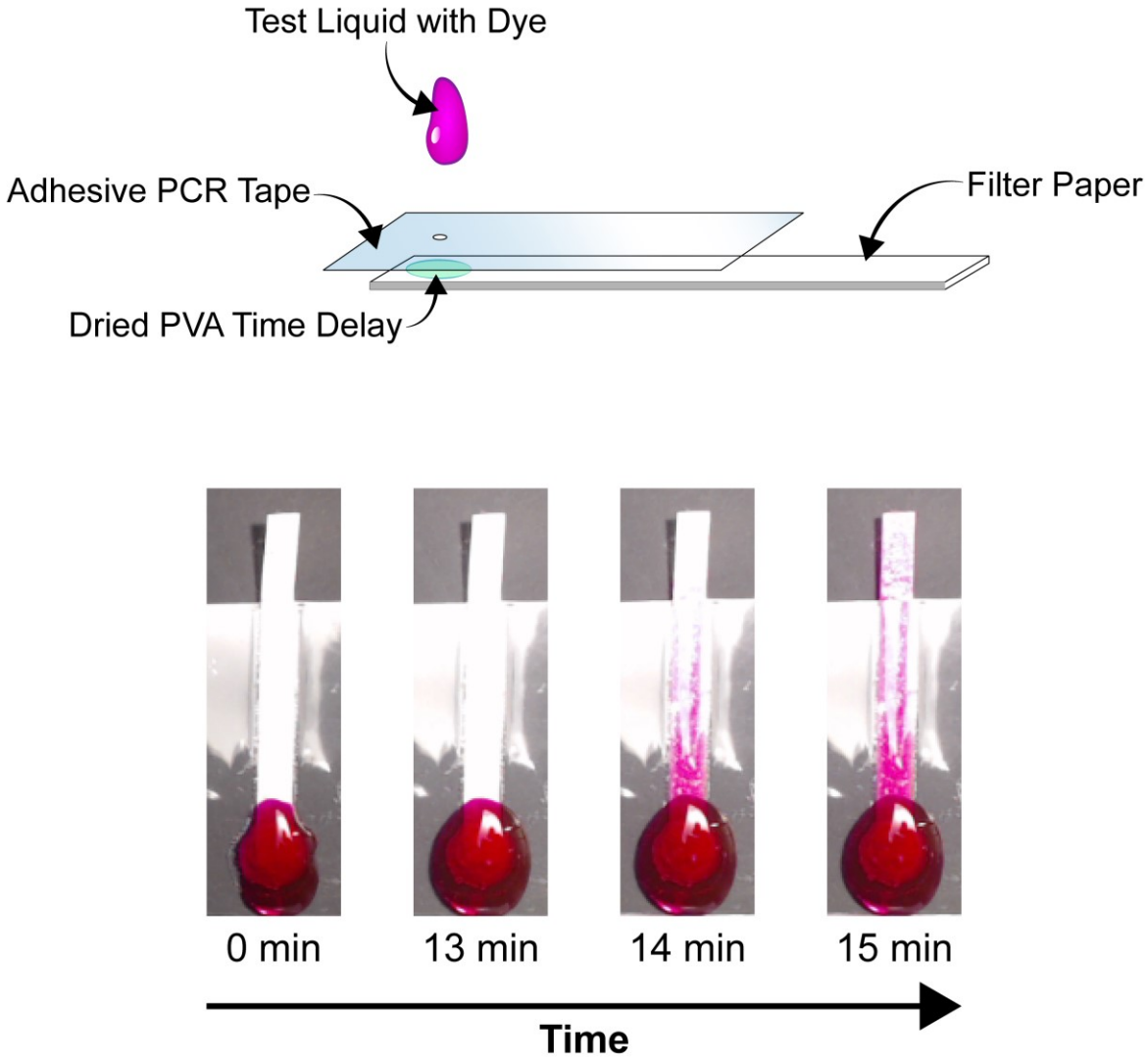

Fig S20. Polyvinyl Alcohol (PVA) time delays for optimized multi-stage wFDCF Reactions. PVA fluidic time delays allow for wearable multi-stage reactions to occur rather than one-pot lyophilized reactions. Testing of the PVA time delays was performed by applying various PVA mixtures to filter paper, allowing to fully dry overnight, covering with impenetrable PCR tape where a 6 mm hole was punched through and aligned directly on top of the dried PVA region. A test aqueous dyed liquid was applied and PVA dissolution and wicking into the filter paper was monitored over time. A representative experiment is shown using a 50 µL dried time delay consisting of ~67,000 MW PVA (Millipore-Sigma, St. Louis, MO) that allows for a time delay of ~15 minutes. For the A-version sensors, 20% (w/v) PVA was used. For the B-version sensors, this was reduced to 18% (w/v) to allow more facile pipetting. No substantial change in delay time was noticed between the 18% and 20% delays.

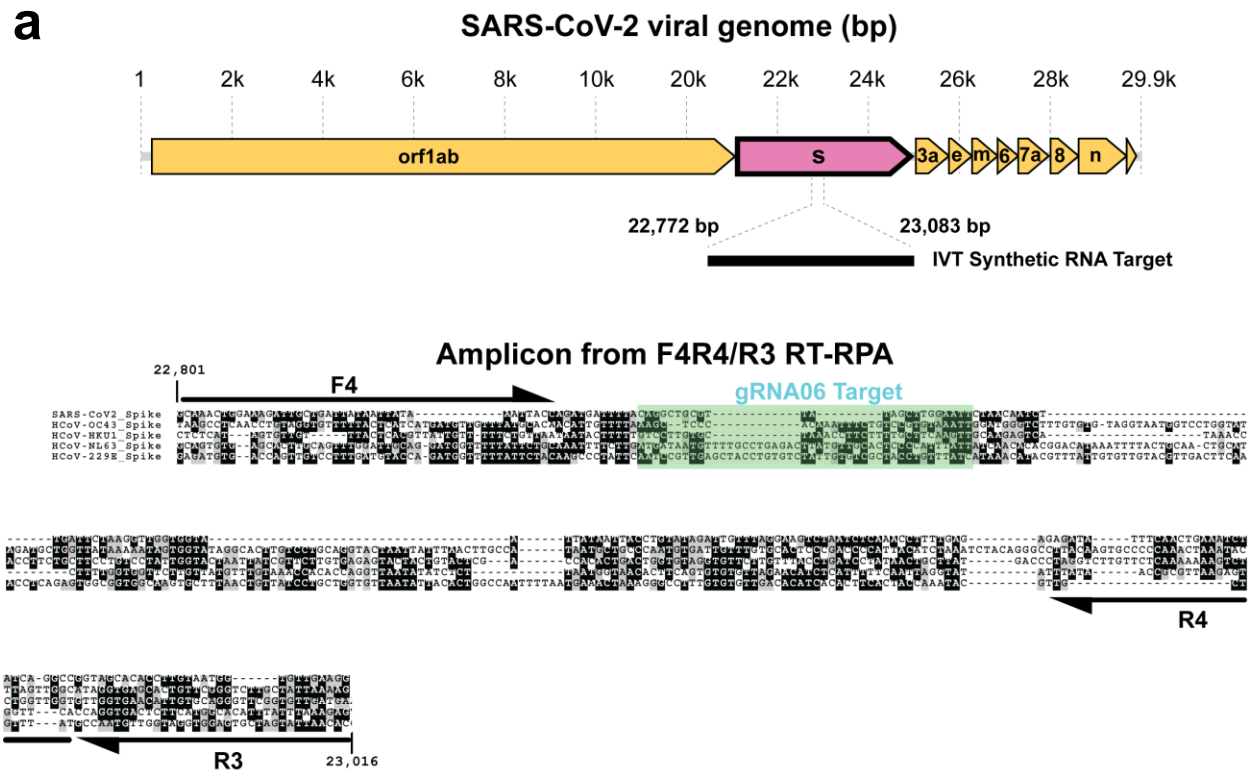
a
SARS-CoV-2 viral genome (bp)
1
2k
4k
6k
8k
10k
20k
22k
24k
26k
28k
29.9k
orf1ab
S
3a
e
m
6
7a
8
n
22,772 bp
23,083 bp
IVT Synthetic RNA Target
Amplicon from F4R4/R3 RT-RPA
22,801
F4
gRNA06 Target
R4
R3
23,016

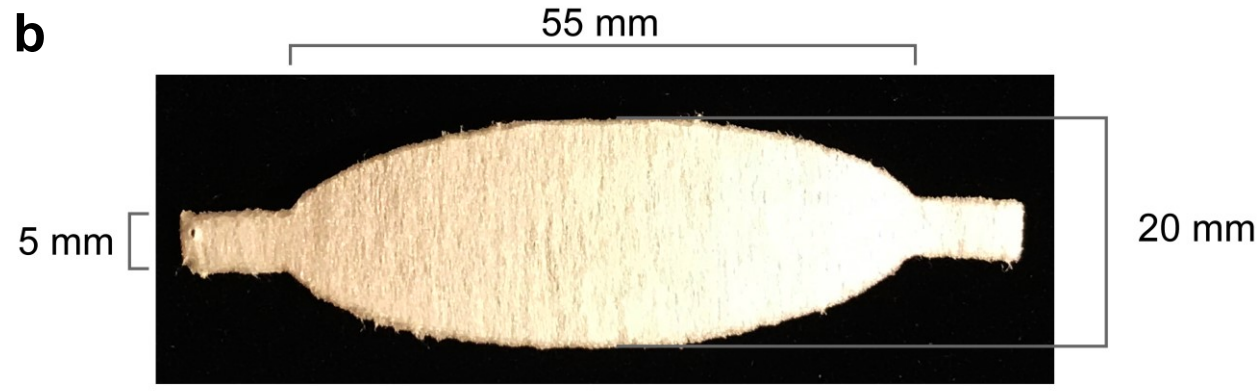
b
55 mm
5 mm
20 mm

c

1. Wax printed patterns for multiple µPADs.

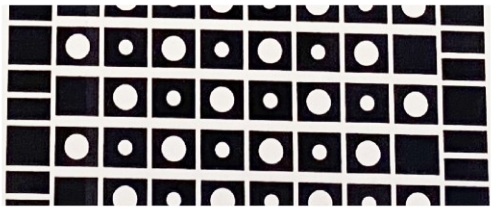

2 . After wax reflow by hot pressing.

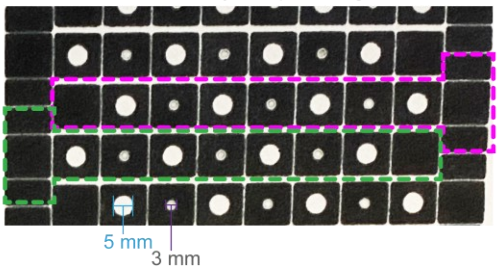

3. Individual µPADs arrays are cut from each sheet.

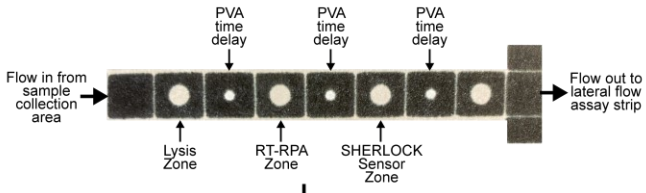

4. PVA time delays are applied and dried overnight.

5. Lysis, RT-RPA, and SHERLOCK reactions are pipetted onto zones, snap-frozen, and lyophilized.

6. µPADs are folded to overlap all zones on one axis..

5

d

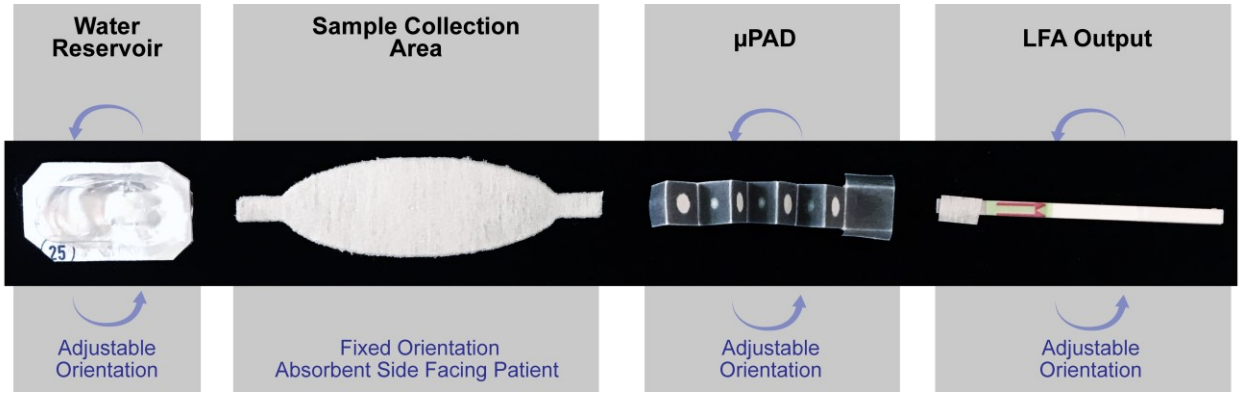

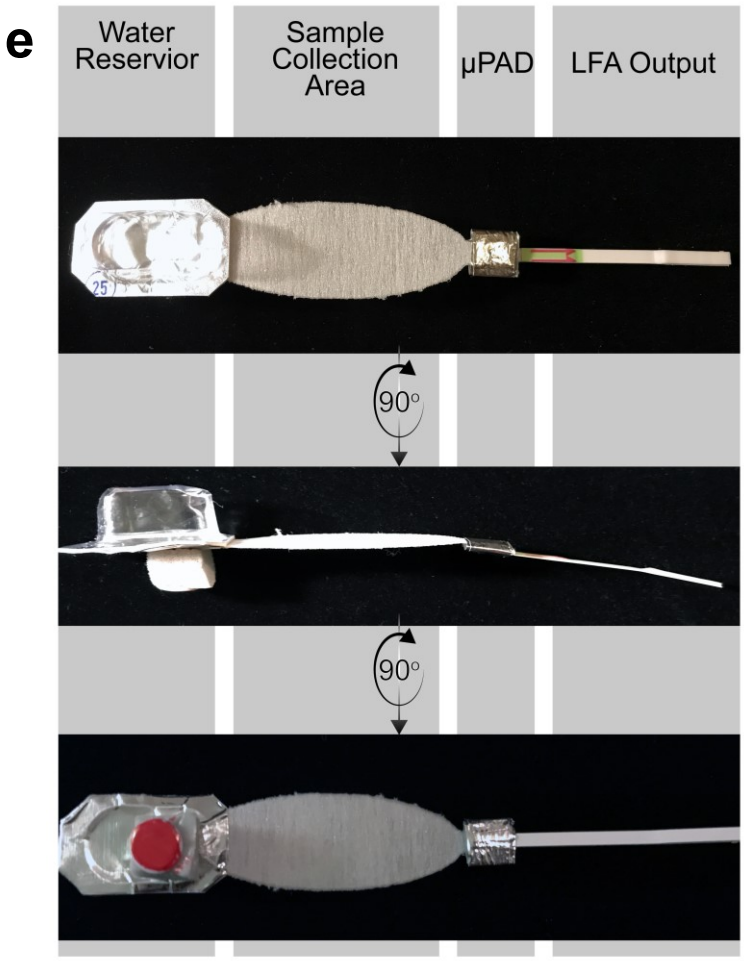
e
Water Reservior
Sample Collection Area
µPAD
LFA Output
90°
90°


f
0 min
1 min
6 min

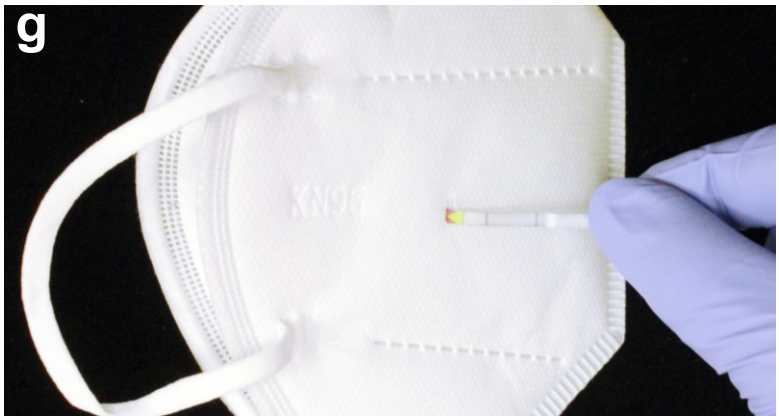
g

Fig S21. SARS-CoV-2 face-mask diagnostic A-version sensor design and construction. **a,** SARS-CoV-2 genomic region targeted by the RT-RPA and SHERLOCK sensor utilized in the face-mask diagnostic of our A-version sensors, used for the experiments shown in Figure 4d-g. Our Cas12a gRNA sensor targets a region (highlighted in green in the multiple sequence alignment) in the Spike protein gene between 22-23k of the SARS-CoV-2 region. An *in vitro* transcribed RNA portion of the SARS-CoV-2 genome corresponding to 22,772:23,083 was generated from a synthetized DNA fragment and used in testing. The multiple sequence alignment shows the aligned homologous regions from SARS-CoV-2 and the three circulating human coronavirus strains (OC43, HKU1, NL83, and 229E). The sequence alignment was generated using Clustal Omega (EMBL-EBI) and BoxShade (SIB Swiss Institute of Bioinformatics). The shown region corresponds to the amplicon generated from RT-RPA with the F4/R4/R3 primer mix. The sequences for the gRNA, *in vitro* transcribed RNA targets, and RT-RPA primers are presented in Supplementary Table S2. **b,** Laser-cut sample collection pad from capillary wicking material. A polymeric wicking material was laser-cut with a large sample collection area (55 x 20 mm) that will be positioned inside of the mask to collect respiratory droplets and aerosols for virus detection. **c,** Images of the μPAD construction. Steps for construction the μPAD device portion of the sensor: (1) A solid wax printer is used to print an array of μPADs on filter paper. (2) The printed wax pattern is refluxed by application of a hot press, to fully allow the wax to penetrate the filter paper. (3) The individual μPADs are cut from each sheet. (4) Then, polyvinyl alcohol is added to the time delay zones and allowed to dry at room temperature overnight. (5) Fresh lysis reagents, RT-RPA reactions, and Cas12a SHERLOCK reactions are applied to their respective reaction zones; the μPAD is lyophilized for a minimum of 4 hours. (6) After lyophilization, the μPAD is folded using RNase-free tweezers to overlap the reaction zones. **d,** Components of the face-mask sensor before assembly. From left to right, the water blister allows for user-activation of the rehydration reaction. The sample collection area absorbs viral particles from the patient. The μPAD contains the freeze-dried nucleic acid test sensor reactions, separated by PVA time delays. Finally, a lateral flow assay generates a visual output based on Cas12a-based cleavage of a FAM-Biotin probe. The orientation of the water blister reservoir, μPAD, and LFA components can be adjusted provided the fluidic contacts are properly maintained. These components can also be either placed on the outside or the inside of the face mask. Due to operational requirements, the sample collection pad requires an orientation with the Porex surface facing the patient, and can only be positioned on the inside of the mask. **e,** Fully assembled sensor. **f,** Demonstration of sample flow through face-mask sensor. Bromophenol blue dye was spotted at random locations throughout the sample collection zone. Upon hydration from the reservoir, a sample front can be clearly seen sweeping across the sample zone and into the μPAD. **g**, In order to preserve patient confidentiality, the LFA strip for A-version sensors are oriented with the LFA indicator surface facing the mask to hide the output from external view. The clinician must pull the strip back to observe / record the results.

a

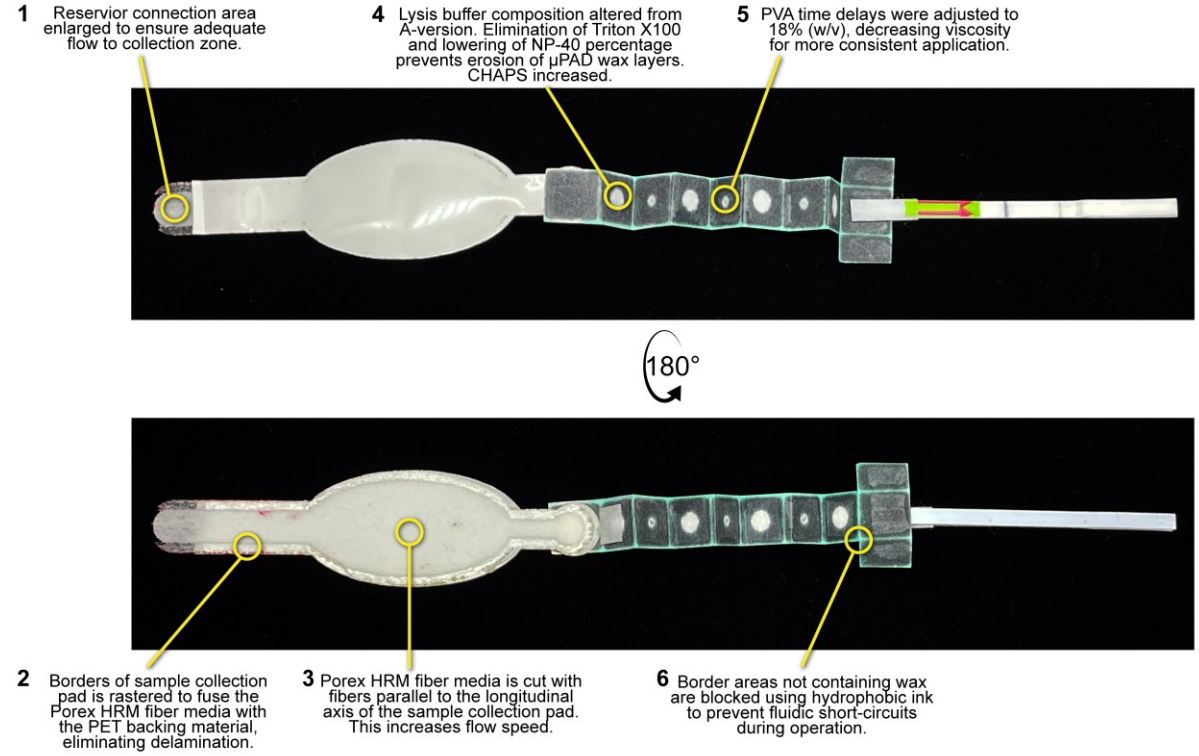
1 Reservior connection area enlarged to ensure adequate flow to collection zone.
4 Lysis buffer composition altered from A-version. Elimination of Triton X100 and lowering of NP-40 percentage prevents erosion of µPAD wax layers. CHAPS increased.
5 PVA time delays were adjusted to 18% (w/v), decreasing viscosity for more consistent application.
180°
2 Borders of sample collection pad is rastered to fuse the Porex HRM fiber media with the PET backing material, eliminating delamination.
3 Porex HRM fiber media is cut with fibers parallel to the longitudinal axis of the sample collection pad. This increases flow speed.
6 Border areas not containing wax are blocked using hydrophobic ink to prevent fluidic short-circuits during operation.

b

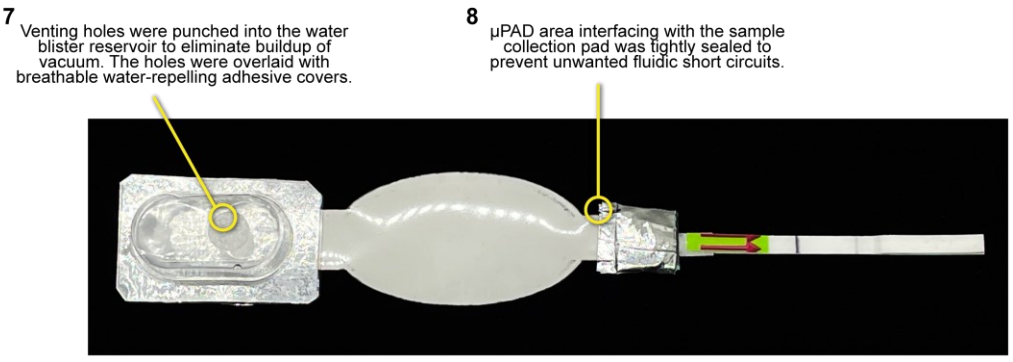
7 Venting holes were punched into the water blister reservoir to eliminate buildup of vacuum. The holes were overlaid with breathable water-repelling adhesive covers.
8 µPAD area interfacing with the sample collection pad was tightly sealed to prevent unwanted fluidic short circuits.

c

Fig S22. SARS-CoV-2 face-mask diagnostic B-version sensor design and construction. The B-version of the SARS-CoV-2 face-mask sensors contain a number of improvements over the A-version sensors that optimize robustness and consistency. These sensors were used for the on-simulator mask experiments shown in Figure 4i-j. **a,** Sub-assembly consisting of the sample collection pad, μPAD (unfolded), and the LFA output strip, highlighting key differences between the B-version and A-version sensor components. **b**, Fully assembled B-version face-mask sensors with indicated changes from A-version sensors. **c**, A B-version sensor fully integrated into a face mask. The water blister reservoir is positioned as a flap on the outside of the mask, to prevent potential crushing of the blister while the mask is being worn.

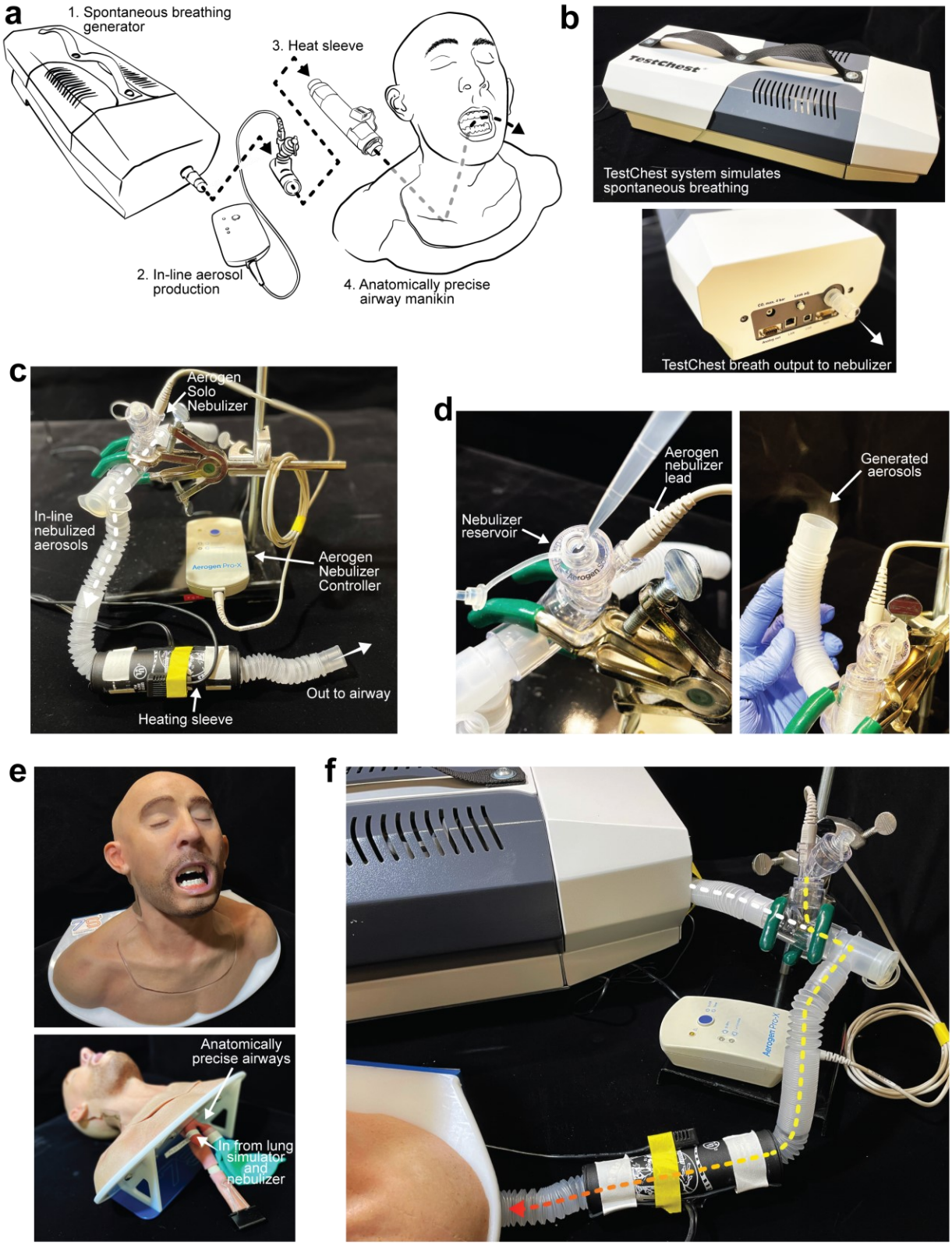
a
1. Spontaneous breathing generator
3. Heat sleeve
2. In-line aerosol production
4. Anatomically precise airway manikin
b
TestChest system simulates spontaneous breathing
TestChest breath output to nebulizer
c
Aerogen Solo Nebulizer
In-line nebulized aerosols
Aerogen Nebulizer Controller
Out to airway
Heating sleeve
d
Aerogen nebulizer lead
Nebulizer reservoir
Generated aerosols
e
Anatomically precise airways
In from lung simulator and nebulizer
f

Figure 23. A breathing simulator for exhaled emission testing of the SARS-CoV-2 face-mask wearable diagnostic. a, A schematic of the key modules used in the breathing simulator. Dotted lines indicate connecting airflow through the different modules via ventilation tubing connectors. **b**, To generate spontaneous breathing rhythms, the TestChest® (Organis GmbH, Switzerland) is a full physiologic artificial lung system that can accurately replicate pulmonary mechanics such as lung vital capacity and functional residual capacity. It allows the user to control the respiration rate and tidal volume to simulate complex breathing mechanics. **c**, The nebulizer and heating assembly. To simulate SARS-CoV-2 laden exhalation breath plumes, the Aerogen® Solo nebulizer system (Aerogen, Inc., Ireland) was used to generate aerosols in the simulated breath stream. The Aerogen® platform is a medical-grade inhalation medicine device that uses vibrating mesh technology. The Aerogen®-produced aerosols have a measured size distribution[12] (0.4 - 4.4 microns) that matches the size range of naturally occurring lung aerosols and droplets[2]. A self-regulating thermal pad sleeve was used to heat the simulated breath to maintain a face mask microclimate of 35°C. **d**, Photos of the nebulizer reservoir being filled (left) and the nebulized aerosols exiting the tubing (right). **e**, A high-fidelity anatomically precise airway manikin (7-SIGMA Simulation Systems, Minneapolis, MN), can simulate exhaled breath as it would exit physiologic airway structures and provides realistic fitment of the mask on a patient's face. **f**, A photograph showing the full air flow path from the TestChest® to the Aerogen® Solo nebulizer, through the heating sleeve, and connecting to the 7-SIGMA manikin.

Supplemental References

1. Gui, M. et al. Electron microscopy studies of the coronavirus ribonucleoprotein complex. *Protein Cell* **8**, 219-224 (2017).
2. Fennelly, K.P. Particle sizes of infectious aerosols: implications for infection control. *Lancet Respir Med* **8**, 914-924 (2020).
3. Patel, A.K. et al. Inhaled Nanoformulated mRNA Polyplexes for Protein Production in Lung Epithelium. *Adv Mater* **31**, e1805116 (2019).
4. Pardee, K. et al. Rapid, low-cost detection of zika virus using programmable biomolecular components. *Cell* **165**, 1255-1266 (2016).
5. Huang, A. et al. BioBits Explorer: A modular synthetic biology education kit. *Sci Adv* **4**, eaat5105 (2018).
6. Stark, J.C. et al. BioBits Health: Classroom activities exploring engineering, biology, and human health with fluorescent readouts. *ACS Synth Biol* **8**, 1001-1009 (2019).
7. Kumar, R.M. et al. Deconstructing transcriptional heterogeneity in pluripotent stem cells. *Nature* **516**, 56-61 (2014).
8. Topp, S. et al. Synthetic riboswitches that induce gene expression in diverse bacterial species. *Appl Environ Microbiol* **76**, 7881-7884 (2010).
9. Chandler, M. et al. Broccoli Fluorets: Split Aptamers as a User-Friendly Fluorescent Toolkit for Dynamic RNA Nanotechnology. *Molecules* **23** (2018).
10. Zhang, S., Huang, J., Chen, Z. & Lai, Y. Bioinspired special wettability surfaces: from fundamental research to water harvesting applications. *Small* **13** (2017).
11. Ju, J. et al. A multi-structural and multi-functional integrated fog collection system in cactus. *Nat Commun* **3**, 1247 (2012).
12. McDermott, K. & Oakley, J.G. Droplet Size and Distribution of Nebulized 3% NaCl, Albuterol, and Epoprostenol by Phase Doppler Particle Analyzer. *Respiratory Care* **64**, 3238831 (2019).